

LANDSAT-BASED LINEAMENT ANALYSIS. EAST TEXAS BASIN,
AND STRUCTURAL HISTORY OF THE SABINE UPLIFT
AREA, EAST TEXAS AND NORTH LOUISIANA

Topical Report

Prepared by

Robert W. Baumgardner, Jr., and
Mary L. W. Jackson

Assisted by

Bruce Gates

Bureau of Economic Geology
W. L. Fisher, Director
The University of Texas at Austin
Austin, Texas 78713

Prepared for
The Gas Research Institute
Contract No. 5082-211-0708
November 15, 1986

QAe7677

DRAFT

DISCLAIMER

LEGAL NOTICE This report was prepared by the Bureau of Economic Geology as an account of work sponsored by the Gas Research Institute (GRI). Neither GRI, members of GRI, nor any person acting on behalf of either:

- a. Makes any warranty or representation, express or implied, with respect to the accuracy, completeness, or usefulness of the information contained in this report, or that the use of any apparatus, method, or process disclosed in this report may not infringe privately owned rights; or
- b. Assumes any liability with respect to the use of, or for damages resulting from the use of, any information, apparatus, method, or process disclosed in this report.

RESEARCH SUMMARY

Title Landsat-Based Lineament Analysis, East Texas Basin, and Structural History of the Sabine Uplift Area, East Texas and North Louisiana

Contractor Bureau of Economic Geology, The University of Texas at Austin, GRI Contract No. 5082-211-0708, entitled "Geologic Analysis of Primary and Secondary Tight Gas Sand Objectives"

Principal Investigator R. J. Finley

Report Period March 1, 1984 - November 15, 1986
Topical Report

Objective Because the Travis Peak Formation of East Texas and North Louisiana is most often hydraulically fractured to achieve economic production rates, it is important to understand the structural geologic setting of these areas. Lineament analysis using satellite imagery has become a standard technique in analyzing for preferred structural orientations and was applied to define relations between subsurface structure and surficial features. Regional stratigraphic studies of the Travis Peak showed that the Sabine Uplift probably postdated Travis Peak deposition. A detailed study of the Travis Peak and younger sediments was required to confirm the timing of relative uplift and to help define mechanisms for structural growth. All data are being utilized to help define past and present stress regimes that relate to current natural and hydraulic fracture orientations.

Technical Perspective Lineaments have been recognized as the surficial expression of geologic structure in many studies. Previous analysis of lineaments in East Texas reported parallelism between trends of lineaments and structural features and correlation between lineaments and faults. This report summarizes a regional study of lineaments mapped on Landsat Thematic Mapper images and describes spatial correspondence and parallelism between lineaments and subsurface structure.

Earlier subsurface studies of the Sabine Uplift area have been limited by shallow and widely spaced well data. Structure and isopach maps presented in this report provide an improved interpretation of the structural and depositional history of the Lower Cretaceous interval in the Sabine Uplift area.

Results

Most lineaments detected in this study are stream network features. Few lineaments display a one-to-one correspondence with mapped faults or geologic contacts. High values of lineament density demarcate major fault zones. Two regional lineament orientations are significant at the 99-percent confidence level: 325 degrees and 21 degrees. The northwest regional trend is parallel to wellbore elongations at depths down to 8,000 ft in the Jurassic Schuler Formation. The East Texas Basin and the Sabine Uplift have the same significant northwest trend, but the significant northeast lineament orientations for these two subregional structural features are different. The northeast trend in the East Texas Basin is subparallel to that of elongate salt structures there. The northeast trend over the Sabine Uplift may result from stresses generated by upward movement of the uplift. The northwest lineament trend, common to the regional and subregional data sets, is thought to result from gulfward extension in the Gulf Coastal Stress Province where the least principal stress is perpendicular to the coast. Hydraulically generated fractures should propagate perpendicular to the minimum compressive stress and, consequently, perpendicular to the northwest trend of lineaments in this study area.

The isopach maps generated in this study show that the Sabine Uplift was part of a large basinal area during the Late Jurassic and Early Cretaceous. The Sabine Uplift does not appear to have been a large Jurassic horst that remained in a structurally high position throughout the Cretaceous and Tertiary, as is commonly shown in the literature. Timing, orientation, and magnitude of Sabine arching indicate that the Sabine Uplift may have been produced by northeast-directed tectonic events related to orogenic activity in the southern North American Cordillera and the Sierra Madre Oriental in Mexico.

Technical Approach

Lineament studies were conducted on four black-and-white Thematic Mapper images at 1:250,000-scale. Each image was interpreted manually on a light table using transmitted light. Standard statistical techniques were used to identify significant lineament orientations.

Subsurface structural studies used 811 electric logs and 24 cross sections. Six Lower Cretaceous units were correlated across the study area, and six isopach and five structure maps were constructed.

CONTENTS

	Page
INTRODUCTION.....	1
LANDSAT-BASED LINEAMENT ANALYSIS OF THE EAST TEXAS BASIN AND SABINE UPLIFT by Robert W. Baumgardner, Jr.	3
ABSTRACT.....	3
INTRODUCTION.....	4
Purpose and scope.....	4
Physiography and land cover.....	10
Previous work.....	11
METHODS AND MATERIALS.....	12
Imagery.....	12
Procedures.....	15
Definition of observed lineaments.....	17
RESULTS.....	21
Correspondence between lineaments and geologic features.....	21
Length-weighted frequency of lineament azimuths.....	22
Graphical display of results.....	26
Selection of polar graphs.....	26
Significance level of peaks.....	28
Definition and validity of peak values.....	28
Vector sums of greater-than-average peaks.....	35
Lineament density.....	39
Subregional lineament orientation.....	42
DISCUSSION.....	52
Relationship between lineaments and stress regime.....	52
Stress in study area.....	53

CONCLUSIONS.....	57
ACKNOWLEDGMENTS.....	57
MESOZOIC AND CENOZOIC STRUCTURAL HISTORY OF THE SABINE UPLIFT AREA, EAST TEXAS by Mary L. W. Jackson.....	59
ABSTRACT.....	59
INTRODUCTION.....	59
PREVIOUS WORK.....	60
METHODOLOGY.....	62
GEOLOGIC SETTING.....	70
DEPOSITIONAL HISTORY OF MESOZOIC AND CENOZOIC SEDIMENTS.....	71
Jurassic depositional history.....	71
Lower Cretaceous depositional history.....	75
Basal Upper Cretaceous depositional history.....	85
Upper Cretaceous and Tertiary depositional history.....	88
MESOZOIC AND CENOZOIC STRUCTURAL HISTORY.....	89
Late Jurassic and Early Cretaceous events.....	89
Arching at the end of the Early Cretaceous.....	91
Late Cretaceous and Tertiary events.....	97
SALT-RELATED STRUCTURES ON THE SABINE UPLIFT.....	99
PROPOSED ORIGIN FOR THE SABINE UPLIFT.....	105
SUMMARY.....	107
ACKNOWLEDGMENTS.....	108
REFERENCES.....	109
APPENDIX A.....	119

FIGURES

1. Location map of study area.....	6
2. Generalized geologic map of study area.....	8

3.	Stratigraphic column of geologic formations.....	9
4.	Spectral range of Landsat satellite sensors. A. Distribution of Landsat bands. B. Reflectance of three basic cover types.....	13
5.	Map of all Landsat lineaments in study area.....	18
6.	Examples of lineament types.....	20
7.	Procedure for statistical evaluation of lineament orientation data. A. Length-weighted frequency (F). B. Vector sum of adjacent larger-than-average peaks of F. C. Bernshtein accuracy criterion for peaks significant at 99-percent confidence level.....	23
8.	Polar graphs of length-weighted frequency for lineaments in 12 subregional zones.....	24
9.	Graph of index of preferred orientation (IPO).....	30
10.	Polar graphs of vector sums for greater-than-average peaks of length-weighted frequency.....	36
11.	Polar graphs of Bernshtein accuracy criterion for 12 subregional zones.....	38
12.	Map of lineament density and major structural features.....	40
13.	Boundaries of East Texas Basin and Sabine Uplift as defined by lineament density.....	43
14.	Polar graphs of values of Bernshtein accuracy criterion. A. East Texas Basin. B. Sabine Uplift.....	44
15.	Map of lineaments and salt-related structures in East Texas Basin.....	46
16.	Polar graph of values of Bernshtein accuracy for lineaments and elongate salt-related structures.....	47
17.	Models of faults related to doming. A. Uplift only. B. Uplift and extension. C. Polar graphs from A and B combined.....	49
18.	Map of breakouts in wells in the Schuler Formation, East Texas.....	55
19.	Geologic and structural setting.....	63
20.	Data points used in this study and cross-section locations.....	64
21.	Type log of the Lower Cretaceous.....	65

22.	Representative west-east cross section of the Lower Cretaceous.....	66
23.	Representative north-south cross section of the Lower Cretaceous.....	68
24.	Isopach map of the combined Sligo and Travis Peak Formations.....	72
25.	Structure map of the base of the Massive Anhydrite.....	73
26.	Structure map of the base of the Austin Group.....	74
27.	Stratigraphic section for the Sabine Uplift area.....	77
28.	Isopach map of the Pine Island, James, and Rodessa Members of the Trinity Group.....	78
29.	Representative stratigraphic dip sections across East Texas and western Louisiana.....	79
30.	Isopach map of the upper Glen Rose and Massive Anhydrite.....	80
31.	Isopach map of the Paluxy Formation.....	82
32.	Isopach map of the Fredericksburg Group.....	83
33.	Isopach map of the Washita Group.....	84
34.	Isopach map of the Eagle Ford Group.....	87
35.	Tectonic and salt-related events in the Sabine Uplift area.....	90
36.	Regional isopach map of the Glen Rose Subgroup.....	92
37.	Regional isopach map of the Paluxy Formation.....	93
38.	Structure map on the top of the upper Glen Rose Formation.....	94
39.	Palinspastic map on the base of the Massive Anhydrite.....	98
40.	Structural features in southwestern United States.....	100
41.	Salt-related structures in the Sabine Uplift area.....	102
42.	Structure map on top of the Paluxy Formation.....	103
43.	Structure map on top of the Fredericksburg Group.....	104

TABLES

1. Landsat Thematic Mapper images used in this study.....	7
2. Descriptions of lineaments.....	19
3. Significant peaks for 5-degree and 10-degree sectors.....	27
4. Data for 12 zones and three areas in order of increasing number of lineaments.....	31
5. Megalineaments and significant peaks of F.....	34
6. Selected subsurface studies that include the area of the Sabine Uplift.....	61
7. References pertaining to mid-Cretaceous erosional history on the Sabine Uplift.....	96

INTRODUCTION

The Travis Peak Formation, an areally extensive tight gas sandstone in East Texas and North Louisiana, serves as a natural laboratory for technology development in tight gas production. Incorporated in the geologic component of the Gas Research Institute's (GRI) program have been regional and local studies of Travis Peak depositional systems, analyses of mineralogy, diagenetic history, and hydrocarbon maturation based on extensive collection of core, and structural geologic studies aimed at understanding states of stress and potential controls on hydraulic fracture propagation. This report includes two elements among several components of the structural geologic studies.

The Landsat-based lineament analysis uses standard remote sensing techniques in an analysis of Thematic Mapper images over a broad area of East Texas and part of North Louisiana. Although difficult to apply in a region of abundant vegetation and intensive agricultural land use, the lineament data reflect regional and salt-related structural features and show correlation with borehole elongation directions. This analysis of Landsat images is being followed up with study of higher-resolution synthetic aperture radar imagery that contains a higher density of detectable lineaments. Further digital processing of Landsat imagery is expected to enhance interpretations of specific areas of interest. All results are being correlated with borehole data collected as part of GRI's first Staged Field Experiment well, drilled in Waskom field, Harrison County, Texas, in August 1986.

The Sabine Uplift is the major structurally positive feature in northeast Texas and northwest Louisiana, but previous stratigraphic studies have shown that it was not present at the time of Travis Peak deposition. By focusing on the post-Travis Peak depositional history of the Sabine Uplift area it has been possible to define the

timing and extent of the uplift and to incorporate these results in burial history curves for estimation of the timing of diagenesis. Future studies of in situ stress analysis must take into account at least two periods of uplift that have now been defined.

LANDSAT-BASED LINEAMENT ANALYSIS OF THE EAST TEXAS BASIN AND SABINE UPLIFT

Robert W. Baumgardner, Jr.

ABSTRACT

Lineament analysis was used to study the relationship between subsurface structure and surficial features in East Texas, southeastern Oklahoma, southwestern Arkansas, and northwestern Louisiana, an area of low topographic relief, moderate vegetation cover, and diverse land use. More than 2,200 lineaments were mapped from four standard 1:250,000-scale Landsat Thematic Mapper images. Operator error and database variation were evaluated in areas of sidelap between adjacent images. Because no significant difference (at $p=.05$ level) in lineament orientations or mean lineament length was detected in these areas, mapping error and differences between images were judged inconsequential. Vector sums of greater-than-average values of length-weighted frequency (F) were used to define significant peaks of lineament orientation. Regional orientation for all lineaments is bimodal, with peaks at 325 degrees and 21 degrees azimuth. The northwest regional peak coincides with mean azimuth of borehole elongations attributed to natural fractures in 50 wells located throughout East Texas. Within the salt structure province of the East Texas Basin the azimuth of the vector sum for lineaments (16 degrees) is not significantly different from that for underlying, elongated salt-related structures (29 degrees) (salt diapirs, salt pillows, turtle structures). These results suggest that lineaments and subsurface structures result from like-oriented stresses. Lineament density (length/unit area) was

measured in 100 km² grid cells throughout the study area, and it successfully delineated some large structural features. An arcuate trend of high values (≥ 20 km/100 km²) demarcates the Mexia-Talco Fault Zone. Other density highs occur near the Angelina Flexure and the Rodessa, South Arkansas, and Elkhart-Mt. Enterprise Fault Zones. Lineament density values have no consistent spatial relationship with salt-related structures, but their relatively small size probably makes these structures difficult to detect. These results indicate that high lineament density coincides with most major surface and subsurface structures in the study area. Furthermore, statistically significant lineament orientations coincide with azimuths of elongated boreholes and deeply buried structures and may be diagnostic of regional and basinwide stress regimes.

INTRODUCTION

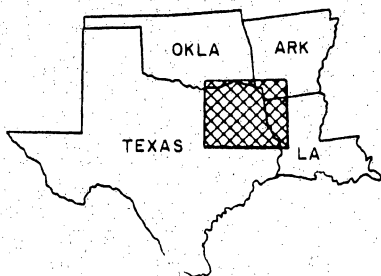
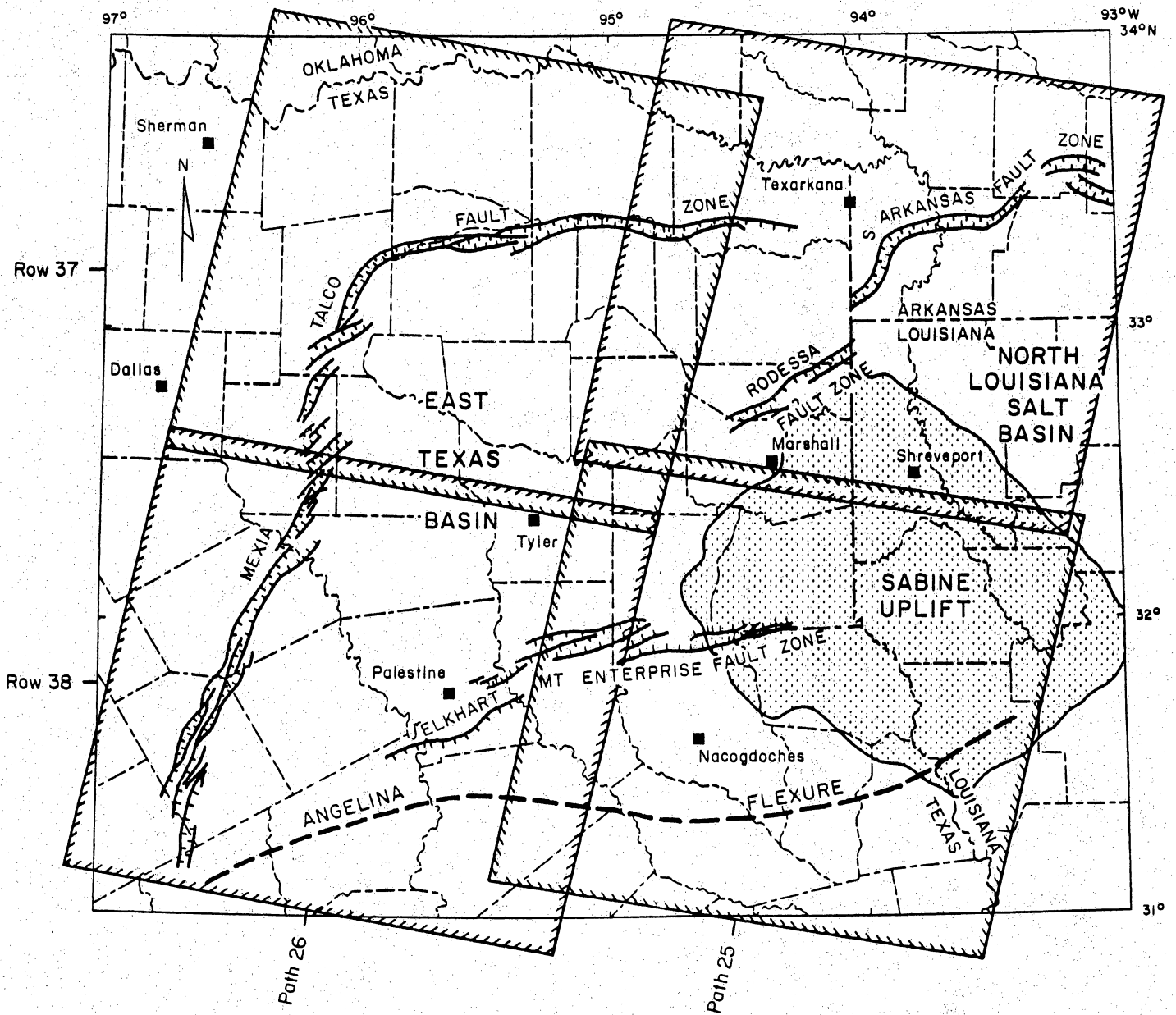
Purpose and Scope

This remote sensing study is part of a comprehensive investigation of the Lower Cretaceous Travis Peak Formation in East Texas and northwest Louisiana. The purpose of this study is to identify and describe lineaments and, if possible, assess their relationships with geologic structures. Lineaments may be spatially correlated with fractures in the subsurface, or they may reflect the regional stress regime. If a correspondence between lineaments and subsurface stress or structure can be demonstrated, then the spatial distribution and orientation of these surface features can be used to assist selection of drilling sites for hydraulic fracturing of low-permeability formations.

First use of the word "lineament" has been attributed to Hobbs (1904) by El-Etr (1976) in a review of the terminology applied to linear features on the Earth's surface. The definition formulated by Woodruff and Caran (1984, p. 8) describes the lineaments mapped in this study: "a pattern of tones, textures, contours and other such features that is straight, linear and more or less continuous, has definable end points and lateral boundaries (high length/width ratio), and hence a discernible azimuth." Features that fit this definition but proved to be man-made were excluded from this analysis.

Four Landsat Thematic Mapper images compose the data base for this study (fig. 1, table 1). All are standard, black and white, 1:250,000-scale prints obtained from EROS Data Center prior to September 1985. These four images provide almost complete coverage of the study area from 93 degrees west to 97 degrees west between 31 degrees north and 34 degrees north (fig. 1). The principal tectonic features in the area are the East Texas Basin, the Sabine Uplift, and the North Louisiana Salt Basin (fig. 1). The East Texas Basin is bounded by the Mexia-Talco Fault Zone on the north and west, by the Sabine Uplift on the east, and by the Angelina Flexure on the south. The boundary of the irregular Sabine Uplift has been defined differently by various authors (Murray, 1948; Andersen, 1960; Granata, 1963; Carlson, 1984). For the sake of uniformity in figure 1, the outcrop contact between the Eocene Wilcox Group and overlying Carrizo Sand (in Texas) or Claiborne Group (in Louisiana) was selected to mark the edge of the uplift. The North Louisiana Salt Basin is delimited by the Sabine Uplift on the west. Its eastern boundary, the Monroe Arch, is outside the study area.

Most of the study area is underlain by rocks of Eocene age (figs. 2 and 3). Except for Quaternary sediments filling the major stream valleys, rocks exposed in the area are progressively younger toward the Gulf coast. Cretaceous rocks crop out north and west of the Mexia-Talco Fault Zone, outside the East Texas Basin.

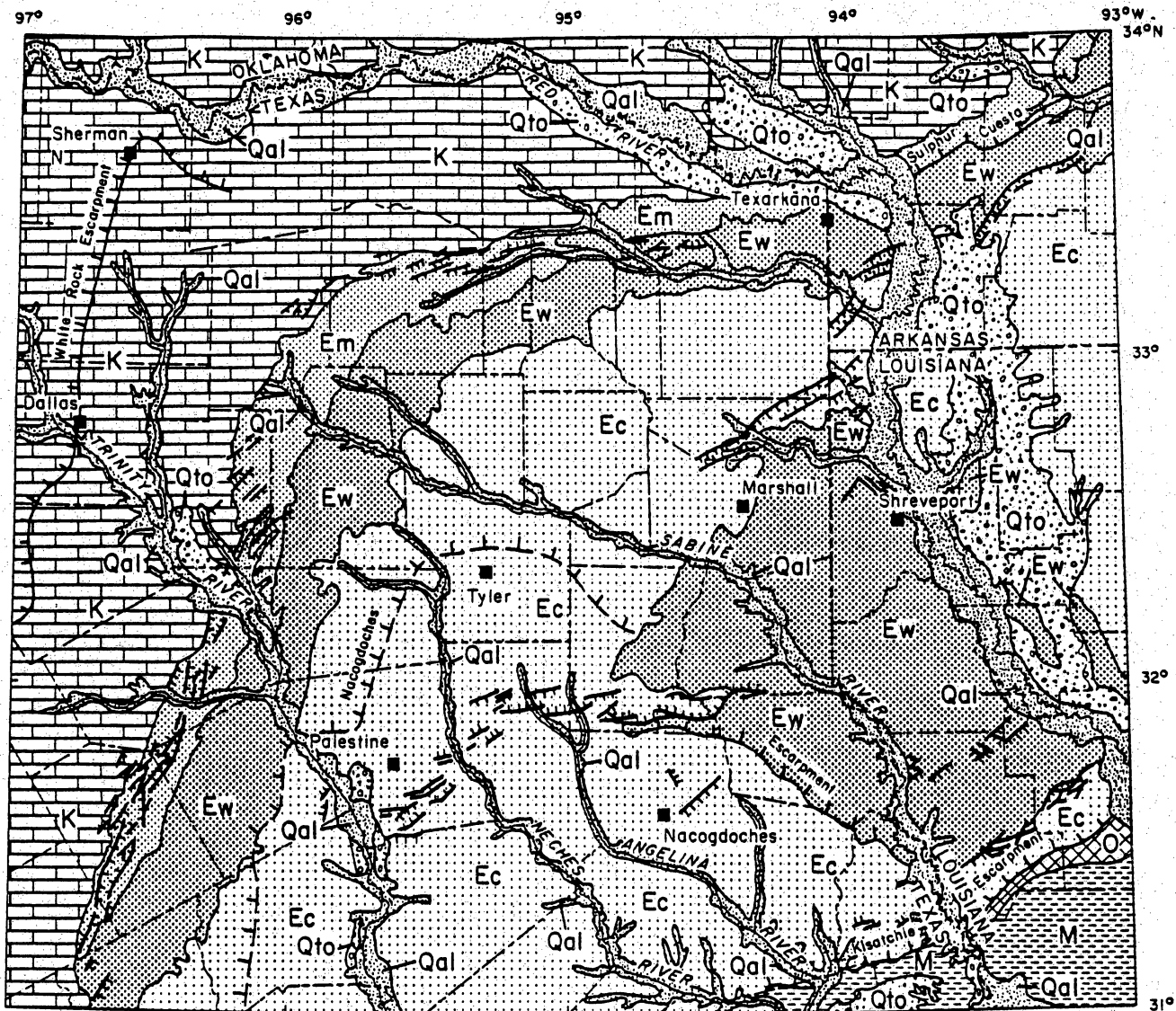


QA 6108

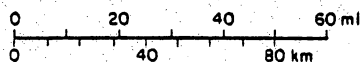
Figure 1. Location map of study area showing major tectonic elements and boundaries of Landsat images. Note area of sidalap between images in Paths 25 and 26. Fault zones in Texas are from Ewing (in preparation).

Table 1. Landsat Thematic Mapper images used in this study. All images were generated using Band 5 data (1.55-1.75 μm). For location of images see figure 1.

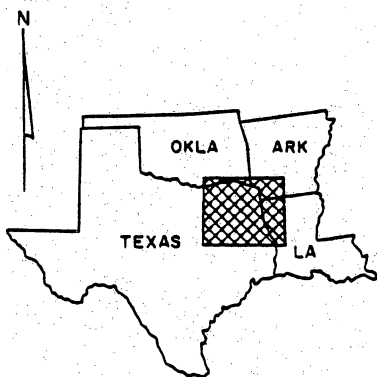
Path/row Landsat 4 or 5	Scene identification number	Date	Sun elevation (degrees)	Sun azimuth (degrees)	Mapping time (hr)	Rate of error (%)
25/37	50249-16194	Nov. 5, 1984	35	150	7.25	5.5
25/38	50265-16200	Nov. 21, 1984	32	150	6.5	5.0
26/37	40202-16250	Feb. 3, 1983	31	142	8.25	1.6
26/38	40202-16252	Feb. 3, 1983	32	141	7.75	3.8



After Fenneman (1938), Barnes (1967a, b, 1972, 1975, 1979a, b),
 Haley (1976), Louisiana Geological Survey (1984)



EXPLANATION



QUATERNARY	EOCENE/PALEOCENE
Qal Holocene alluvium	Em Midway Group
Qto Pleistocene terrace, other	CRETACEOUS
TERTIARY	K Cretaceous undivided
M Miocene undivided	Escarpment, dashed where broken or irregular
O Oligocene undivided	Fault
EOCENE	
Ec Claiborne Group and younger Eocene	
Ew Wilcox Group	

QA 6117

Figure 2. Generalized geologic map of study area. Most rocks exposed at the surface are of Eocene age. Except for Quaternary sediments in stream valleys, rocks decrease in age toward the Gulf Coast (southeast).

ERA	SYSTEM	SERIES	GROUP	FORMATION OR MEMBER	AGE (Ma)						
CENOZOIC	TERTIARY	EOCENE	CLAIBORNE	COOK MOUNTAIN	48						
				SPARTA							
				WICHES							
				QUEEN CITY							
				REKLAW							
		CARRIZO									
		PALEOCENE	WILCOX	UNDIFFERENTIATED	56						
				MIDWAY		UNDIFFERENTIATED					
						MESOZOIC	CRETACEOUS	UPPER CRETACEOUS	NAVARRO	UPPER NAVARRO CLAY	66
										UPPER NAVARRO MARL	
	NACATOC SAND										
	LOWER NAVARRO										
	TAYLOR	UPPER	73								
		PECAN GAP CHALK									
	LOWER	WOLF CITY SAND									
	AUSTIN	GOBER CHALK	86								
		AUSTIN CHALK									
	ECTOR CHALK										
	LOWER CRETACEOUS	EAGLE FORD	EAGLE FORD	92							
			WOODBINE		LEWISVILLE						
DEXTER											
MANESS SHALE											
BUDA LIMESTONE											
GRAYSON SHALE											
WASHITA	GEORGETOWN	103.5									
	MAIN STREET LIMESTONE										
	WENO-PAWPAW LIMESTONE										
	DENTON SHALE										
	FORT WORTH LIMESTONE										
	DUCK CREEK SHALE										
	DUCK CREEK LIMESTONE										

ERA	SYSTEM	SERIES	GROUP	FORMATION OR MEMBER	AGE (Ma)		
MESOZOIC	CRETACEOUS	LOWER CRETACEOUS	FREDERICKSBURG	KIAMICHI SHALE	103.5		
			GOODLAND LIMESTONE				
			JURASSIC	UPPER JURASSIC	TRINITY	PALUXY/WALNUT	105
						UPPER GLEN ROSE	
						MASSIVE ANHYDRITE	
						RODESSA LIMESTONE	
						JAMES LIMESTONE	
						PINE ISLAND SHALE	
						PETTET LIMESTONE	
						TRAVIS PEAK	112
	SCHULER						
	BOSSIER	135					
	GILMER						
	BUCKNER	138					
	SMACKOVER						
	NORPHLET	140					
	LOUANN SALT						
	WERNER	143					
	156						

After Seni and Jackson (1984, fig. 3)

QA 6127

Figure 3. Stratigraphic column of geologic formations mentioned in report.

Physiography and Land Cover

Physiography in the study area is the product of fluvial erosion of mostly weakly indurated sediments. Generally, topography is flat to slightly rolling, reflecting the gentle regional structural dip toward the Gulf Coast and the relatively high erodibility of most exposed rocks. The pattern of outcrop belts gives rise to inland-facing, generally northeast-southwest-trending, cuestas (Fenneman, 1938; Stenzel, 1938; Murray, 1961). Major cuestas are, from northwest to southeast, White Rock Escarpment, Sulphur Cuesta in southwestern Arkansas, Nacogdoches Escarpment, and Kisatchie Escarpment (fig. 2). Each cuesta is developed on resistant strata with scarp faces up to 30 m (100 ft) high (Fenneman, 1938). All but the Nacogdoches Escarpment are narrow, continuous scarps in the study area. The Nacogdoches scarp has been eroded into a series of hills capped, locally, by iron-oxide cemented marl and greensand (Fenneman, 1938). Its general position is shown in figure 2 by a line that was drawn on 1:250,000-scale topographic maps through groups of topographic highs above 152 m (500 ft) elevation. Locally, drainage is controlled by these resistant strata, and obsequent streams flow parallel to the outcrop belts along more erodible beds. Except in the vicinity of scarps, topographic relief throughout the study area is low. Major river valleys and their interfluves slope to the east, southeast, and south at 0.2 to 1.1 m/km (1 to 6 ft/mi). Tributary streams have slopes up to 3 m/km (16 ft/mi). Maximum topographic slope values, measured on 1:250,000-scale U. S. Geological Survey topographic maps, reach 34 m/km (180 ft/mi), but they cover less than one percent of the study area.

The study area in Texas covers parts of three north-south-trending physiographic-vegetative provinces. From east to west these are the Pineywoods, Post Oak Savannah, and Blackland Prairies (Orton, 1964; McMahan and others, 1984). Native vegetation of the Pineywoods, as its name implies, is mostly pine (Pinus spp.). The Post Oak Savannah contains mostly blackjack oak (Quercus marilandica). The Pineywoods and Post Oak Savannah extend into northern Louisiana and southern Arkansas. They are referred to collectively as the Ouachita-Red River Rolling Lands by Murray (1961, his Landform Map). Native vegetation on the Blackland Prairies, in the westernmost part of the study area, is various grasses, except along watercourses, where hardwood trees are found.

All of these vegetation types have been altered by man. Roads, towns, reservoirs, agricultural fields, and new-growth areas in forests are some of the most common signs of human activity that are visible on Landsat imagery. Areas of grassland have been introduced in the Pineywoods and Post Oak Savannah. The Blackland Prairies are almost entirely cultivated (McMahan and others, 1984).

Previous Work

Lineaments have been recognized as the surficial expression of geologic structure in many published studies (Frost, 1977; Caran and others, 1981; Williams, 1983; Bailey and others, 1984; Woodruff and Caran, 1984). For areas where sedimentary cover and vegetation are relatively thin or absent, such results are readily achieved. But even where unconsolidated sediments and vegetation obscure bedrock, lineament studies have revealed geologic structures such as uplifted basement blocks (Thomas, 1974) and domal structures (Berger, 1982).

Successful detection of buried or obscured structures via analysis of lineaments in the study area presents several challenges. Structures formed by salt movement (domes, pillows, and turtle structures) and basement structures are covered by sediments ranging from less than 100 m (330 ft) to more than 6,000 m (20,000 ft) thick (Jackson and Seni, 1984). Natural vegetation patterns of evergreen and deciduous forests and prairies have been much altered by land-use practices such as cultivation for agricultural crops and clear-cutting in woodlands. Furthermore, man-made linear features of the landscape, such as roads, power lines, and dams, hamper detection of natural lineaments.

Previous studies of lineaments in East Texas reported (1) parallelism between the trends of lineaments and structural features (Dix and Jackson, 1981), (2) correlation between lineaments and faults (Caran and others, 1981), and (3) correlation between lineament intersection and a producing oil field (Berger, 1982). Other workers have discussed the application of lineament studies to mineral exploration (Norman, 1976; Halbouty, 1980). Thus, precedent has been set for this study's approach to lineament analysis based on Landsat data.

METHODS AND MATERIALS

Imagery

All Landsat Thematic Mapper (TM) images used for this study were generated with data from band 5. This band detects reflective infrared energy between wavelengths of 1.55 and 1.75 μm . It was used because within its range the reflectances of three basic land cover types are quite different (fig. 4), making them easier to see on the Landsat image. Furthermore, vegetation moisture differences can

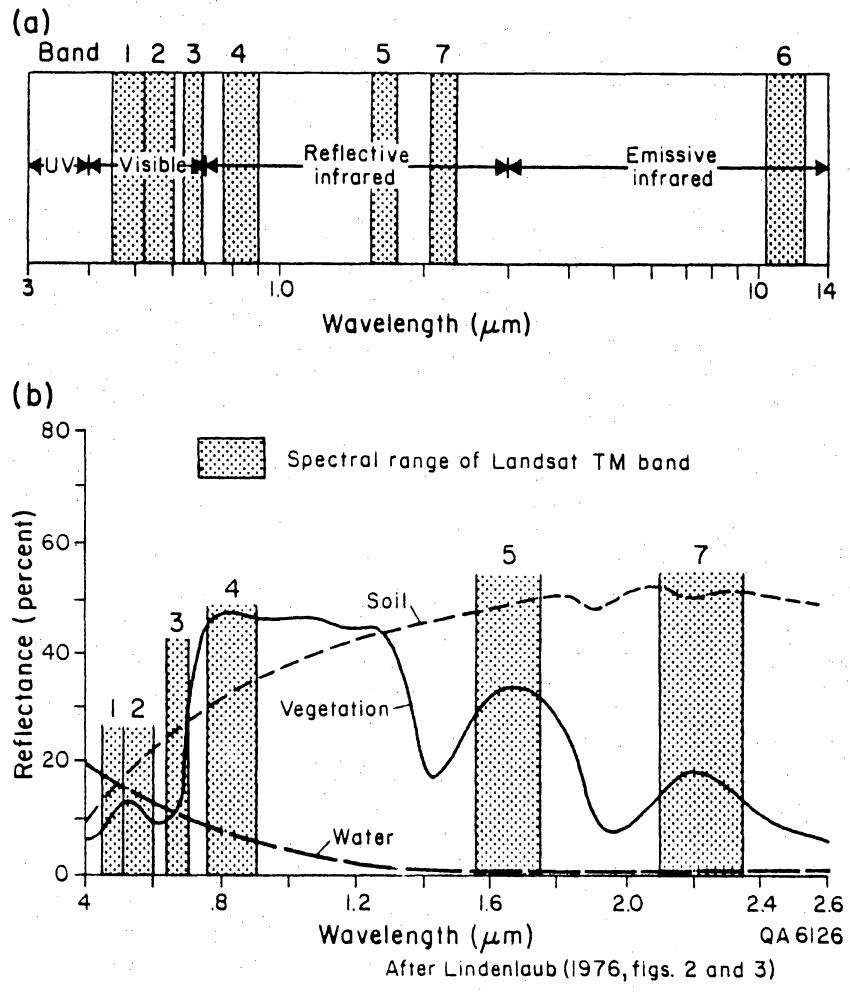


Figure 4. Spectral range of Landsat satellite sensors. Each band represents that part of the electromagnetic spectrum that each of the sensors detects. A. Distribution of Landsat bands in visible, reflective infrared, and emissive infrared wavelengths. B. Reflectance of three basic land cover types in the visible and reflective infrared wavelengths. Percent reflectance is a measure of relative brightness on a Landsat image. In band 5 bare soil is the most reflective cover type. Water appears black. Vegetation displays an intermediate brightness.

be detected in this band, and these may reveal subtle differences in plant cover that are related to soil types. Different soil types can result from different parent materials or other geologic and geomorphic factors. Recent work by Drury (1986) has shown that band 5 is especially useful for detection of geologic structure in agricultural terrain, which covers much of the study area.

The resolution of the Thematic Mapper in band 5 is 30 m (100 ft). Under most conditions, an object on the ground must be 30 m wide to be detected by the satellite sensor. An exception to this general rule occurs when an object less than 30 m wide having very high reflectance, such as a dry, gravel-topped road, occurs in low reflectance surroundings, such as a wet, grass-covered field. Because of the large difference in reflectance, the sensor will detect the narrow road. However, natural land surface features seldom display such contrast.

Images acquired during late fall and winter (table 1) were used for two reasons: (1) low sun angle was needed to enhance low topographic relief of the study area, and (2) because parts of the study area are covered by woods and cultivated fields. Leaf canopy is absent or thinner in the winter than in other seasons (except in areas of evergreen forest), which allows the satellite sensor to detect the spectral signature of the ground rather than the vegetation (Uttamo, 1979).

The sun's azimuth for all scenes is between 141 and 150 degrees (table 1). As a result, in this area of relatively low relief and surface dissection, linear features perpendicular to the sun's azimuth (51 to 60 degrees) may be preferentially illuminated or shaded, similar to the effect of look direction on features detected by side-looking radar (Yamaguchi, 1985). However, in only one part of the study area does the interval between 51 and 60 degrees azimuth have a length-weighted frequency that is significantly higher than the mean value (discussed in a later section). Thus, any

excessive enhancement by solar shading or highlighting of features with azimuths of 51 to 60 degrees is minimal.

Procedures

Lineaments were mapped in four steps. First, the Landsat image was placed on a light table and viewed with transmitted light in a darkened room. A transparent sheet of mylar was placed over the image and the end points of each lineament were marked. Second, after thorough visual inspection was completed, a second sheet of transparent mylar was placed over the first, and the end points were connected by a line drawn on the second sheet. In this way the image was not obscured during the initial visual inspection by a growing network of lines. Third, the mapped lineaments were checked against larger-scale photomosaics (1:63,360-scale) and, when available, aerial photographs (1:20,000- and 1:40,000-scale). Lineaments were transferred from the second mylar overlay to the photomosaics using a proportional projector to enlarge the lineament overlay to the scale of the photomosaics. Lineaments corresponding to man-made features such as fences, straightened river channels, levees, power line rights-of-way, and the like, were erased from the overlay. Rates of error varied from image to image (table 1), but for all four Landsat images, the number of man-made features erroneously mapped amounted to 3.8 percent of the lineaments checked. Lineaments that were neither man-made, nor clearly associated with some natural feature, such as a straight stream valley, were not erased. These were usually mapped on straight tonal boundaries that were visible on the Landsat images but were not apparent on the larger-scale photographs. In the fourth step, those lineaments confirmed as natural features were transferred from the second mylar

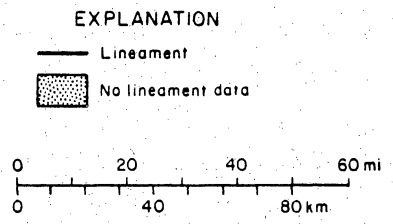
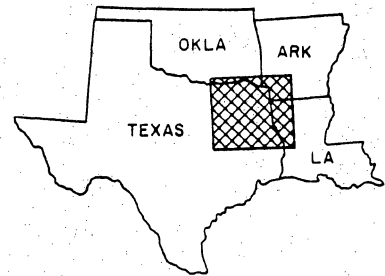
overlay to U.S. Geological Survey topographic maps at the same scale (1:250,000). In areas where images overlapped (between Rows 37 and 38) or sidelapped (between Paths 25 and 26) (fig. 1) lineaments from only one image were transferred to the topographic maps to avoid creating false high lineament density along image boundaries. At this point, lineaments were compared with maps of surface geology to determine whether spatial correspondence existed between lineaments and mapped geologic features, such as faults and formation contacts. Finally, from the maps the lineaments were digitized for computer-assisted analysis.

To ensure that each image was given equally rigorous inspection, records were kept of time spent per image, and statistical tests were used on lineaments in the sidelap area between adjacent images. Each scene was examined for 6.5 to 8.25 hours (table 1). This time included using a mask to view 1/9 of an image at a time. The mask was placed over the image and each 1/9 of the image was studied for 10 minutes. During this procedure all parts of the image received equal attention. Differences in time spent on each image were caused by differences in contrast on each image, but this did not significantly affect mapping of the lineaments, as shown by comparison of lineament data from sidelap areas between Paths 25 and 26 (fig. 1). Larger-than-average azimuth peaks from different images in the sidelap area coincide. Mean lengths of lineaments in the sidelap area in Path 25 are not significantly different (at $p=.05$ level) from the mean lengths in Path 26. These results indicate that the difference in quality of different Landsat images causes no significant change in the perceived length of lineaments, nor does it affect the azimuth of larger-than-average peaks. Furthermore, this procedure proved that the investigator found the same larger-than-average peak azimuth for the same area on different images at different times. Thus mapping error was determined to be insignificant.

Initially, lineaments transferred to the 1:250,000-scale topographic maps were digitized in one-degree-latitude by one-degree-longitude zones. Then, azimuth data for all lineaments in the study area were compiled to define regional lineament orientation. Finally, the data were examined for each one-degree square zone and for subregional structural features such as the East Texas Basin and the Sabine Uplift. In each case lineaments were analyzed for length-weighted frequency (F) and Bernshtein accuracy criterion (H) as described by Dix and Jackson (1981). These measurements of azimuth are discussed more fully in the Results section of this report.

Definition of Observed Lineaments

Of the 2,250 lineaments in the study (fig. 5) 1,860 (83 percent) were checked against photomosaics. Of these, 236 were compared with larger-scale (1:20,000- or 1:40,000-scale) aerial photographs and described as shown in table 2 and figure 6. More than 90 percent of the described lineaments are stream network features. Because the visibility of streams is not affected by land cover or land use, it is unlikely that differences in these factors affected the detection of most lineaments. Topographic features, such as scarps, account for only 2 percent of all described lineaments. This is not surprising, given the low local relief in the study area. Although large-scale photographic coverage of the study area is incomplete, no evidence suggests that the percentage of each lineament type in table 2 would change if more photographs were available. It is reasonable to expect that these 236 lineaments are representative of the other 2,014 in the study.



QA 6124

Figure 5. Map of all Landsat lineaments mapped in the study area.

Table 2. Descriptions of lineaments checked against large-scale aerial photographs. See figure 6 for examples.

Description	Number	Percent
Meandering/sinuuous stream with overall straight plan view	79	34
Straight valley with straight or meandering stream	62	26
Meandering/sinuuous valley with overall straight plan view	29	12
Straight reach of river channel	25	11
Straight stream	17	7
Straight edge of lake	8	3
Straight scarp/topographic feature	5	2
Streams aligned across valley or drainage divide	5	2
Other (tonal anomaly, unidentified)	6	3
TOTAL	236	100

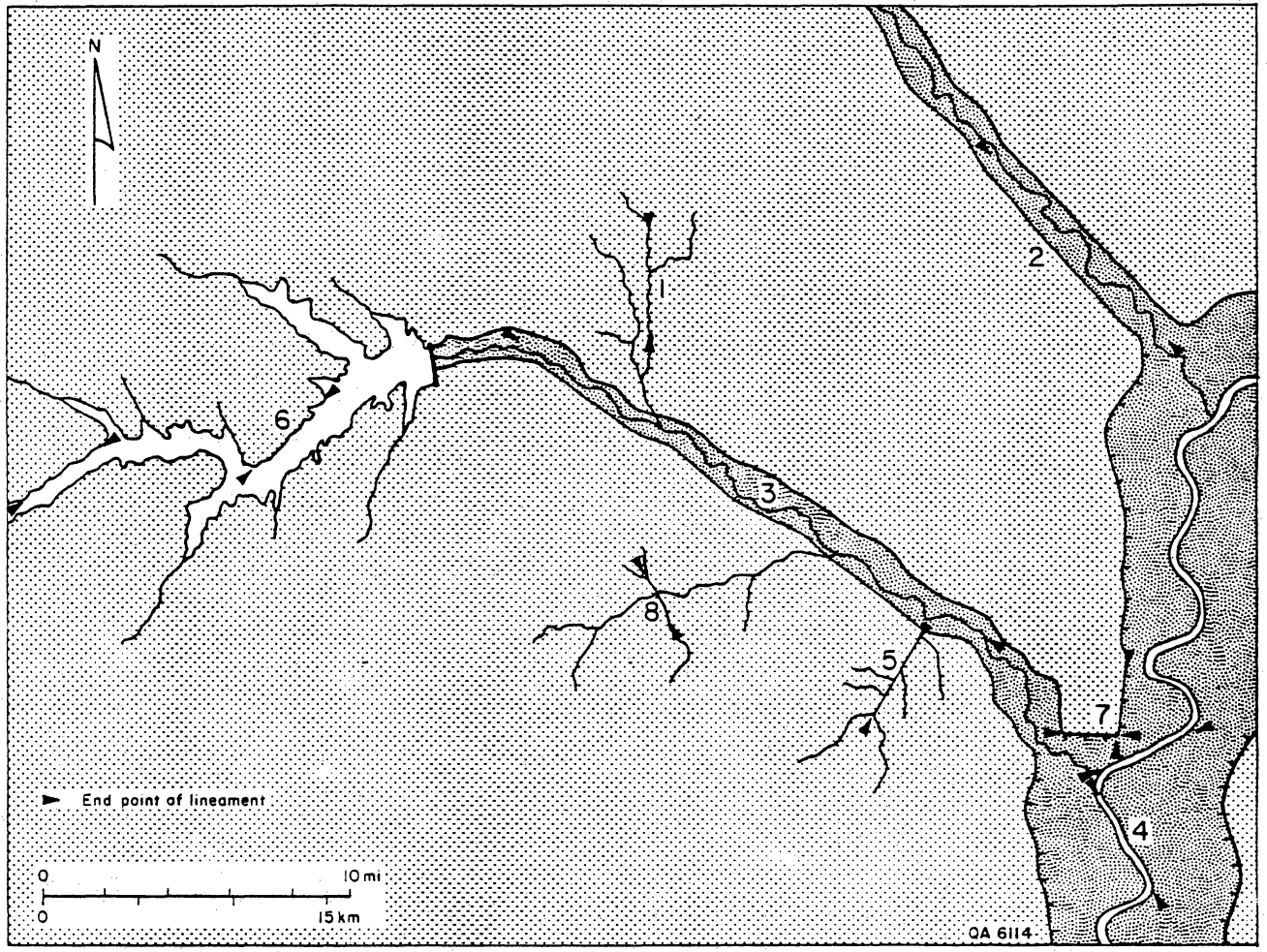


Figure 6. Examples of lineament types described from large-scale photographs. See table 2 for description of each type.

RESULTS

Correspondence Between Lineaments and Geologic Features

Detection of features on the Earth's surface by the Thematic Mapper is constrained by the resolution of its sensor. Under most conditions of natural land cover an object must be at least 30 m (100 ft) wide to be detected by the sensor. Most lineaments in this study are stream network features because they are the most common physiographic features in the area large enough to be detected by the sensor. In addition, the difference in reflectance between vegetation-covered banks and water or between cultivated uplands and bottomland vegetation (fig. 4) renders streams and their valleys especially noticeable.

Few lineaments display a one-to-one correspondence with mapped faults or geologic contacts. Whether the straight streams mapped as lineaments are flowing along unmapped faults or fractures is not known. Less than 0.5 percent of all lineaments in the study directly overlie faults mapped at scales of 1:250,000 and 1:500,000 (Barnes, 1967a, 1967b, 1972, 1975, 1979a, 1979b; Haley, 1976; Louisiana Geological Survey, 1984). This is due to their lack of spectral contrast in band 5 and the small part of the study area that faulted terrain comprises (fig. 2). Many faults in the study area are intraformational, so that rocks on either side of the fault have similar lithology, and support similar kinds of vegetation. Unless a discernible scarp develops along the fault or local hydrologic conditions lead to vegetation differences across the fault, it will not be visible on Landsat imagery in band 5. A slightly higher number of lineaments coincide with geologic contacts (0.9 percent). Some of these are cuestas that are large enough to be visible at the resolution of the satellite sensor (fig. 2). More than 2 percent of all lineaments are parallel to faults

and formation contacts but are laterally offset from them. Most of these are straight streams. Some are obsequent streams, flowing parallel to outcrop belts along the bases of cuestas where less resistant rocks crop out.

Length-Weighted Frequency of Lineament Azimuths

Lineament azimuth data were initially displayed as polar graphs of length-weighted frequency (F) (figs. 7A and 8). As described by Dix and Jackson (1981) this parameter expresses the total lineament length in a 10-degree sector of the graph, weighted in proportion to the number of lineaments in the area in question:

$$F = \frac{L_s \times n}{L_t} \quad (1)$$

where F = length-weighted frequency

L_s = total lineament length in 10-degree sector

L_t = total lineament length in area

n = number of lineaments in area

The area in question can be the entire study area, or any one of the 12 subregional zones (fig. 8), or a subset of those data over a structural feature.

Length-weighted frequency is used to combine lineament length and number of lineaments in a single parameter. The advantage in using this measure is that values from different areas can be compared while allowing for differences in number of lineaments in each area.

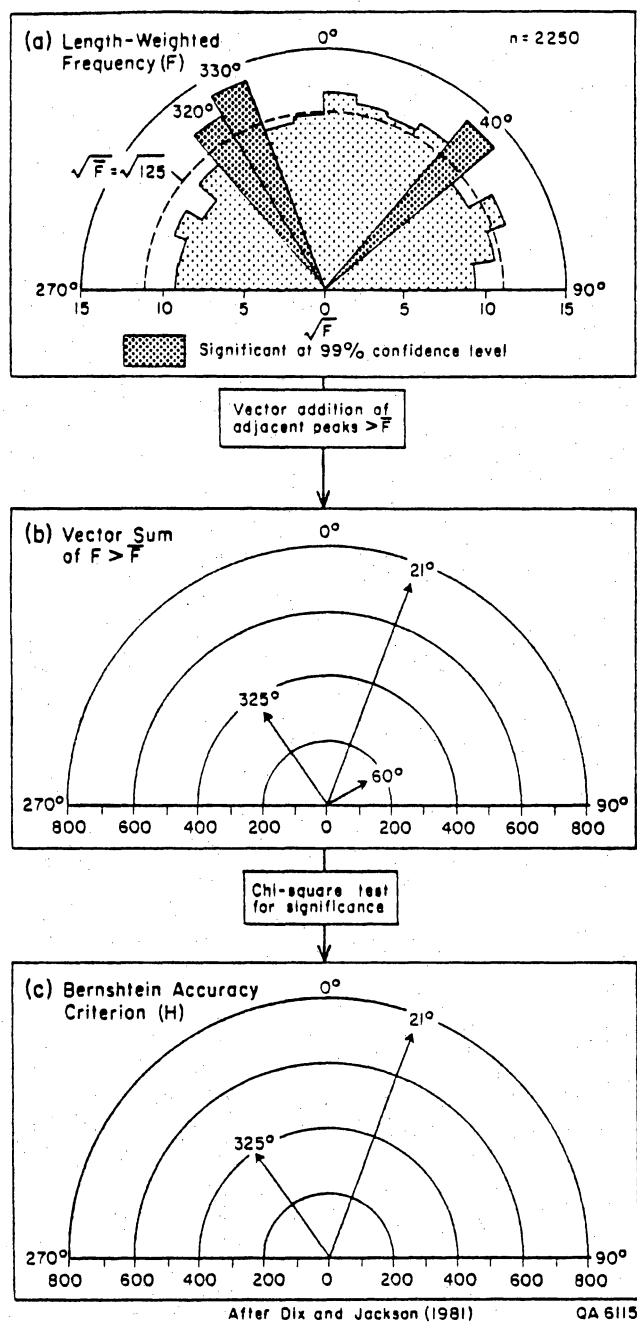


Figure 7. Procedure for statistical evaluation of lineament orientation data. Polar graphs of orientation data for all 2,250 lineaments in the study area. A. Length-weighted frequency (F) of lineaments has three peaks significant at the 99-percent confidence level. The square root of F is plotted to prevent areal exaggeration of large peaks. B. The vector sum of adjacent larger-than-average peaks of F also has three peaks, but orientations are different. C. Two peaks of Bernshtein accuracy criterion are significant at the 99-percent confidence level: 325° and 21°. These are referred to as the significant regional peaks.

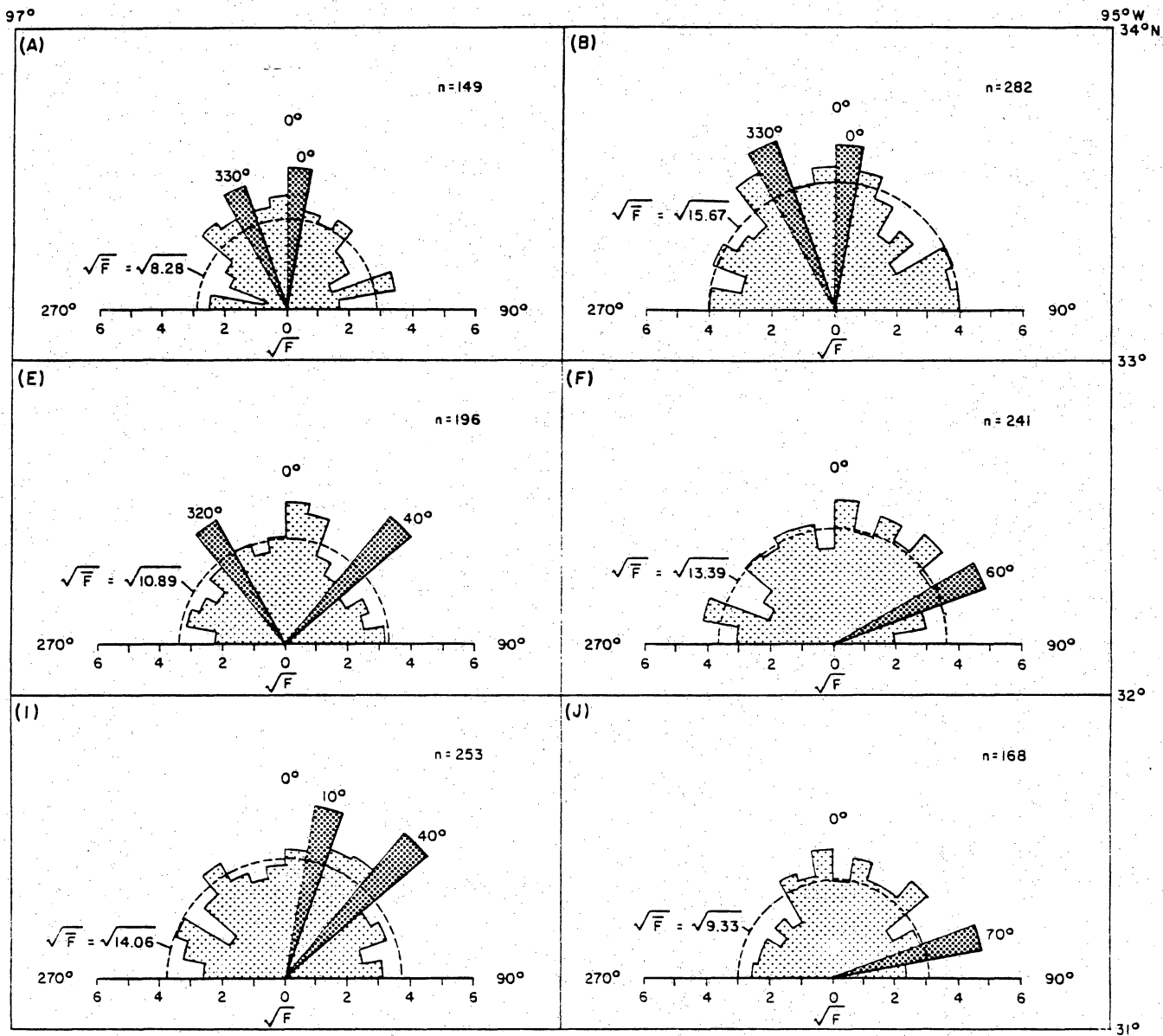
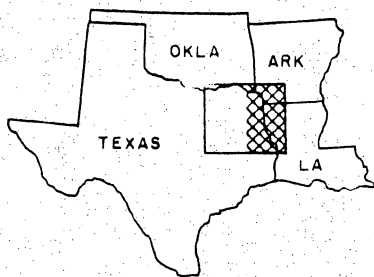
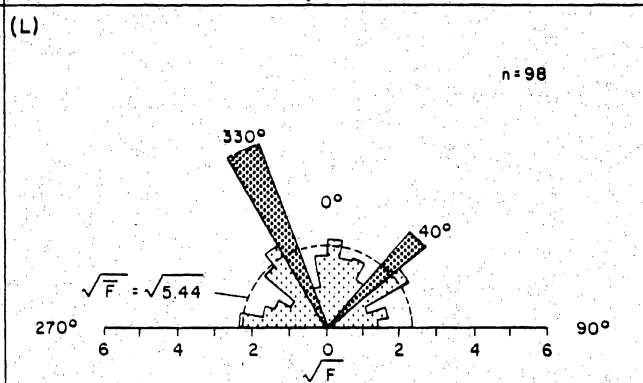
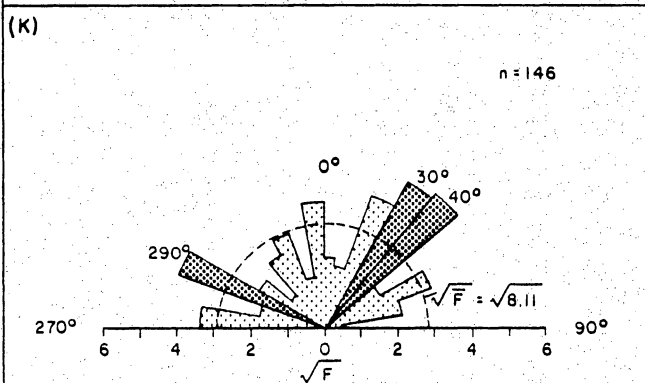
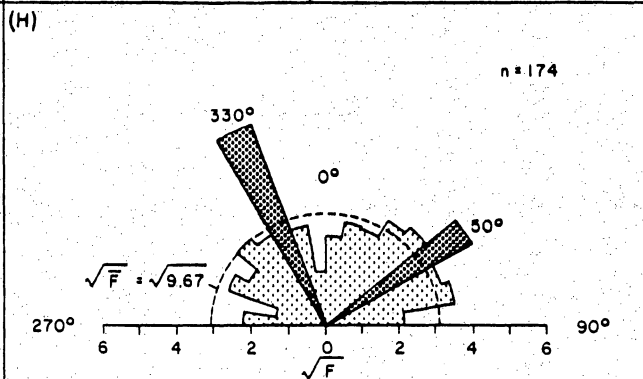
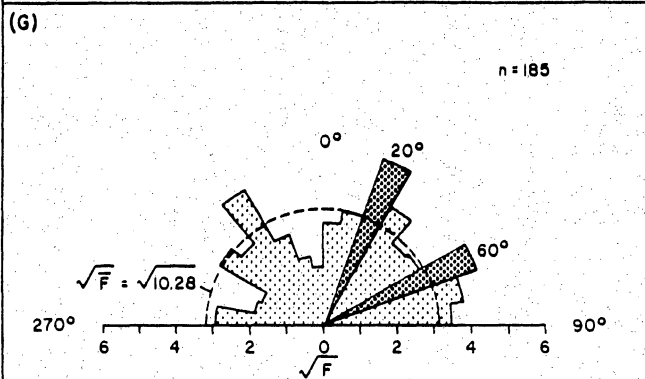
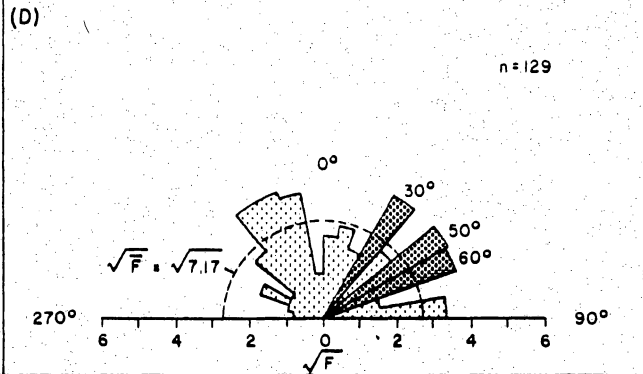
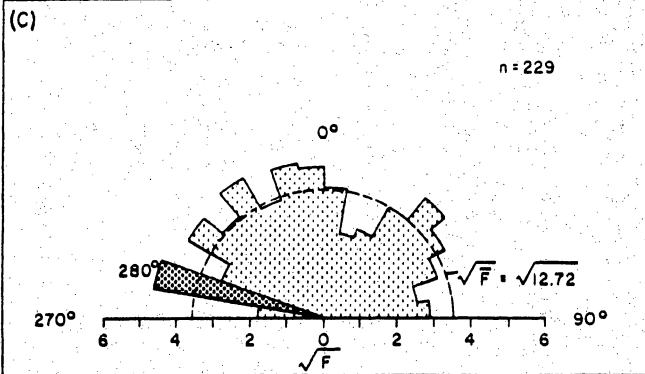


Figure 8. Polar graphs of length-weighted frequency for lineaments in 12 subregional zones. Zones are labelled in sequence from left to right in rows of four zones each. Number of lineaments shown by n.

QA 6110

95°

93°W
34°N



QA 6149

Graphical Display of Results

Selection of polar graphs

Polar graphs are used in this study to display directional data because of their familiarity and ease of interpretation (figs. 7A and 8). Because lineament data are symmetrical about the axis of a polar diagram, only the northern half, from 270 degrees through 360 degrees to 90 degrees, of these diagrams is used. However, polar plots have two disadvantages.

The first disadvantage is that the width of sectors used to divide the polar plot arbitrarily limits the number and magnitude of significant peaks. When grouped with a few high F values, several low F values can lower the cumulative value for a sector. Significant peaks may be obscured that would appear if narrower sectors were used.

This problem was evaluated using 5-degree and 10-degree wide sectors. Length-weighted frequency was computed for each sector and all peaks significant at the 99-percent confidence level were identified (table 3). Significant 5-degree sectors numbered 34, whereas there were only 23 significant 10-degree sectors. However, there is close correspondence between the two groups of significant sectors. Nineteen of the significant 10-degree sectors coincide with significant 5-degree sectors. Eighteen of these are the most significant 5-degree sectors (having the highest F values). Thus, because the 10-degree sectors include the most significant 5-degree sectors, and because 10-degree sectors are commonly used in the literature of lineament studies (Wise, 1969; Dix and Jackson, 1981; Finley and Gustavson, 1981), they are used here.

Table 3. Significant peaks for 5-degree and 10-degree sectors. The peaks for each zone are listed in order of descending F value. All are significant at 99-percent confidence level. Note that for zones A and L, one 10-degree peak corresponds to two 5-degree peaks. The 10-degree peaks correspond to 19 of the 23 most significant 5-degree peaks. Locations of zones are shown in figure 8.

Zone	Azimuths of significant 10° peaks			Azimuths of significant 5° peaks				Correspondence between 10° and 5° peaks
	1	2	3	1	2	3	4	
A	0	330	--	335	5	0	--	3 of 3
B	330	0	--	75	330	--	--	1 of 2
C	280	--	--	275	300	--	--	1 of 2
D	50	30	60	320	25	85	330	1 of 4
E	40	320	--	35	325	355	--	2 of 3
F	60	--	--	60	35	15	--	1 of 3
G	20	60	--	60	15	35	85	2 of 4
H	330	50	--	330	50	--	--	2 of 2
I	40	10	--	15	40	25	--	2 of 3
J	70	--	--	70	--	--	--	1 of 1
K	40	30	290	45	35	275	20	2 of 4
L	330	40	--	325	330	45	--	3 of 3
Subtotal	12	9	2	12	11	8	3	21 of 34
TOTAL		23			34			

The second disadvantage of polar graphs is that the area of a sector of the graph increases in proportion to the square of its radius. As a result, a relatively large sector will appear disproportionately larger than its smaller neighbors. For example, a sector with a value of 8 will appear, not twice as large as 4, but four times as large:

$$(8)^2/(4)^2 = 64/16 = 4 \quad (2)$$

To avoid this areal exaggeration of high F values, all data were plotted as the square root of F (figs. 7A and 8).

Significance level of peaks

The method and format of the following discussion of F values is adapted from Dix and Jackson's (1981) statistical treatment of lineament data. Results of the current study are explained fully, but the reader desiring more background on these techniques is referred to the cited publication.

Definition and Validity of Peak Values

In this study a peak on a polar graph of \sqrt{F} is defined as any 10-degree wide sector with a magnitude larger than the average for that graph. The "peakedness" of a graph is affected by the number of lineaments in the sample. Dix and Jackson (1981) devised a measure of peakedness called the index of preferred orientation (IPO).

$$\text{IPO} = \frac{\sum_{i=1}^{18} |L_r - 0.05| \times 100}{1.8} \quad (3)$$

where L_r = total lineament length in 10-degree sector
relative to total lineament length in data set

They observed that values of IPO for computer-generated, geologically meaningless, random "lineaments" decreased as sample size increased. The decrease in value was rapid from 50 to 200 lineaments, but changed more slowly as the number of lineaments increased above 200. As a result, they proposed that data sets should contain at least 200 lineaments to "minimize the effects of randomly oriented lineaments on geologically significant trends" (Dix and Jackson, 1981, p. 12). Although a similar, rapid decrease in IPO values occurred between 100 and 200 lineaments in the present study (fig. 9), a different conclusion is proposed.

Values of IPO are higher in this study than in Dix and Jackson's report for equivalent numbers of random model lineaments (fig. 9). This suggests that the peakedness of data in this study is not random, but results from directional control of lineaments, which produces IPO values as much as twice as high as those generated randomly. In addition, although IPO value decreases as sample size increases, this is not a steady decrease (between 100 and 370 lineaments) like that shown by the randomly generated "lineaments" of Dix and Jackson (1981) (fig. 9, table 4, this study). Apparently, in this study IPO declines as sample size increases not because random peaks resulting from randomly oriented lineaments are gradually obscured, but because larger-than-average peaks become "imbedded" in a matrix of lineaments with different azimuths. Some of these lineaments comprise the larger-than-average peaks, and cause IPO values to increase with increasing number of lineaments (as from 129

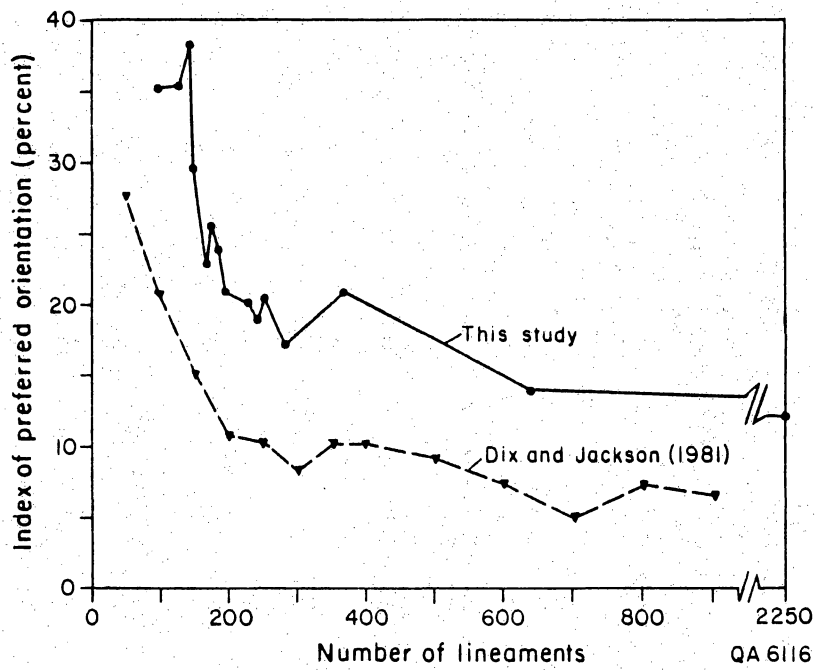


Figure 9. Graph of index of preferred orientation (IPO). Values of IPO are higher in this study than in Dix and Jackson's model study (1981) for equivalent numbers of lineaments. However, in both studies, values of IPO decrease rapidly as numbers of lineaments increase to 200, then decrease more slowly for more than 200 lineaments.

Table 4. Data for 12 zones and three areas in order of increasing number of lineaments. Index of preferred orientation (IPO) decreases discontinuously. No significant decrease in the number of significant 10-degree peaks accompanies the increase in number of lineaments. See figure 9 for graph of IPO values. For location of zones see figure 8. For location of Sabine Uplift and East Texas Basin see figure 13.

Number of lineaments (n)	IPO value	Number of significant 10-degree peaks at 99% level	Zone/Area
98	35.1	2	L
129	35.3	3	D
146	38.2	3	K
149	29.6	2	A
168	22.8	1	J
174	25.6	2	H
185	23.7	2	G
196	20.7	2	E
229	20.1	1	C
241	18.8	1	F
253	20.4	2	I
282	17.2	2	B
368	20.9	3	Sabine Uplift
639	13.9	1	E. Tx. Basin
2250	12.1	3	Entire area

to 146, 168 to 174, and 241 to 253 lineaments; fig. 9, table 4). Lineaments that do not comprise large peaks cause IPO value to decrease as number of lineaments increases.

To determine which greater-than-average peaks were significant a chi-square test was used to measure the difference between each peak and the mean F value for each data set (Siegel, 1956, p. 42-47). Dix and Jackson (1981) concluded that the 99-percent confidence level ($p=.01$ level) should be used to define geologically meaningful peaks because none of their samples with more than 100 computer-generated "lineaments" had significant peaks at that level. In this study each of the 12 one-degree-by-one-degree zones has one or more peaks significant at the 99-percent confidence level. In addition, the number of significant peaks does not decrease as the number of lineaments increases (fig. 8, table 4). For this reason, the 99-percent peaks from all 12 zones (and the three larger areas, table 4) are considered valid.

It should be noted that the random model set used by Dix and Jackson (1981) was enlarged by adding more randomly generated "lineaments" to those that had been previously generated. Thus, theirs was a "homogeneously random" data set (Martin P. A. Jackson, personal communication, 1986). By contrast, the increase in the number of lineaments shown in table 4 and figure 9 is a rank-ordering of 12 independent zones and 3 larger areas. Comparing these with Dix and Jackson's data is difficult because it is not known whether more or fewer significant peaks would form as a result of incrementally enlarging the data set in any single zone. However, by comparing data from Zone G, the Sabine Uplift, and the entire study area (table 4, fig. 9), Dix and Jackson's method of incremental enlargement is duplicated. Zone G is in the Sabine Uplift and both are part of the entire study area. For these three data sets the number of lineaments increases steadily while the number of significant peaks actually increases from 2 to 3 (table 4). This result supports the

conclusion that the number of significant peaks in this study does not decrease as the number of lineaments increases.

The azimuth and number of significant 10-degree-wide peaks vary from zone to zone (fig. 8). The most frequent significant peaks are at 40 degrees and 330 degrees, occurring four times each. Three peaks with azimuth of 60 degrees exist, and others occur less often. The 12 zones can be assembled into groups on the basis of azimuths of significant peaks. From Zone I in the southwest to Zone D in the northeast extends a group with only northeast-trending peaks. Zones A, B, and C have north- and northwest-trending peaks. The remaining zones have peaks in both northeast and northwest quadrants (E, H, K, L, fig. 8).

These groups do not correspond to any known geologic structures. Because of their size and arbitrary position, some of the zones cross boundaries between subregional structural features. The orientations of lineaments within the boundaries of these structures are examined in a later section.

Significant peaks may be composed of many short lineaments, or a few long ones, or a combination of both. To describe the composition of significant peaks a category of megalineaments was defined. A megalineament is a single lineament with an F value greater than the average 10-degree sector on a polar graph. Among the 12 zones there are 23 separate 10-degree-wide sectors with significant peaks (table 5). Eight of these peaks contain at least one megalineament.

Most megalineaments make the peak they occupy significant. However, in one zone (H), the other lineaments in the significant peak are long enough to make it significant without the megalineament (table 5). In two zones (L and E) the megalineaments are long enough to be significant by themselves. Thus, of the 23 significant peaks, 7 are significant because of the presence of megalineaments, but only 2 peaks would be significant solely on the basis of megalineaments.

Table 5. Megalineaments and significant peaks of length-weighted frequency (F) for 10-degree wide sectors from 12 zones in study area. Megalineaments, longer than the average sector length, compose more than 35 percent of 8 peaks. The length of megalineaments has no correlation with mean sector length. Location of zones shown in figure 8.

Mean sector length (F)	Number of significant peaks	Number of significant peaks with megalineaments	Length of peak sector with megalineaments (F)	Length of megalineament (F)	Difference between length of peak sector and megalineament (F)	Zone
5.44	2	1	28.75*	25.17*	3.58	L
7.17	3	0	-	-	-	D
8.11	3	1	21.20*	8.87	12.33	K
8.28	2	0	-	-	-	A
9.33	1	1	22.73*	11.57	11.16	J
9.67	2	1	34.17*	12.50	21.67*	H
10.28	2	1	23.29*	11.69	11.60	G
10.89	2	1	26.79*	20.29*	6.50	E
12.72	1	1	22.42*	14.16	8.26	C
13.39	1	0	-	-	-	F
14.06	2	1	35.17*	14.14	21.03	I
15.67	2	0	-	-	-	B

*significant at 99-percent confidence level

Megalineaments determine, or at least contribute to, less than a third of the significant peaks in the 12 zones. The other significant peaks are composed of lineaments that are shorter than the average 10-degree sector's length.

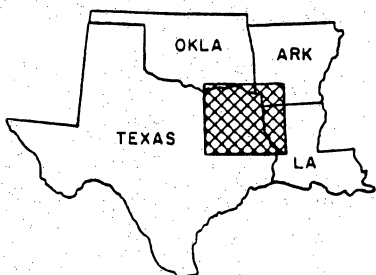
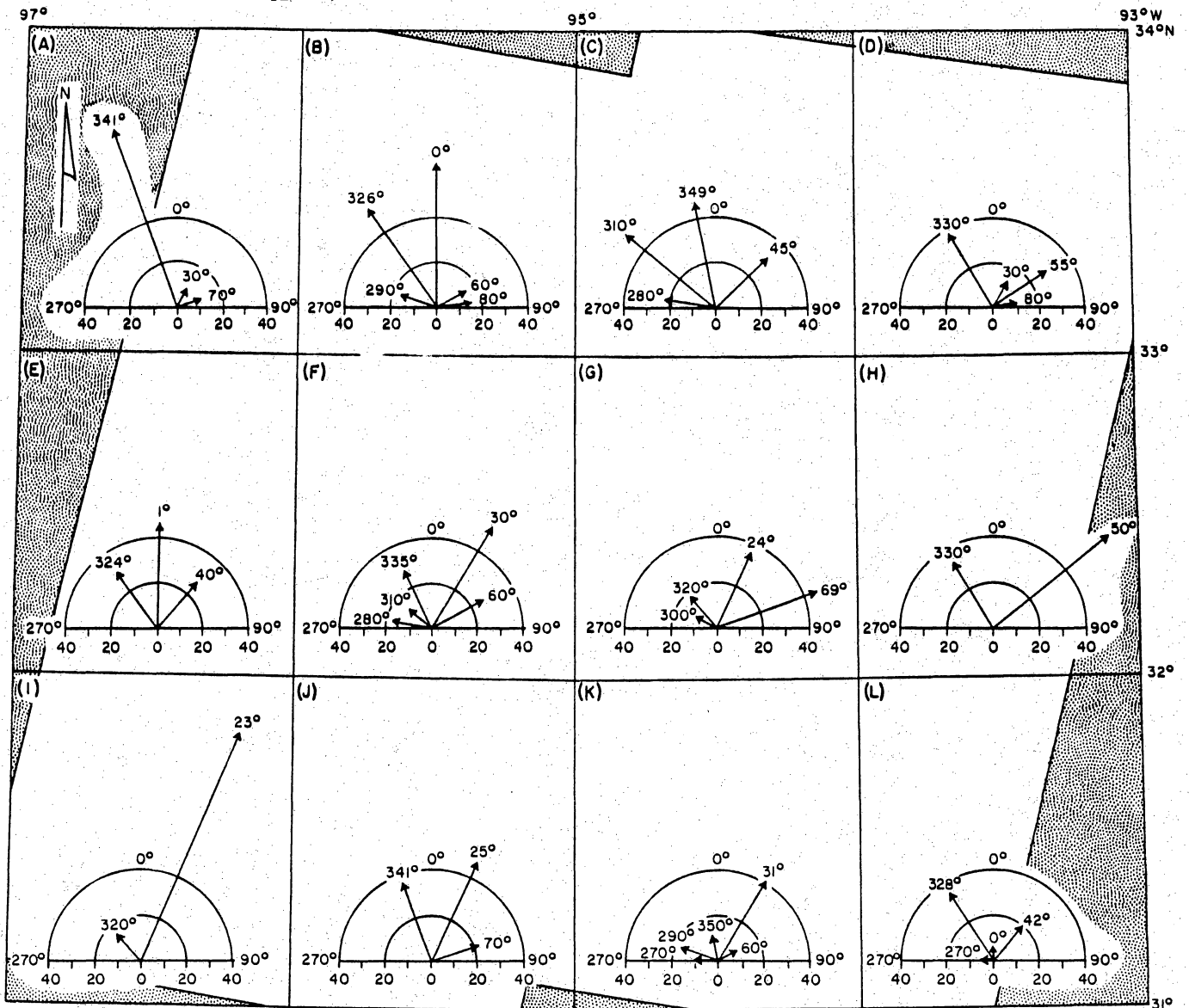
The length of megalineaments has no correlation with the mean sector length of a zone. Megalineaments are not simply functions of the mean sector length, which is determined by the number of lineaments in a zone. They can be more than four times longer than mean sector length (zone L, table 5).

Vector Sums of Greater-Than-Average Peaks

Although the significant azimuths of lineament orientation data can be determined using 10-degree-wide sectors, significant trends that are split between two adjacent sectors may be obscured. To avoid this potential loss of important data, vector sums of greater-than-average peaks are calculated (Dix and Jackson, 1981). A greater-than-average peak is any sector or group of adjacent sectors with a value of F greater than the mean.

The vector sum of greater-than-average peaks for all data combined and for the 12 subregional zones produces peak azimuths ranging from 270 to 80 degrees. For all data combined there are peaks at 325 degrees, 21 degrees, and 60 degrees azimuth (fig. 7B). In the subregional zones, similar orientations can be seen (fig. 10). Ten-degree wide sectors at 320, 30, and 60 degrees have the largest number of vector sum peaks. The 10-degree wide sector most frequently represented among the vector sums is 320 degrees, with five peaks between 320 and 329 degrees. Sectors at 30 and 60 degrees have four peaks each (fig. 10).

Not all vector sums of greater-than-average peaks are statistically significant, however. To determine which peaks are significant a chi-square test is applied to



 No data

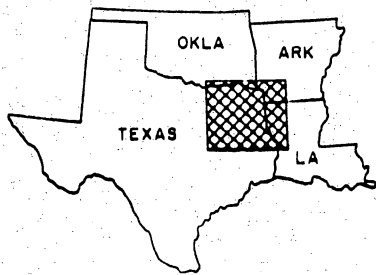
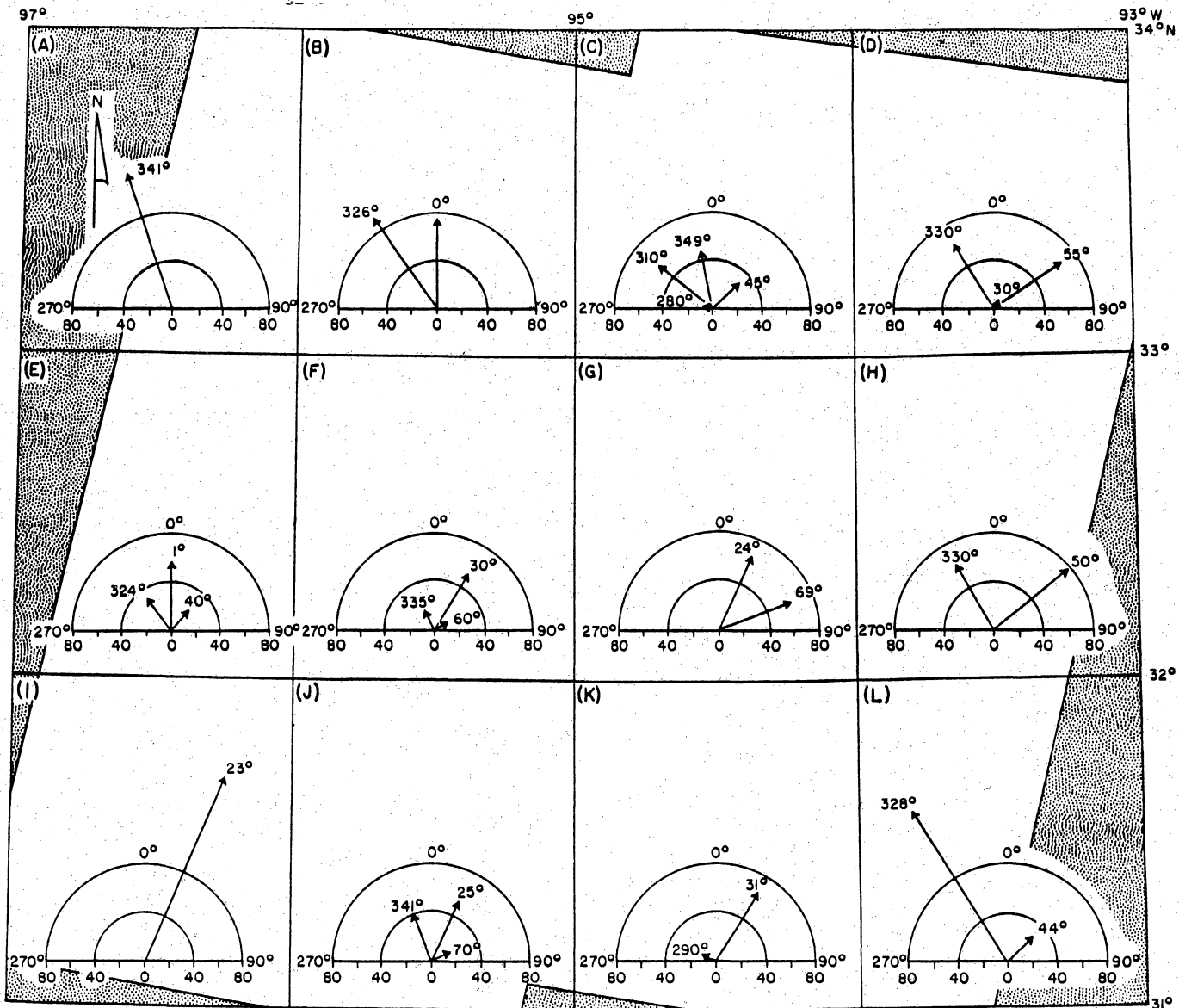
QA 6109

Figure 10. Polar graphs of vector sums of greater-than-average peaks of length-weighted frequency. Each graph represents a subregional zone (see fig. 8).

each vector sum peak (fig. 7C). For all data combined, 2 of the 3 peaks are significant at the 99-percent confidence level. In the subregional zones, 28 of the 44 peaks are significant at the 99-percent confidence level (fig. 10). As a further refinement, the chi-square value for each significant peak is divided by the degrees of freedom ($v=k-1$, where k equals the number of 10-degree sectors forming the peak) to yield the Bernshtein accuracy criterion (H) (Vistelius, 1966; Dix and Jackson, 1981). The values for the significant peaks are plotted using magnitude of the Bernshtein criterion and azimuth of the vector sum peak (figs. 7C and 11).

The distribution of Bernshtein values is mostly bimodal. For all data combined, peaks occur at 21 degrees and 325 degrees (fig. 7C). Hereafter, these are referred to as the significant regional northeast and northwest trends. Similar orientations are seen among the 12 subregional zones (fig. 11). Confidence intervals were calculated for each regional peak (Cheeney, 1983, p. 98-106) to quantify this similarity. In the subregional zones, 10 peaks occur in the 99-percent confidence interval around the regional northwest peak, between 307 and 343 degrees. Nine peaks occur in the 99-percent confidence interval around the regional northeast peak between 358 and 44 degrees (fig. 11).

These results provide the rationale for the next stage of this study. The geographic distribution of peak H values does not clearly delineate any subregional geologic structure, probably because the boundaries of the 12 subregional zones do not correspond with boundaries of subregional structures (fig. 1). However, the presence of groups of like-oriented adjacent subregional zones (fig. 11) suggests that subregions of similar lineament orientation may exist that coincide with geologic structure. The correspondence between geologic structure and lineament trends is examined by:



 No data

QA 6113

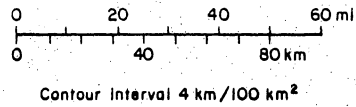
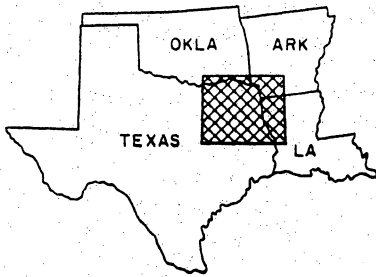
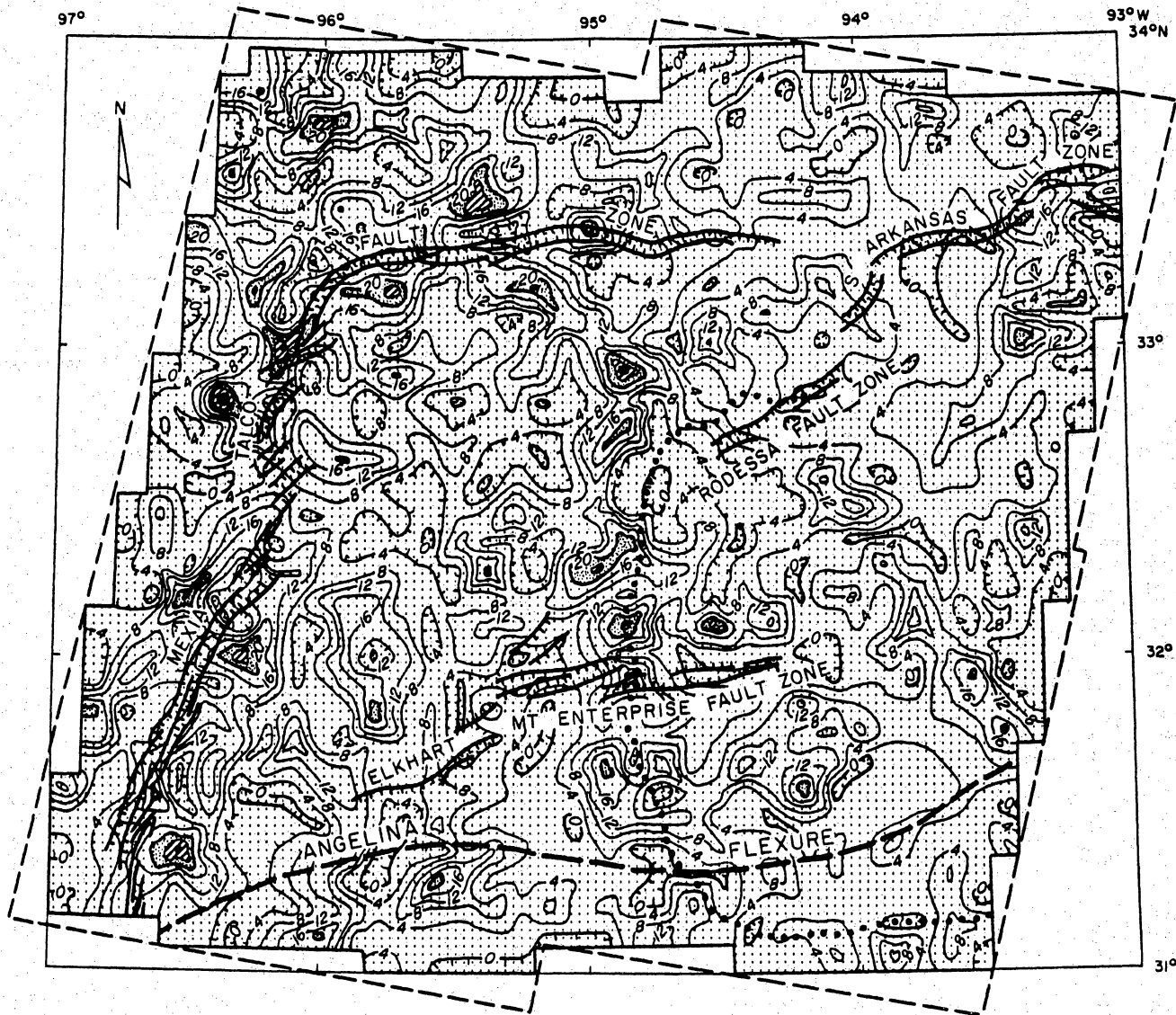
Figure 11. Polar graphs of Bernshtein accuracy criterion for 12 subregional zones (see figs. 8 and 10).

(1) mapping lineament density to determine whether density follows structural trends, and (2) analyzing lineament trends in areas that coincide with buried geologic structures.




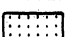


Lineament Density

Lineament density is calculated by measuring lineament length in 100-km² grid cells. The results, expressed as lineament length/100 km², are contoured as shown in figure 12. High values (≥ 20 km/100 km²) delineate the boundaries of the East Texas Basin. On the western and northern sides of the basin the high density values correspond spatially to the Mexia-Talco Fault Zone at the surface and to the updip limit of the Louann Salt in the subsurface. On the eastern side the high values overlie the updip limit of the Woodbine Formation in the subsurface, which marks the edge of the Sabine Uplift at depth. Along the northeastern edge of the basin a series of highs connects the Mexia-Talco Fault Zone with the subsurface limit of the Woodbine Formation. To the south, high values are offset from, but adjacent to, the Angelina Flexure. In addition, the high values on the southern, eastern, and northeastern sides of the basin are concentric to or overlie the outer limit of (Louann) salt pillows in the basin, mapped by Jackson (1982, his fig. 4). By connecting these density highs, a boundary can be drawn completely encircling the East Texas Basin.

The connection between the lineaments and structure is less obvious for the eastern and southern sides of the East Texas Basin than for the western and northern sides where faults are present at the surface. Movement of salt or of the Sabine Uplift may have enhanced lineament development without producing surface faults. To determine whether movement of the Sabine Uplift could account for the density highs along the Woodbine limit separating the uplift from the East Texas



EXPLANATION

-  $\geq 28 \text{ km}/100 \text{ km}^2$
-  $\geq 24 \text{ km}/100 \text{ km}^2$
-  $\geq 20 \text{ km}/100 \text{ km}^2$
-  $< 20 \text{ km}/100 \text{ km}^2$
-  Limit of Woodbine
-  Image boundary

QA 6112

Figure 12. Map of lineament density ($\text{km}/100 \text{ km}^2$). High values demarcate the Mexia-Talco Fault Zone, as well as other structural features. Limit of Woodbine from Ewing (in preparation).

Basin, the position of these high values was compared to the slope of the underlying uplift measured on Horizon B (Massive Anhydrite or Paluxy Formation [fig. 3]) of structure contour maps of the area by Geomap Co. (1981). No consistent relationship between slope on the uplift and position of these density highs was found.

High density values correlate well with some of the other geologic structures in the area. The South Arkansas and Mt. Enterprise Fault Zones have high values either directly overlying them or slightly offset to one side (fig. 12).

Other high density values on figure 12 are not clearly associated with geologic structures. Some include straight streams parallel to regional dip, formation contacts, or straight scarps, but about half exhibit no geologic control of the lineaments they contain. Because the mechanics of lineament formation are not completely understood, it is not surprising that all lineaments cannot be linked to some underlying feature. However, it is clear that the lineament density highs around the East Texas Basin coincide with geologic features, either in the subsurface (Woodbine limit or limit of salt pillows) or at the surface (Mexia-Talco Fault Zone).

Stream networks in areas of high lineament density were examined to determine if they are affected by lithologic boundaries or surface faulting. Most high values of lineament density along the Mexia-Talco Fault Zone include streams that are parallel to outcrop belts or faults (obsequent streams) or perpendicular to these features (consequent streams). Development of drainage along nonresistant beds and down the slope of tilted strata is common throughout this fault zone. Although there is almost no one-to-one correspondence between individual lineaments and mapped faults (as was discussed previously), linear streams parallel to faults and formation boundaries, evidently controlled by structure and lithology, have been mapped as lineaments. A

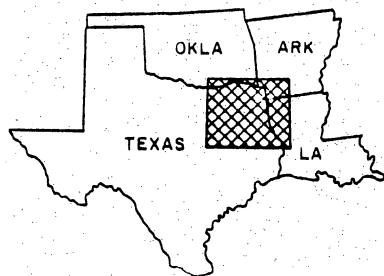
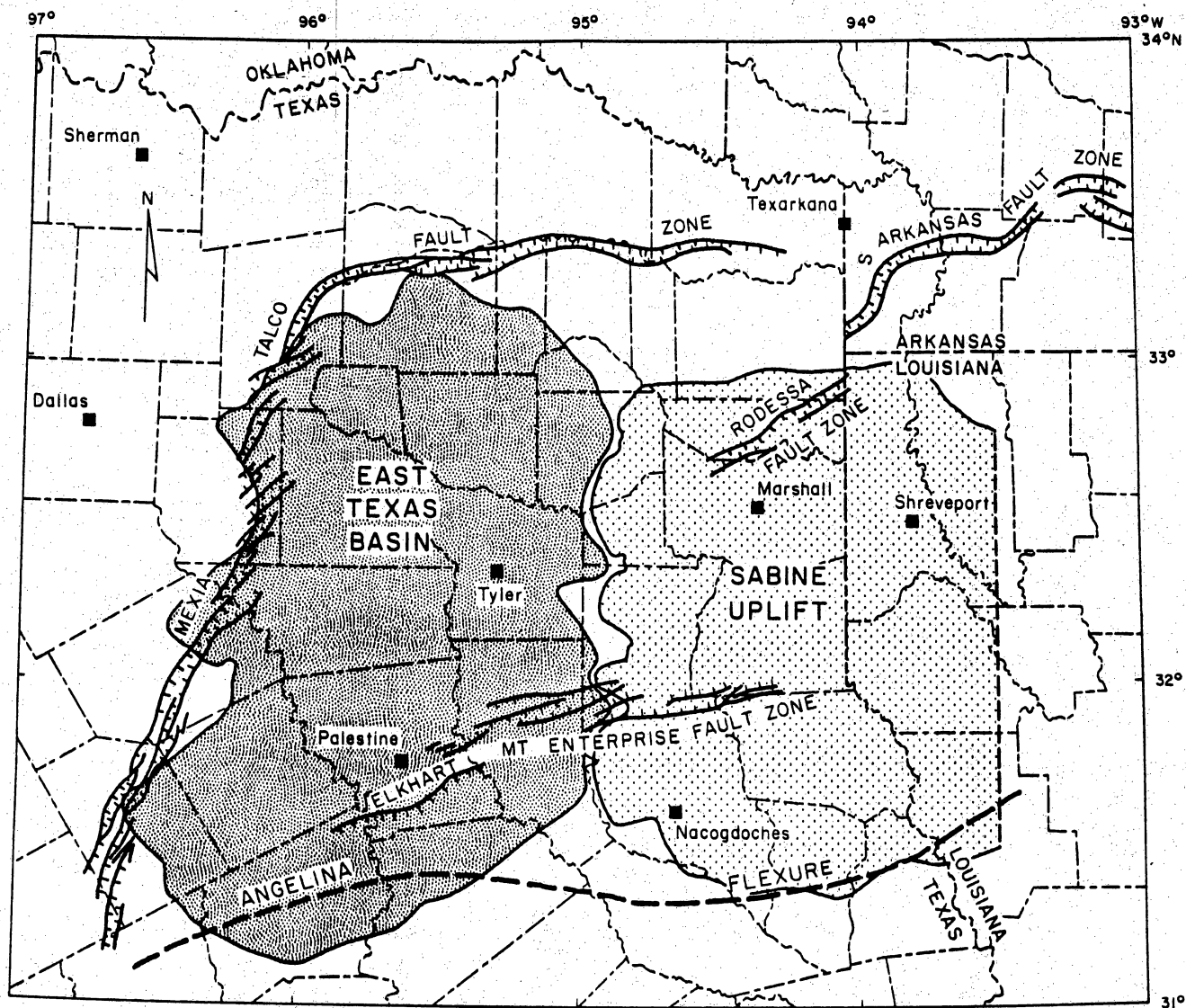
similar situation exists at the Angelina Flexure. Streams there have various orientations, but those parallel or perpendicular to outcrop belts appear to have developed on nonresistant outcrops or as a result of regional gulfward tilting, respectively.

On the other hand, in some high values of lineament density, there is no evidence of surface geologic control of drainage. At the South Arkansas and Mt. Enterprise Fault Zones and along the northeastern boundary of the East Texas Basin, streams mapped as lineaments have no obvious correlation with surface structure or formation contacts.

Subregional Lineament Orientation

Because high values of lineament density successfully outline the East Texas Basin and partly define the boundary of the Sabine Uplift, these boundaries are used to subdivide the study area for analysis of lineament orientation (fig. 13). The partial boundary of the Sabine Uplift defined by high density values on its western flank was extended around the uplift along a line of equal slope as measured on the base of the Massive Anhydrite or of the Paluxy Formation (Geomap Co., 1981). Connecting the density highs surrounding the East Texas Basin defines its boundary. The empty space between the basin and the uplift results from the method used to connect high density values. It avoids, for the most part, dividing lineaments that cross the boundary between the two structures.

Significant peak values of length-weighted frequency (F) were identified for these two subregional areas. The same method described above was used for these data sets. Each area has a bimodal distribution of significant peaks (fig. 14). Both have a northwest peak essentially the same as the regional peak at 325 degrees azimuth (fig. 7C). However, the northeast peaks (at 6 degrees and 40 degrees) are not the



QA 6111

Figure 13. Boundaries of the East Texas Basin and Sabine Uplift as defined by high values of lineament density.

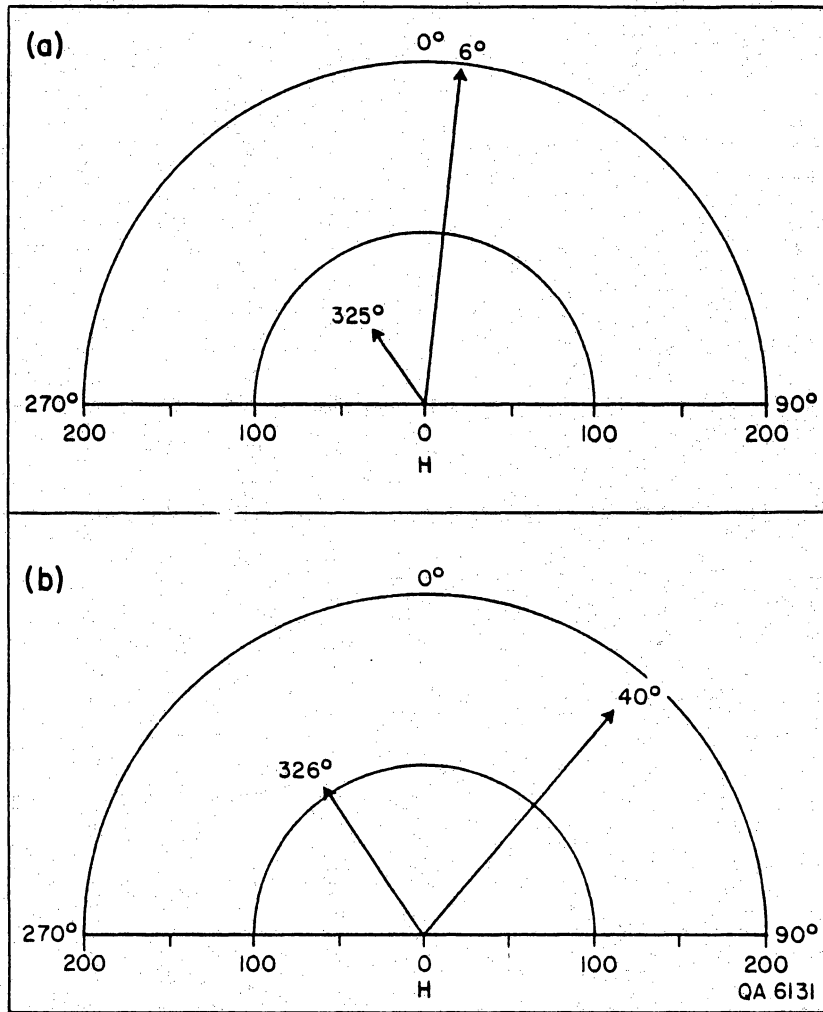


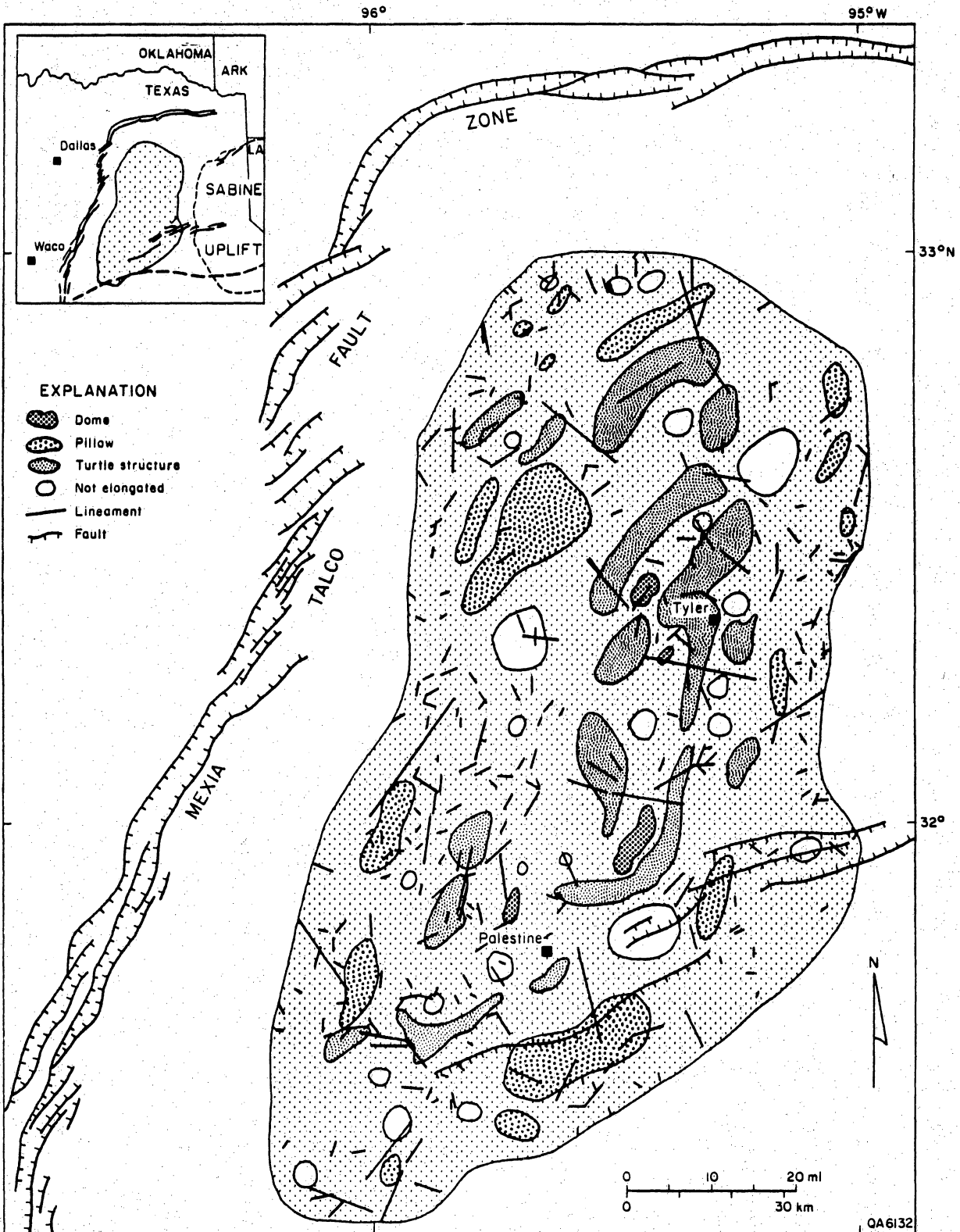
Figure 14. Polar graphs of Bernshtein accuracy criterion for lineaments. A. East Texas Basin. B. Sabine Uplift. Both have northwest azimuths essentially identical to the regional northwest peak shown in figure 7C. The northeast peak azimuths are significantly different from one another.

same as the northeast regional peak (21 degrees), and they are significantly different from one another. This difference could be attributed to geologic differences between the two areas.

To investigate this possibility, significant orientations of lineaments and geologic features in each area were compared. In the East Texas Basin, the relationship between lineaments and elongate salt-related structures was analyzed (fig. 15). Using maps of salt diapirs, salt pillows, and turtle structures from Jackson and Seni (1984), elongated structures were defined as those with a maximum axis at least 1.5 times longer than the axis perpendicular to it. Azimuths of the elongate structures were grouped into 10-degree-wide sectors and examined just as the lineament azimuths were. Lineaments in the same area were excerpted from the regional data and studied. Vector sums were calculated for greater-than-average values of F (as described above), and the Bernshtein accuracy criterion (H) was determined for each vector sum peak (fig. 16).

Azimuths of H for lineaments (16 degrees) and salt-related structures (29 degrees) are subparallel, separated by only 13 degrees (fig. 16). The results of a t test (Cheeney, 1983, p. 98-106) show that the two azimuths are not statistically different. This similarity in orientations and the total absence of other significant peaks suggest that the salt structures and lineaments are caused by similar stress in the rocks.

Although there is a strong correlation between the orientation of salt-related structures and surface lineaments, no consistent spatial relationship exists between them (fig. 15). Most salt diapirs have no overlying lineaments, which is partly a function of their relatively small areal extent. The relationship between the orientations of elongate axes of most structures and those of overlying lineaments appears to be random. In addition, no systematic offset exists between lineaments and elongate structures. Apparently, the lineaments formed independently of the



After Jackson and Seni (1984, figure 5)

Figure 15. Map of lineaments and salt-related structures in the salt structure province of the East Texas Basin. After Jackson and Seni (1984, their fig. 5).

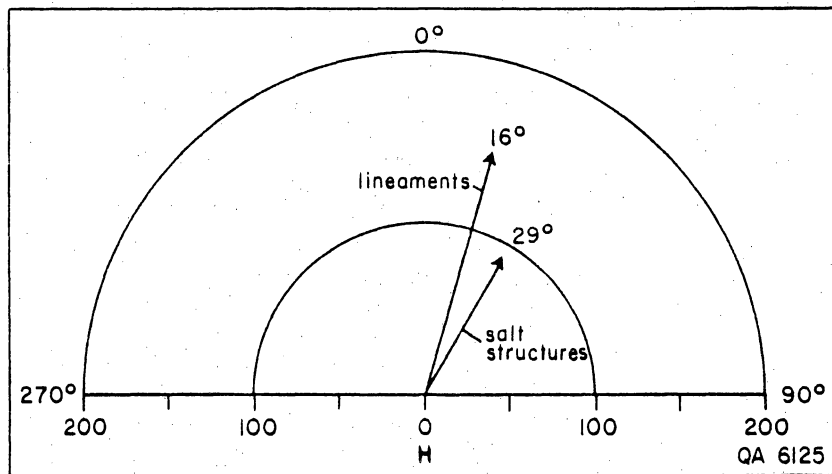
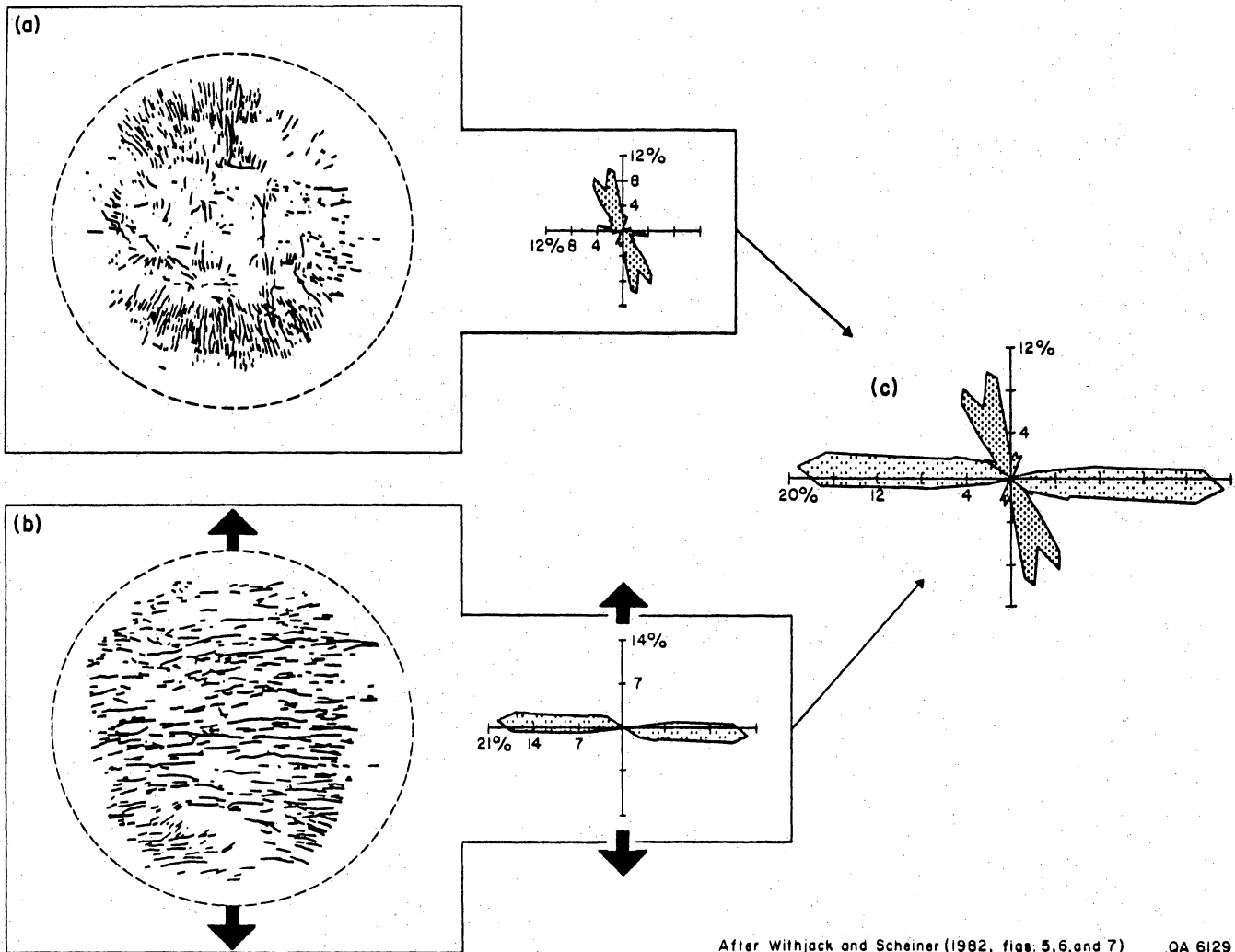


Figure 16. Polar graph of Bernshtein accuracy criterion for lineaments and elongate salt-related structures in the East Texas Basin. The azimuths are not significantly different.

elongate salt structures, but may have been produced by the same basinwide stress regime.

To explain lineament azimuths over the Sabine Uplift, results from this study were compared with those obtained in a study of experimental models of faults produced by doming (Withjack and Scheiner, 1982). An important assumption involved in this comparison is that lineaments over the Sabine Uplift formed as a result of stress analogous to that which caused faulting in the experimental model. Two models were relevant to the current study: (1) doming and (2) doming with extension. These were applicable to the Sabine Uplift for the following reasons: (1) The Sabine Uplift has risen episodically since the early Cretaceous (Carlson, 1984). (2) The Uplift is in the tensional Gulf Coastal Plains stress province (Zoback and Zoback, 1980, their fig. 5). Because the uplift has undergone periods of quiescence and doming over long periods of time, the relative magnitude of vertical and horizontal stresses due to uplift and extension have probably changed during these times. Similarly, in their experiments, Withjack and Scheiner (1982, their table 1) varied the ratio of extension to uplift from 0.0 to 1.7. At a ratio of 0.0 no extension was applied, and at a ratio of 1.7, the rate of extension was 1.7 times greater than the rate of uplift.

Model faults that resulted from uplift alone were not randomly oriented. Instead, they had a prominent northwest azimuth (in terms of the local, arbitrary orientation of the model) (fig. 17A). This result was not discussed by the authors. It may have been the result of some anisotropy in the clay cake or the rubber sheets used in the experimental apparatus. It is tempting to draw an analogy between this anisotropy and those in clastic rocks (due to facies changes, fracturing, and/or uneven compaction) that may influence lineament development.



After Withjack and Scheiner (1982, figs. 5, 6, and 7) QA 6129

Figure 17. Models of faults related to doming. A. Uplift alone. B. Uplift with extension. Extension is 1.7 times greater than uplift. C. Polar graphs of A and B combined. Note that scale changes from B to C.

When extension was applied simultaneously with doming, the model results were radically altered. As much as 64 percent of all faults were perpendicular (± 10 degrees) to the applied extension direction (fig. 17B). Few faults formed at the same orientation as those in the model of uplift alone.

Neither one of these models, by itself, adequately describes the lineament trends over the Sabine Uplift, but by combining the two the result obtained is very similar to those observed in the present study. The combined polar graphs for both experimental models are bimodal (fig. 17C). Azimuths of Bernshtein accuracy criterion for lineaments over the Sabine Uplift are also bimodal (fig. 14B). This similarity, in itself, is not significant, but it suggests that the lineaments may be the products of two different stress regimes: one dominated by extensional stress and one dominated by uplift. As stated previously, these two regimes probably have alternated during episodic doming since the Cretaceous.

Regional extensional stress of the Sabine Uplift is perpendicular to the continental margin (Zoback and Zoback, 1980), which has an azimuth of about 350 degrees along the Upper Texas Gulf Coast. According to the Withjack and Scheiner (1982) model, faults should form perpendicular to the extensional stress direction, in this case at an azimuth of about 80 degrees. However, no significant lineament peaks have this azimuth. Instead, lineament peaks occur over the uplift at 326 degrees and 40 degrees azimuth.

Two important factors may be affecting the formation of lineaments over the Sabine Uplift that are not taken into account by the models proposed by Withjack and Scheiner (1982). First, the model dome is hemispherical, whereas the Sabine Uplift is flat-topped and "broken by numerous structural anomalies" (Murray, 1948, p. 146). These structural anomalies may exert local directional control on the orientation of lineaments forming at the surface. Second, the Sabine Uplift may be

affected by stress regimes in adjacent areas. For example, Fisk (1944, his fig. 6) mapped fault zones next to the eastern edge of the uplift with azimuths of 47 degrees, 52 degrees, and 317 degrees. He attributed alignment of tributaries and parallelism of drainage lines in the Mississippi alluvial valley to control by these and other regional structures. The similarity between these fault orientations and peak lineament azimuths (40 degrees and 326 degrees) suggests that lineaments over the uplift may result from similarly oriented stresses.

The lineament azimuth peak at 326 degrees may be analogous to the azimuth peak for faults that formed in Withjack and Scheiner's (1982) model for uplift alone. That is, the lineaments may be the result of some anisotropy in the rocks. Because this orientation occurs as part of the regional data (fig. 7C) and in the East Texas Basin (fig. 14A), the proposed anisotropy must be a regional feature as well.

One candidate for this anisotropy is unmapped transfer (transform) faults. Generally, transfer faults form in extensional basins at high angles to extensional normal faults (Etheridge and others, 1985). They accommodate extension by transferring movement between sets of normal faults. In the study area transfer faults may have formed approximately at right angles to the northeast trend of normal faults (Mexia-Talco, South Arkansas, Rodessa, and Elkhart-Mt. Enterprise Fault Zones, fig. 1). Pilger (1981) proposed a model of tectonic evolution of the northern Gulf Coast in which the East Texas Basin formed by crustal spreading with transform faults oriented northwest-southeast. The direction of spreading has the same general orientation as the northwest lineament peak at 325 degrees azimuth.

DISCUSSION

Relationship Between Lineaments and Stress Regime

Previous studies have shown that lineaments can overlie basement structures with similar azimuth (Frost, 1977) and that lineament zones can correspond to regional structural patterns (Caran and others, 1981). Thus far, this study has shown that azimuths of lineaments and elongated salt-related structures in the East Texas Basin are near-parallel. In addition, zones of high lineament density generally correspond with structural features.

The mechanism that produces linear surficial features parallel to deeply buried structures is not completely understood. Berger (1982, p. 580) listed four processes by which a buried structure could indirectly influence surface conditions:

- (1) Differential loading of sediments;
- (2) Renewed or continued movement of buried structures;
- (3) Differential compaction of sediments; and
- (4) Disruptions of near-surface ground water flow.

The first three mechanisms are most likely to have affected formation of lineaments detected in this study. The humid climate in the study area probably masks lineaments that form owing to disruption of ground-water flow.

Regardless of the mechanism affecting surface conditions, Berger (1982) reported that most lineaments he observed on Landsat data were caused by zones of closely spaced fractures. Surface fractures form in response to stresses in near-surface rocks, which may be different from those in the deep subsurface. Haimson (1978, 1979), Zoback and others (1980), and Zoback and Zoback (1980) observed shallow, horizontal stresses (less than 100 m [330 ft] depth) quite different from deeper stresses at the

same site. They attributed these differences to the effects of local topography, weathering, and erosion. Zoback and Zoback (1980) concluded that local fractures and joints can disconnect surface rocks from the tectonic stress field. On the other hand, Tullis (1981) observed that near-surface horizontal stress directions are likely to be similar to those at depth if enough measurements are taken to allow an average over local variations induced by individual nearby fractures.

Similarly, measurement of lineaments over a large area may cancel the random effects of local topography and reveal patterns that are representative of more deeply seated stresses. These linear patterns may be the result of stresses in the rock inherited from a previous period of deeper burial. When the rocks are exposed at the surface, these stresses are relaxed and the rocks fracture. For example, Bannister (1980) concluded that the joint pattern in outcrops he studied was the result of previous stress-strain fracture patterns that, upon exposure to the atmosphere, weathered into joint planes. Lineaments in this study may have a similar origin.

Whether lineaments in the study area are caused by fracturing is not known. However, the parallelism between lineaments and elongated salt structures in the East Texas Basin suggests that subsurface stresses exert significant control on the development of surface lineaments. Similar results have been derived from well data and lineament orientations for the entire study area, as described in the following section.

Stress in Study Area

Gough and Bell (1982) summarized data on the stress regime for East Texas and northwest Louisiana. Citing the presence of extensional normal faults in the East Texas Basin and growth faults to the south, they concluded that the area south of

the Mexia-Talco Fault Zone is a tensional tectonic province, one in which the maximum principal stress is approximately vertical and the minimum principal stress is horizontal and approximately perpendicular to the traces of extensional faults.

According to the McKenzie (1978) model of basin formation, the subsidence that formed the Gulf of Mexico was driven by stretching of the lithosphere and was enhanced by sediment loading of the basin. Other authors (Zoback and Zoback, 1980) have concluded that present-day stress in the Gulf Coastal Plains stress province probably is the result of sediment loading and is not a function of stress in the bedrock underlying Gulf Coast sediments, which remains unknown. Jackson (1982) studied seismic data and concluded that all principal fault systems of the East Texas Basin formed by processes associated with differential gravity sliding of cover over the Louann Salt. Although data from the Elkhart-Mt. Enterprise zone were scarce, he found no evidence to suggest that fault zones formed by marginal flexure of the basin.

Data from 50 wells scattered throughout East Texas (fig. 18) provide important additional information about regional stress directions. Brown and others (1980) measured the azimuths of breakouts (wellbore elongations) in the Schuler Formation at depths below about 2,800 m (9,200 ft). Mean breakout azimuth for each well is shown in figure 18. Based on the orientations of vertical hydraulic fractures (east-west) and recently active normal faults (northeast-southwest) in the area, Gough and Bell (1982) concluded that the northwest to north-northwest orientations of these breakout azimuths were approximately parallel to the least principal stress. According to their interpretation, the breakouts formed by spalling of the borehole in a direction parallel to the minimum compressive stress.

The similarity in orientations of lineaments from the present study and from breakouts suggests that the regional stress regime in this area is exerting a significant control on lineament formation. The mean azimuth of all breakouts, 325 degrees

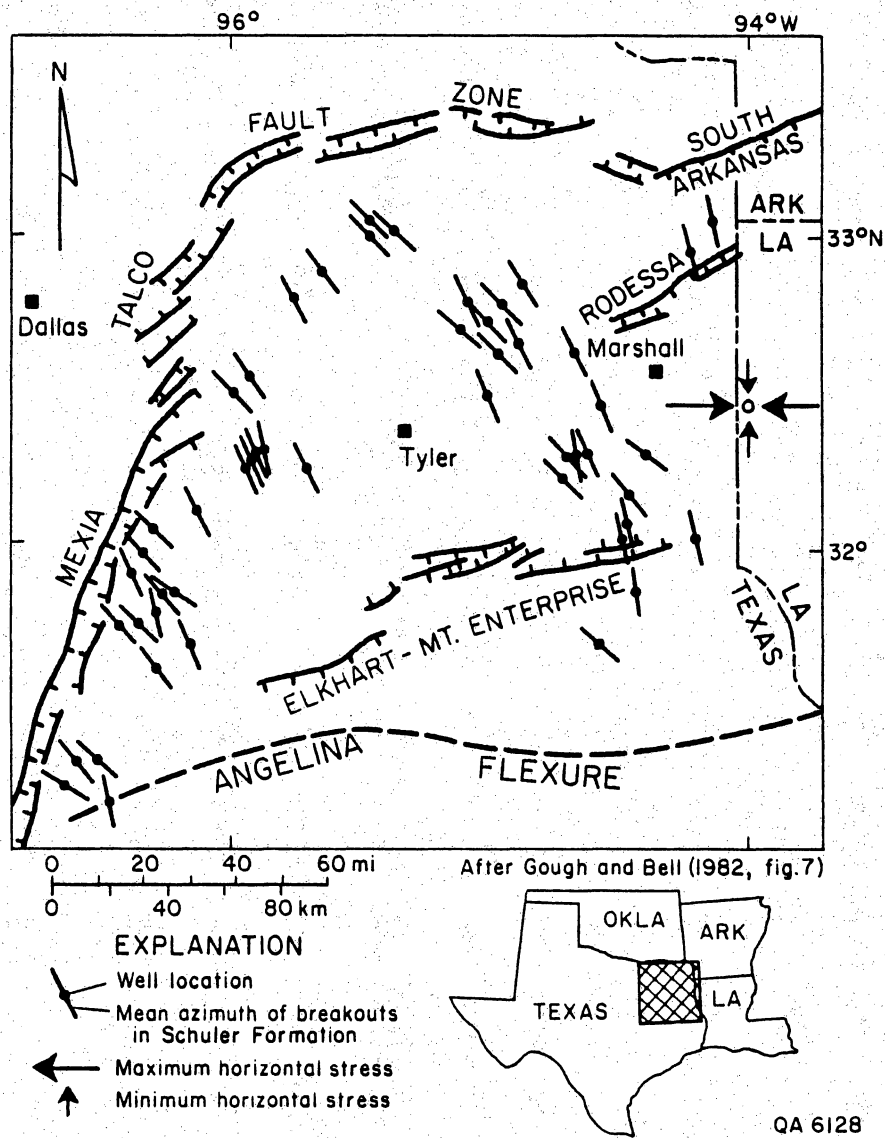


Figure 18. Map of breakouts in wells in the Schuler Formation, East Texas. Mean azimuth of all breakouts in 50 wells is 325°. This is exactly the same as the significant northwest regional azimuth for lineament data in the study area (fig. 7C). Well data from Brown and others (1980), cited in Gough and Bell (1982, their fig. 7). Data for horizontal stresses from well near Texas-Louisiana border are from Strubhar and others (1975). Maximum horizontal stress is oriented east-west.

(Gough and Bell, 1982), is identical to the significant northwest regional peak for all lineaments, as well as for just those in the East Texas Basin (figs. 7C and 14A). Furthermore, the northwest azimuth peak for the Sabine Uplift, 326 degrees, is virtually identical (fig. 14B).

A problem arises when trying to explain why lineaments, if they are formed by fracturing, would form parallel to the least compressive stress, whereas tensional fractures form perpendicular to the same stress. One possible explanation depends on the presence of transfer faults, as discussed previously. Generally, these faults form perpendicular to normal faults. In the study area they would be perpendicular to the major mapped fault zones (fig. 1). Because most lineaments are stream network features (fig. 6, table 2), this theory requires that streams selectively erode along the traces of transfer faults. This may be true near mapped fault zones, where consequent streams flow down the slope of tilted strata, but the role of transfer faulting elsewhere remains untested and unproven. The process by which deeply buried transform faults might affect lineament formation is not known, but differential loading and/or compaction of sediments across faults may be important.

Nevertheless, hydraulic fractures normally propagate parallel to the maximum horizontal compressive stress, opening against the minimum compressive stress. If Gough and Bell (1982) are correct in their analysis of wellbore elongations, hydraulic fractures in the Schuler Formation should propagate from east-northeast to northeast throughout the area covered by the wells shown in figure 18. Furthermore, if lineaments form as a result of regional stresses, they may be useful predictors of fracture propagation direction where wellbore data are lacking.

CONCLUSIONS

Remote sensing of lineaments has been used to study geologic structure on a regional scale. Although one-to-one correspondence between lineaments and mapped faults occurs only rarely, spatial correspondence between most high values of lineament density and major tectonic features is consistently close. Vector sums of length-weighted frequency of lineaments produce bimodal azimuth peaks for the study area as a whole, in addition to the East Texas Basin and the Sabine Uplift. The northwest azimuth peak is essentially identical for all three data sets, but the northeast peaks are not. The northeast peak in the salt structure province of the East Texas Basin is parallel to the peak azimuth for elongated salt-related structures. The northeast peak over the Sabine Uplift is not parallel to any known geologic structure. The northwest lineament peaks are all parallel to the mean azimuth of borehole elongations in wells located throughout East Texas. These elongations are attributed to spalling of the boreholes and interpreted to be parallel to the minimum horizontal compressive stress in the area. Hydraulically generated fractures should propagate perpendicular to the minimum compressive stress and, consequently, perpendicular to the northwest peak azimuth of lineaments in this study.

ACKNOWLEDGMENTS

The Gas Research Institute funded this project under contract number 5082-211-0708, Robert J. Finley, Principal Investigator. Martin P. A. Jackson and Stephen E. Laubach offered useful suggestions at critical junctures. Computer programming for digitization and compilation of lineament data was done by Dale Clark, Jack W. Lund,

and Gerry White under the direction of Michael P. Roberts. Cartography was done by Kerza A. Prewitt and Joel L. Lardon under the direction of Richard L. Dillon. Word processing was by Dorothy C. Johnson under the direction of Lucille C. Harrell. Editing was by Diane Callis Hall. Helpful criticism of the manuscript was provided by Jules R. DuBar, Technical Editor, and by Edward W. Collins, Martin P. A. Jackson, and Stephen E. Laubach.

MESOZOIC AND CENOZOIC STRUCTURAL HISTORY OF THE SABINE UPLIFT AREA, EAST TEXAS

Mary L. W. Jackson

ABSTRACT

Identification of the timing, extent, and orientation of arching episodes in the Sabine Uplift area is important in providing a regional structural framework within which detailed stress and fracture studies of the Travis Peak Formation can be conducted. In this study, estimation of movement on the Sabine Uplift was made from isopach maps, using six units in the Lower Cretaceous interval between the Sligo Formation and the base of the Austin Group. The isopach maps, based on 811 logs, show that the Sabine Uplift was part of a large basinal area during the Late Jurassic and Early Cretaceous. The Sabine Uplift does not appear to have been a large Jurassic horst that remained in a structurally high position through the Cretaceous and Tertiary, as it is commonly shown in the literature. Timing, orientation, and magnitude of arching episodes on the uplift in the mid-Cretaceous and Early Tertiary indicate that the Sabine Uplift may have been produced by northeast-directed tectonic events related to orogenic activity in the Mexican Cordillera.

INTRODUCTION

Investigation of the Travis Peak Formation by researchers at the Bureau of Economic Geology (BEG) is a part of geologic and engineering research on low-permeability gas sandstones that has been supported by the Gas Research Institute (GRI) since 1982. In a recent BEG report, Finley (1984) estimated the maximum recoverable gas-in-place in the Travis Peak Formation in the area of the Sabine Uplift

at 13.8 to 17.3 Tcf, assuming 12 to 15 percent ultimate reservoir production. Other BEG reports concern the sand-body geometry and diagenetic history of the Travis Peak Formation (Fracasso and others, 1986; Dutton, 1985; Saucier, 1985). Reservoir engineering aspects of the Travis Peak Formation have been examined by Lin (1985). Ongoing BEG studies of the Travis Peak Formation include construction of burial history curves for estimation of the timing of diagenesis, and natural fracture distribution and in situ stress analysis.

This report is a subsurface study focused on the timing, extent, and orientation of uplifts that produced deformation of the Travis Peak Formation in the area of the Sabine Uplift. An understanding of the stress history and current states of stress in the Travis Peak is important to optimization of the hydraulic fracturing necessary for gas extraction in low-permeability gas reservoirs. This study provides a structural history of the Sabine Uplift area as a framework within which detailed stress and fracture studies of the Travis Peak Formation can be conducted. In addition, knowledge of the regional structure can assist in identification of possible hydrocarbon source rocks and paths of hydrocarbon migration for the Travis Peak Formation.

PREVIOUS WORK

Early studies of stratigraphic intervals in the Sabine Uplift area were done by Moody (1931), Powers (1920), Huntley (1923), and Murray (1948) in Tertiary and Upper Cretaceous intervals. Studies of deeper intervals were undertaken by Bornhauser (1958), Halbouty and Halbouty (1982), and many other authors (table 6). The most comprehensive study of the Sabine Uplift to date was done by Granata (1963) and includes isopach maps of 10 intervals from the Upper Jurassic Cotton Valley Group to the Upper Cretaceous Navarro Group.

Table 6. Selected subsurface studies that include the area of the Sabine Uplift.

TERTIARY

Waters and others, 1955
Murray and Thomas, 1945
Kaiser and others, 1986

UPPER CRETACEOUS

Granata, 1963
Halbouty and Halbouty, 1982
Waters and others, 1955
Stehli and others, 1972
Nichols, 1964
Oliver, 1971

LOWER CRETACEOUS

Saucier, 1985
Granata, 1963
Halbouty and Halbouty, 1982
Waters and others, 1955
Caughey, 1977
Forgotson, 1956
Pittman, 1985
Nichols, 1964
Bushaw, 1968

JURASSIC

Waters and others, 1955
Nichols, 1964
Dickinson, 1968

Some published Sabine Uplift studies contain stratigraphic and structural interpretations based on shallow or limited data. The large database used in this study allows improved interpretations not possible in earlier studies.

METHODOLOGY

The study area is located in East Texas and Louisiana (fig. 19), encompassing the region generally known as the Sabine Uplift. Over 810 electric and induction-electric logs, of which more than 97 percent penetrate the complete section mapped, were used for this project (fig. 20). A cross-section network constructed for correlation purposes includes 16 cross sections in Texas and 8 in Louisiana. The cross sections and the logs are available in open file at the BEG. Cross sections in this study were correlated to the East Texas Basin cross-section network (Wood and Guevara, 1981a).

Estimation of the timing and orientation of movement on the Sabine Uplift was made from isopach maps. Such maps are interpreted on the assumption that the thickness of sediment accumulation within a certain time interval reflects facies changes and structural movement during that interval. Stratigraphic time lines necessary for making isopach maps in the study area are best approximated by Cretaceous limestones.

Six units in the Lower Cretaceous interval between the Sligo Formation and the base of the Austin Group (fig. 21) were mapped. Each of the stratigraphic markers used to define the units can be identified by a distinctive electric log signature across most or all of the study area (figs. 22, 23). The markers used are (1) base of the Massive Anhydrite, (2) top of the Glen Rose Formation, (3) base of the Fredericksburg Group (base of the Goodland limestone), (4) base of the Washita Group (base of the Duck Creek limestone), and (5) base of the Austin Group (base of

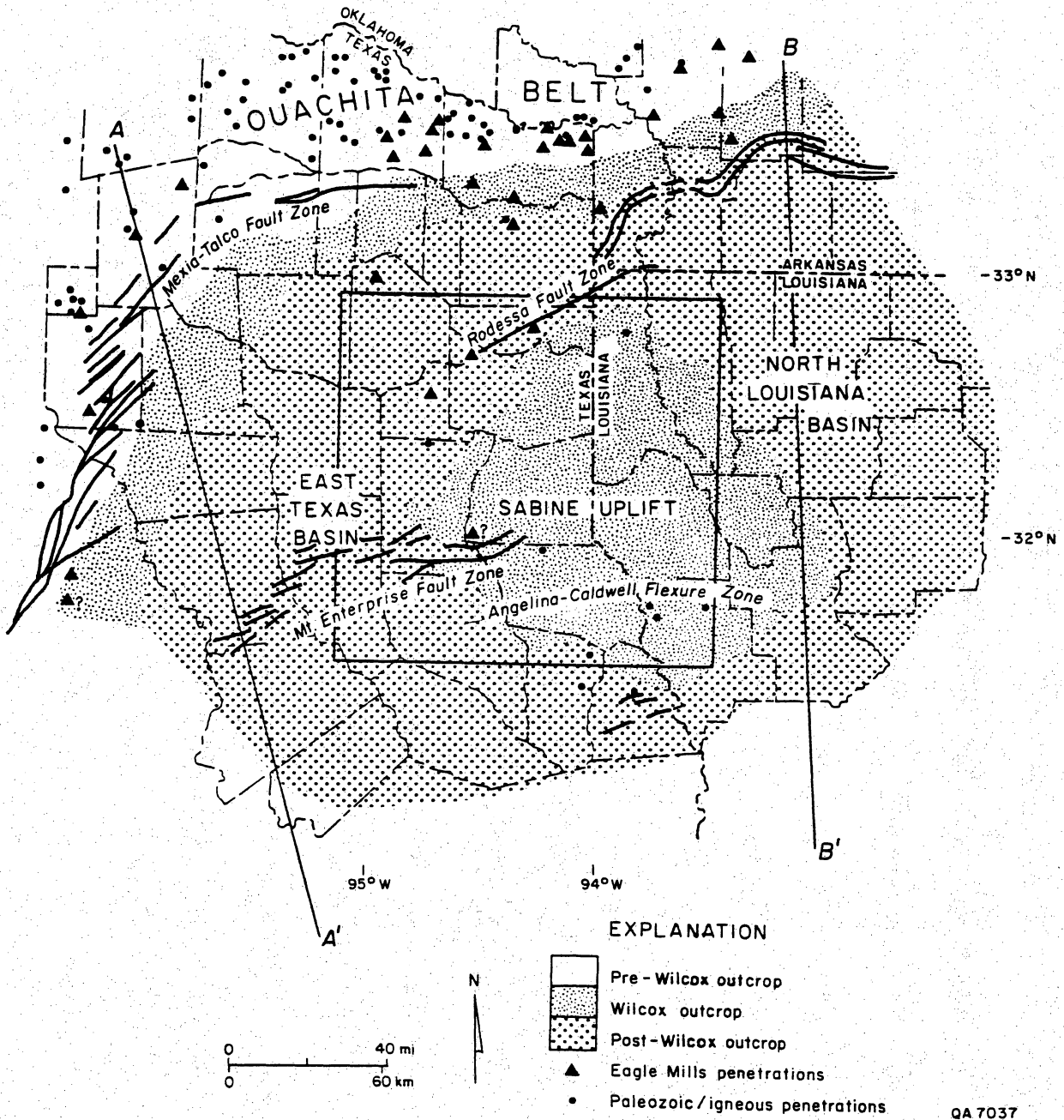
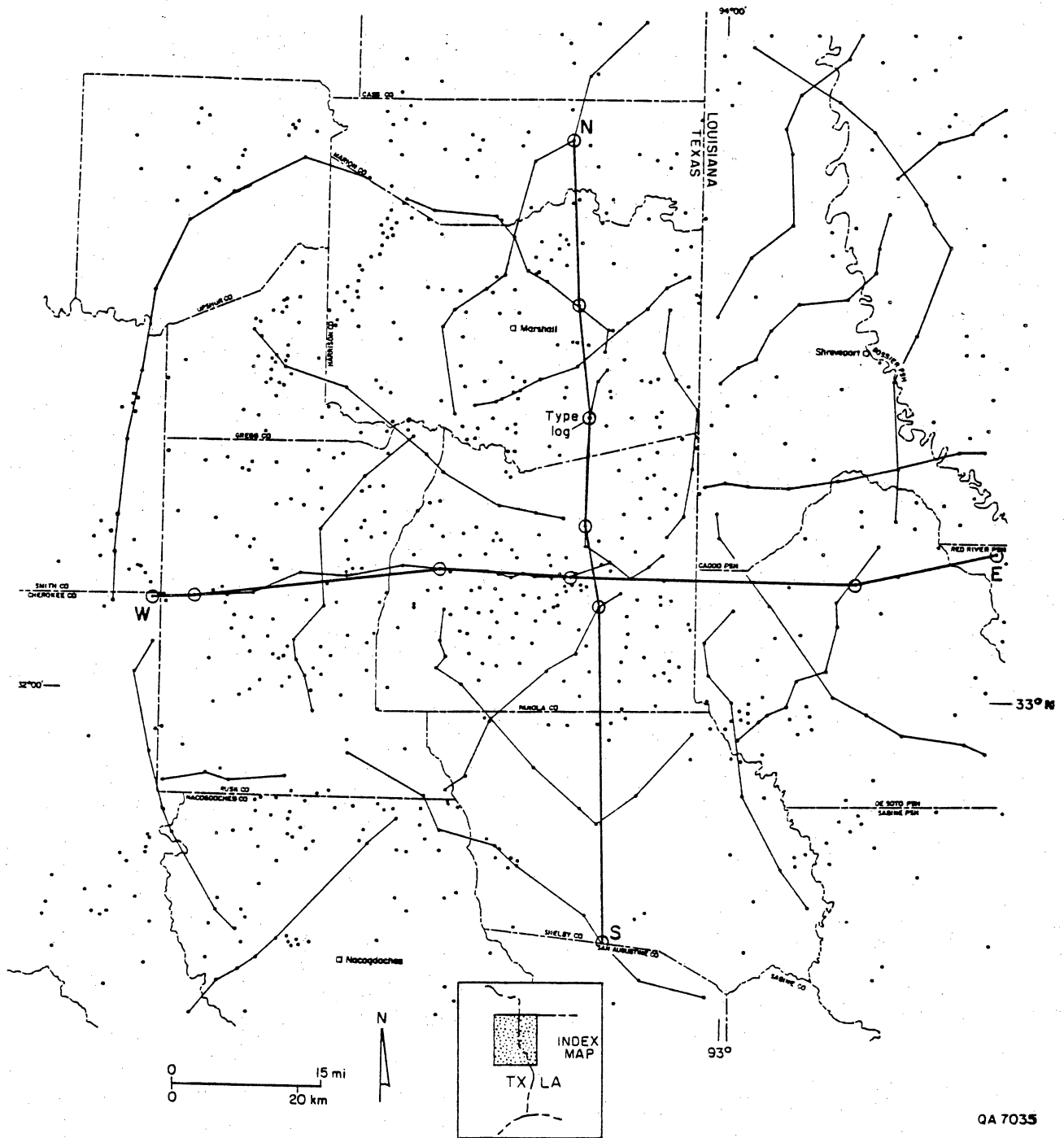


Figure 19. Geologic and structural setting, Sabine Uplift area.



QA 7035

Figure 20. Data points used in this study and representative cross-section, correlation cross-section, and type log locations.

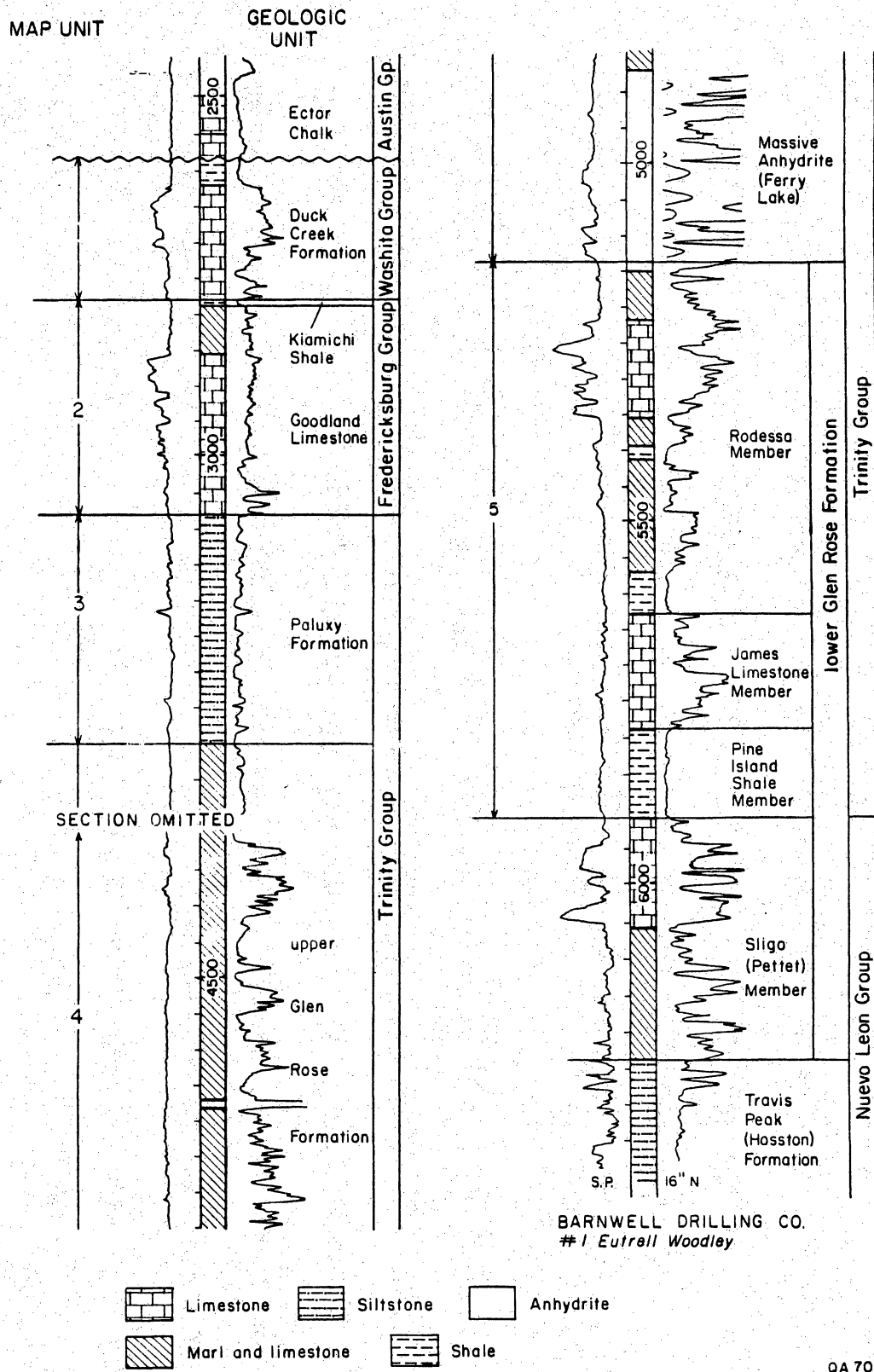
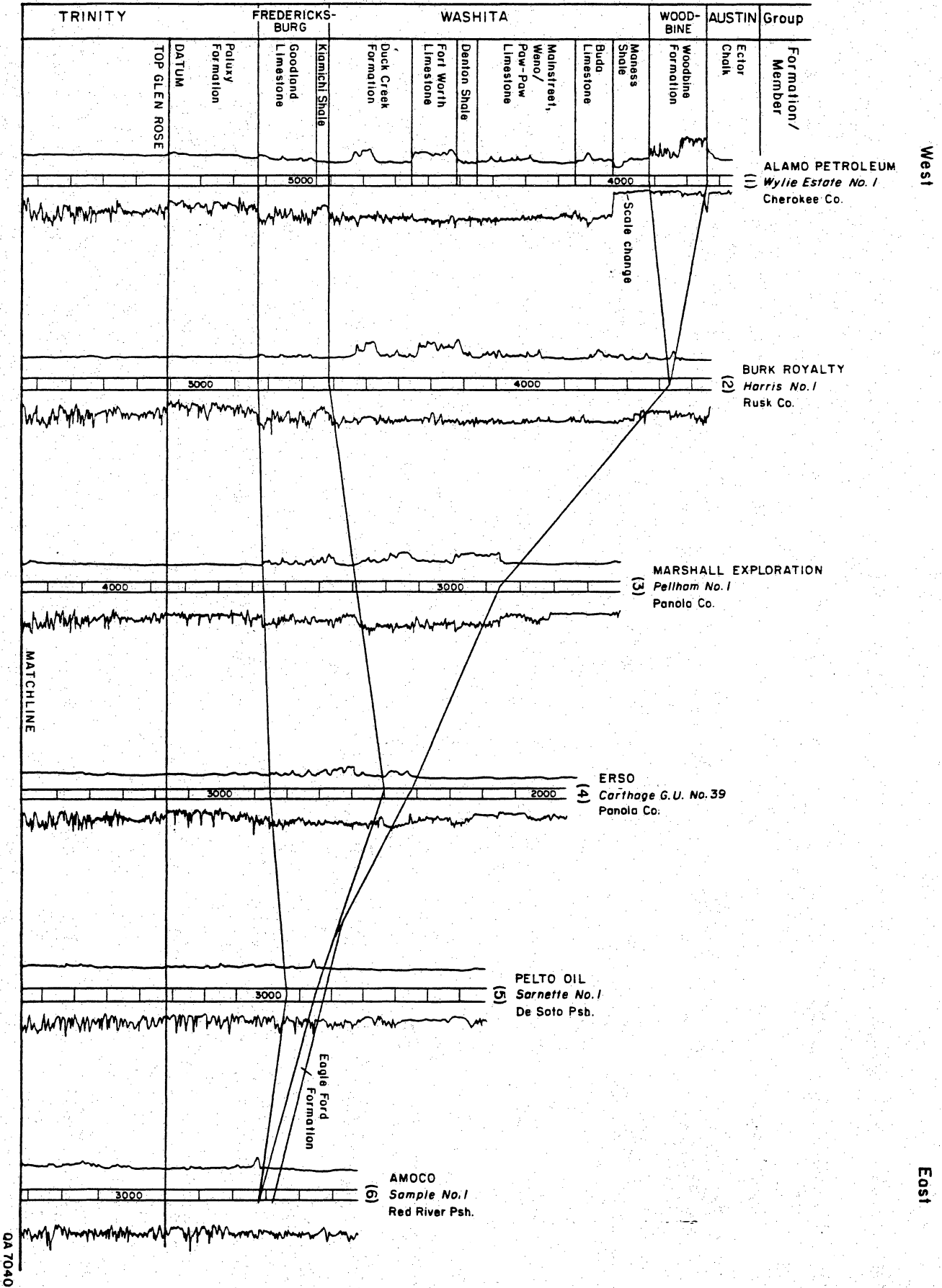
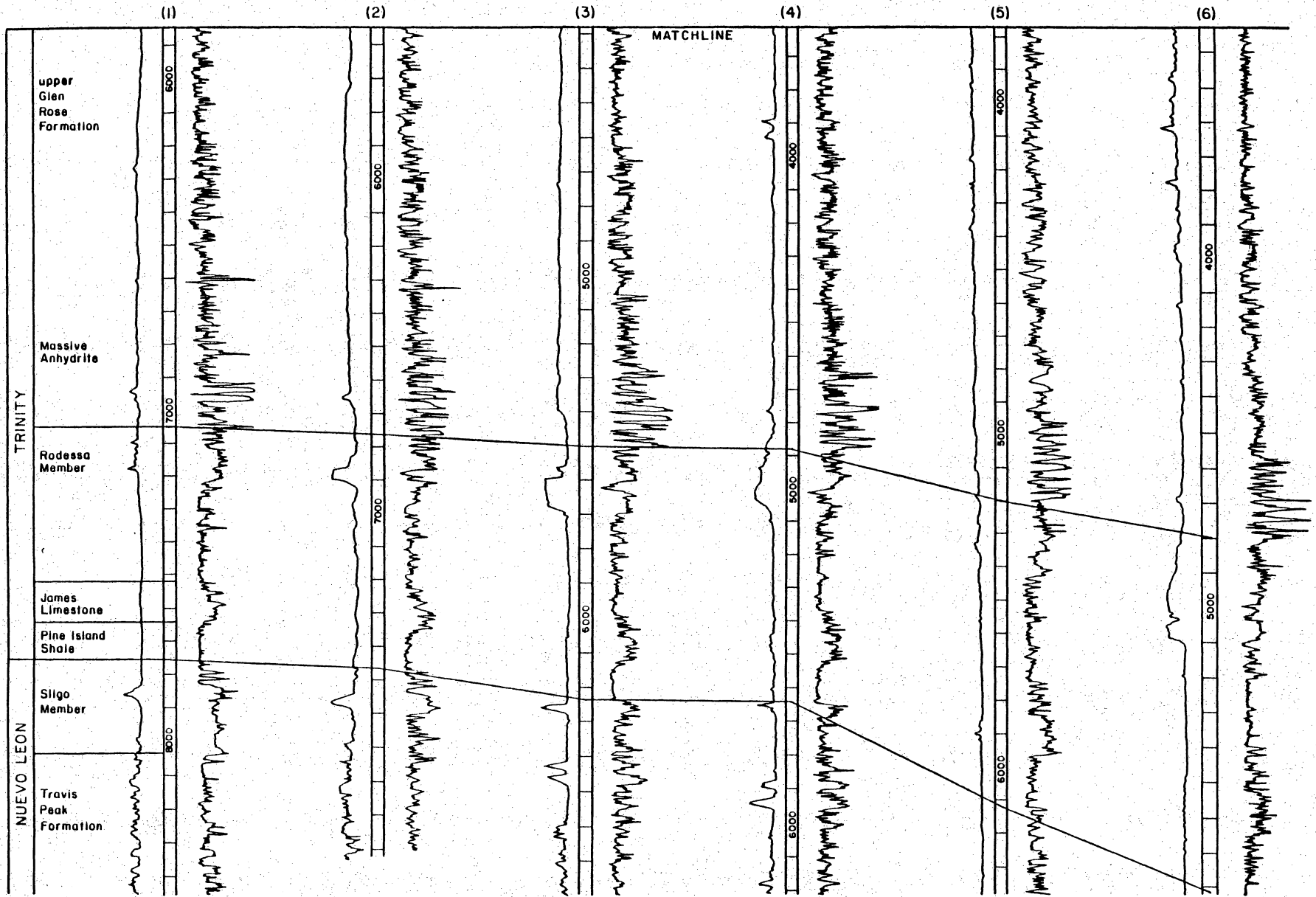


Figure 21. Type log of the Lower Cretaceous, Sabine Uplift area. Location shown on figure 20. Louisiana terminology in parentheses.

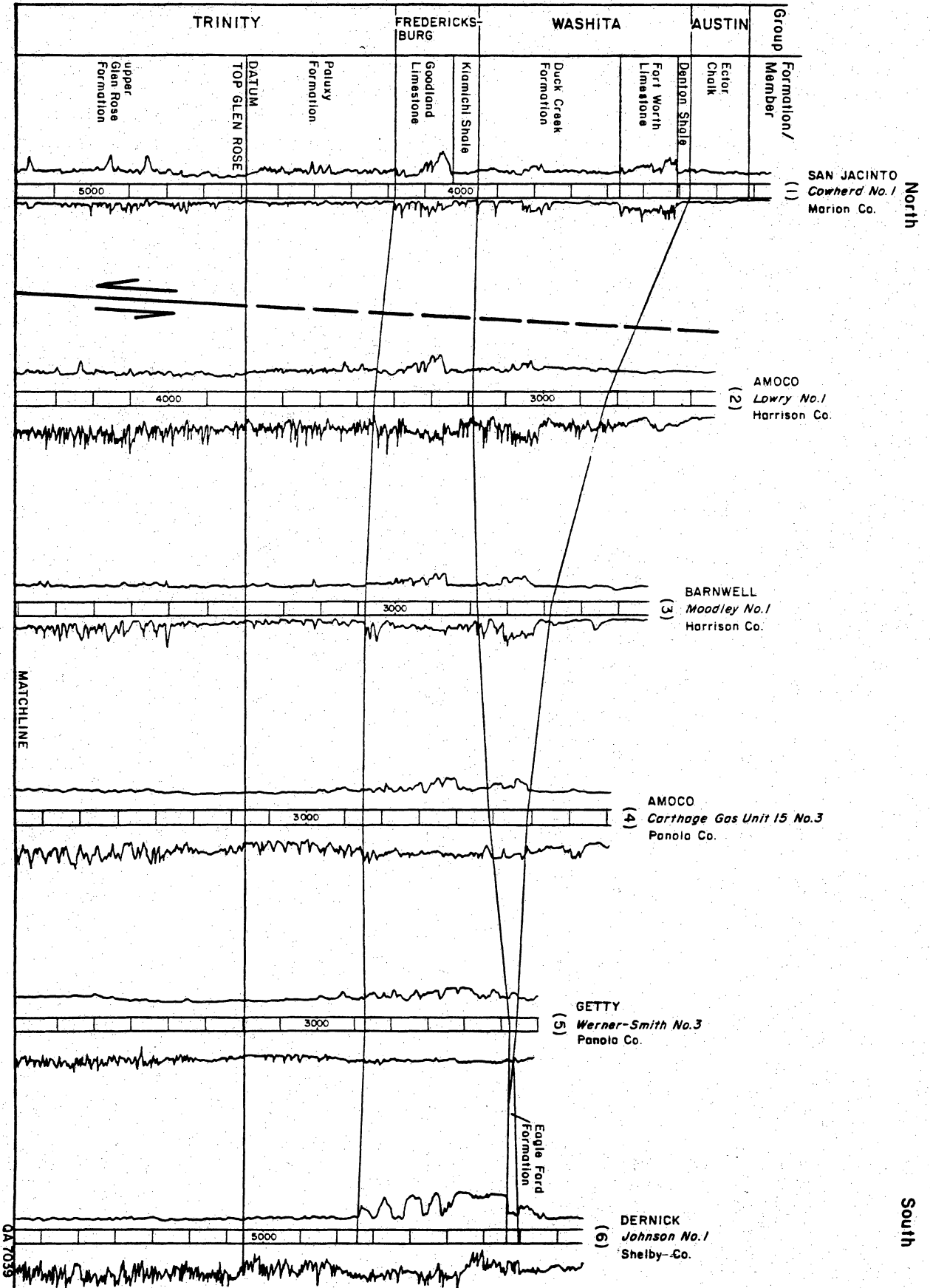


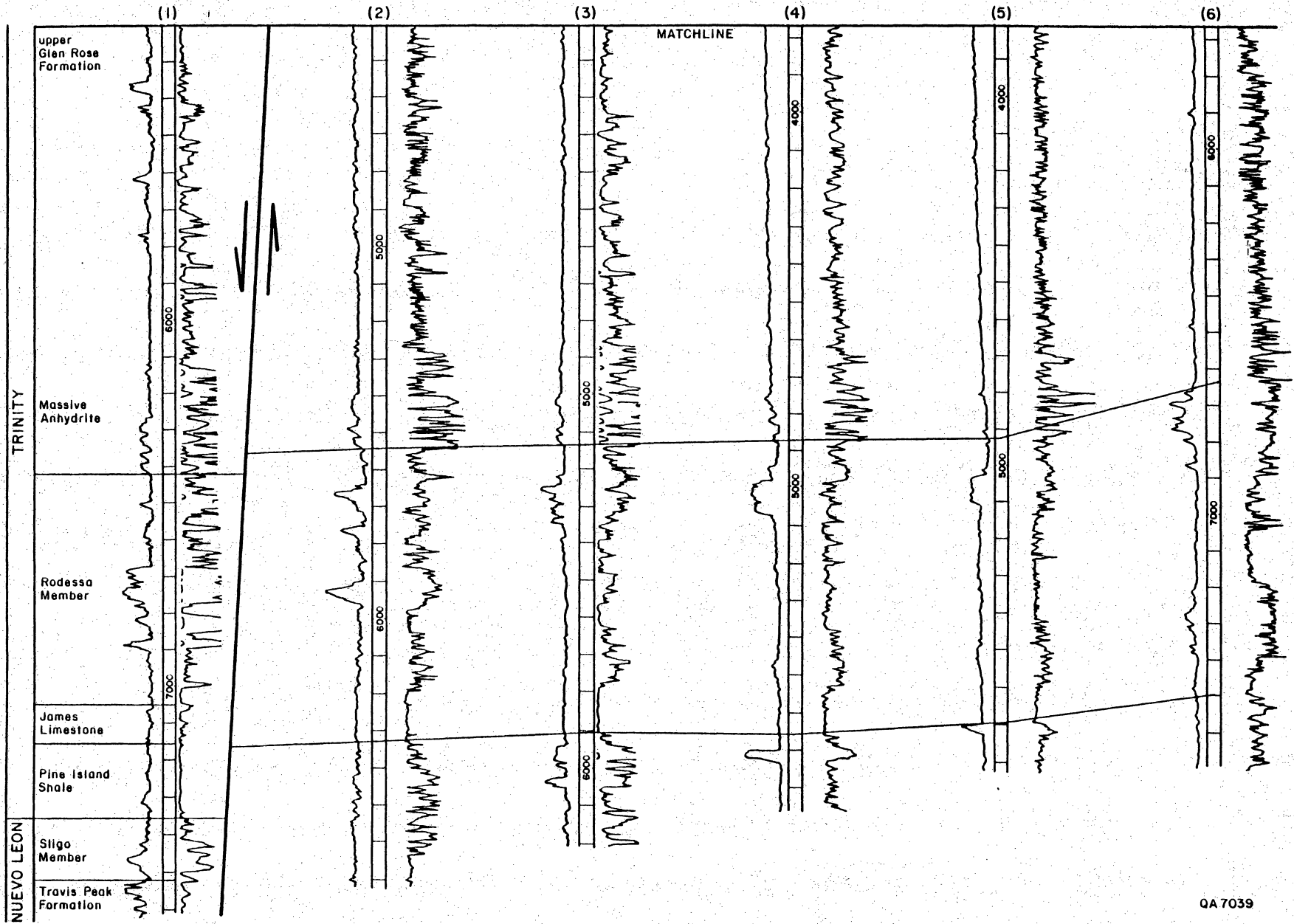
0A 7040



QA 7040

Figure 22. Representative west-east cross section of the Lower Cretaceous in the Sabine Uplift area. Cross-section location on figure 20.





QA 7039

Figure 23. Representative north-south cross section of the Lower Cretaceous in the Sabine Uplift area. Cross-section location on figure 20.

the Ector Chalk). Saucier (1985) included the Sligo Formation in his maps of the Travis Peak Formation, and his top of Sligo marker was used in this study. In the eastern part of the Sabine Uplift area, the Woodbine Group occurs between the Austin and Washita Groups, and the base of the Woodbine was used as the upper contact for the Washita Group interval (fig. 22).

The isopach intervals mapped in this report are actually isochore intervals; unit thicknesses have not been adjusted for structural dip. Because structural dip in the study area is low, the difference between true isopach maps and isochore maps is insignificant.

A palinspastic map was constructed on the base of the Massive Anhydrite to determine the extent of pre-Austin Group uplift in the study area. This type of map excludes structural deformation that occurred after deposition of the horizon chosen for a datum, in this case the base of the Austin Group; the map shows only the structural attitude that was present before the Austin Group was deposited. Vitrinite reflectance data were also used in determining depth of sediment burial.

GEOLOGIC SETTING

The Sabine Uplift lies on the Texas-Louisiana border, and can be defined by the Wilcox outcrop (fig. 19). The Uplift is about 105 miles (169 km) long in the north-northeast direction (longest axis) and about 113 mi (182 km) wide. It is bounded on the west by the East Texas Salt Basin and on the northeast by the North Louisiana Salt Basin. A smaller basin that bridges the two salt basins forms the northern boundary of the Sabine Uplift. On the south the uplift merges into the Angelina-Caldwell Flexure Zone.

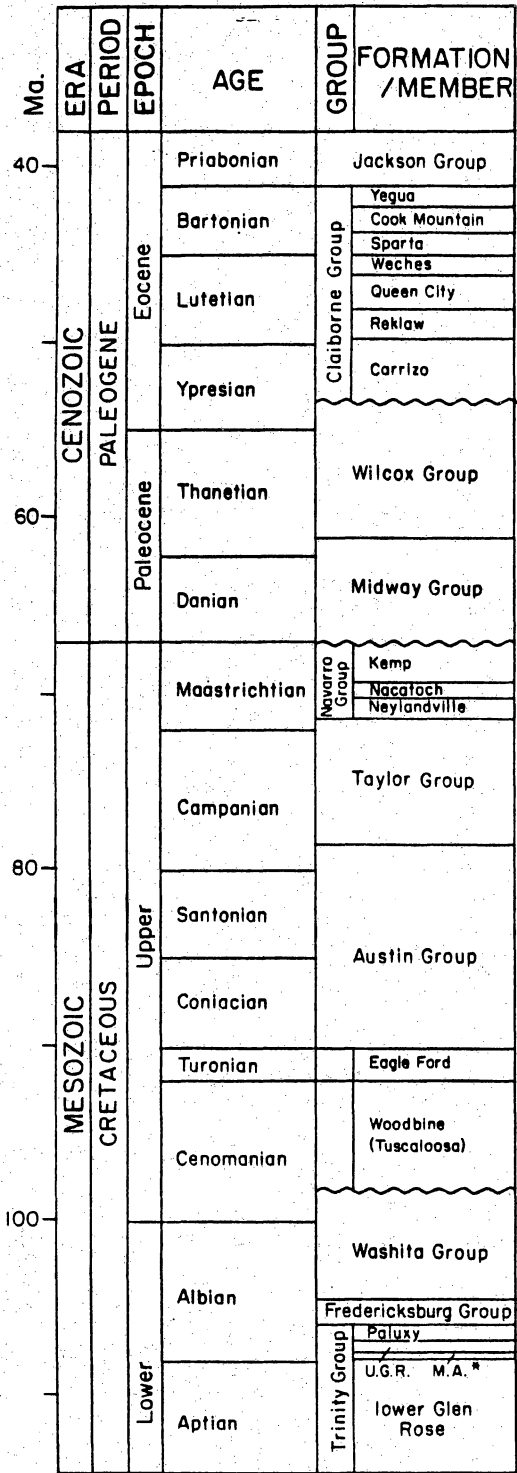
Major fault zones in the area are the Mexia-Talco, which bounds the East Texas Salt Basin on the updip west side, and the east-west trending Mt. Enterprise Fault Zone, which lies to the southwest of the Sabine Uplift. Both of these fault zones are interpreted to be caused by gravitational sliding over the structurally weak Louann Salt (Jackson, 1982). The Rodessa Fault Zone forms an east-northeast-trending graben that cuts the northern edge of the Sabine Uplift.

The Sabine Uplift is underlain by Triassic, Jurassic, Cretaceous, and Tertiary sediments (fig. 24). Lower Cretaceous rocks dip gently toward the East Texas Basin and more steeply on the flanks of salt pillows and domes in Louisiana (fig. 25). A major erosional unconformity overlies these, and Upper Cretaceous and Tertiary rocks dip even more gently toward the East Texas Basin (fig. 26). Lower Eocene (Wilcox) strata form most of the outcrop on the Sabine Uplift today (fig. 19). Nomenclature for some stratigraphic units differs between Texas and Louisiana; in this report Texas nomenclature will be used.

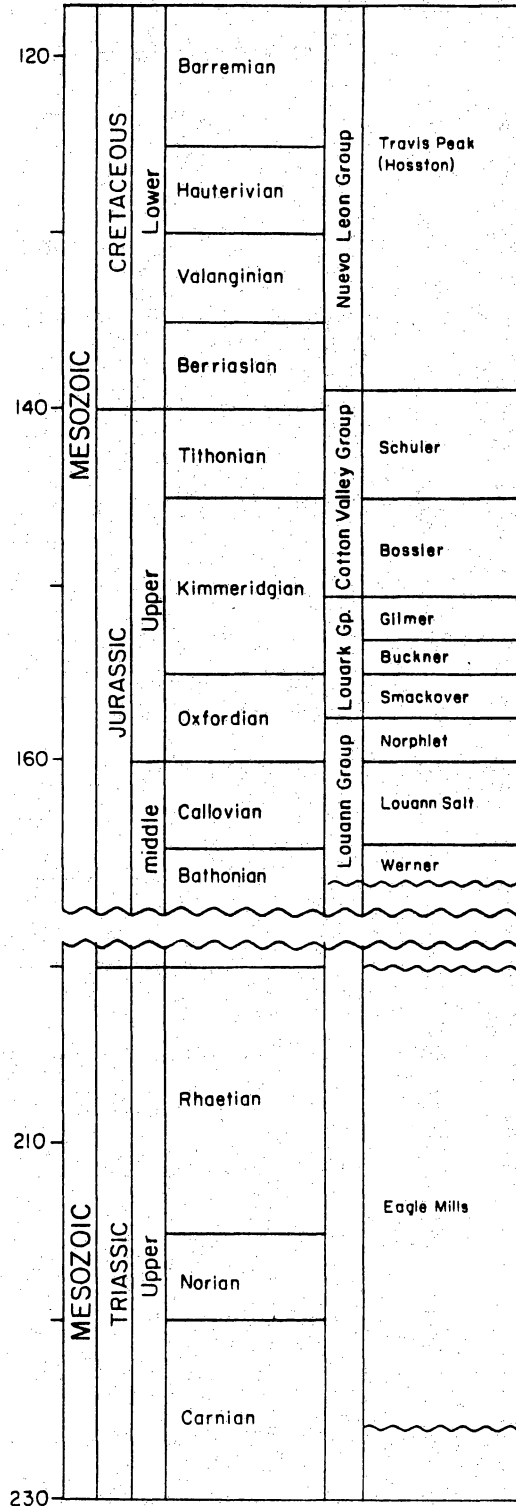
DEPOSITIONAL HISTORY OF MESOZOIC AND CENOZOIC SEDIMENTS

Jurassic Depositional History

The first episode of Mesozoic deposition in the Sabine Uplift area began when tectonic rifting formed grabens into which Eagle Mills fan deltas were deposited (Jackson and Seni, 1984b). The extent of the Eagle Mills Formation is difficult to estimate because it is thin and deeply buried. Eagle Mills well penetrations are mostly in updip areas adjacent to the Ouachita front (fig. 19). No Triassic continental deposits have been drilled in northern Caddo Parish, but Eagle Mills has



* U.G.R. = upper Glen Rose
M.A. = Massive Anhydrite (Ferry Lake)



QA7032

Figure 24. Isopach map of the combined Sligo and Travis Peak Formations. Hachured pattern to northwest is area of Monroe Uplift. Adapted from Saucier (1985).

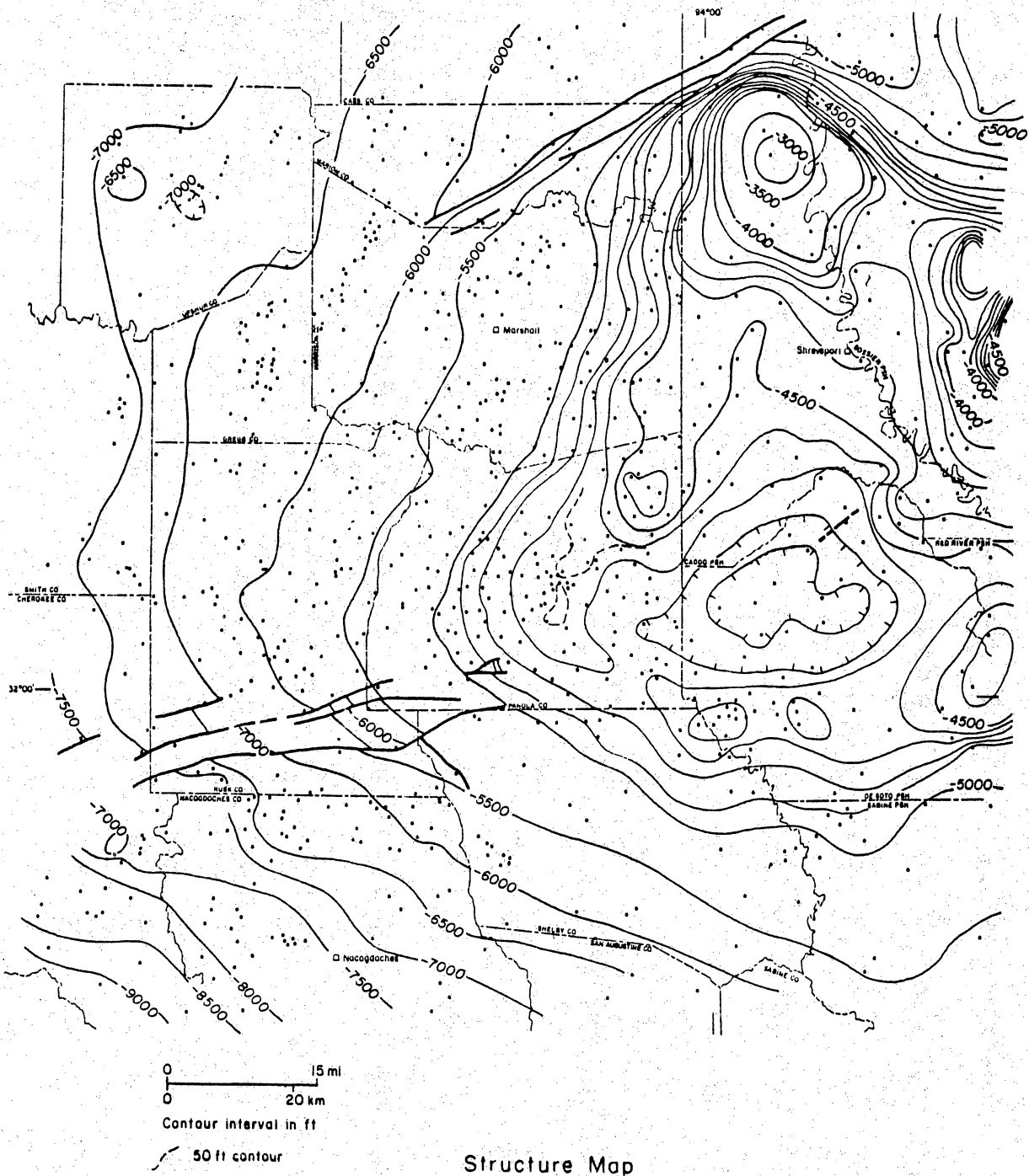
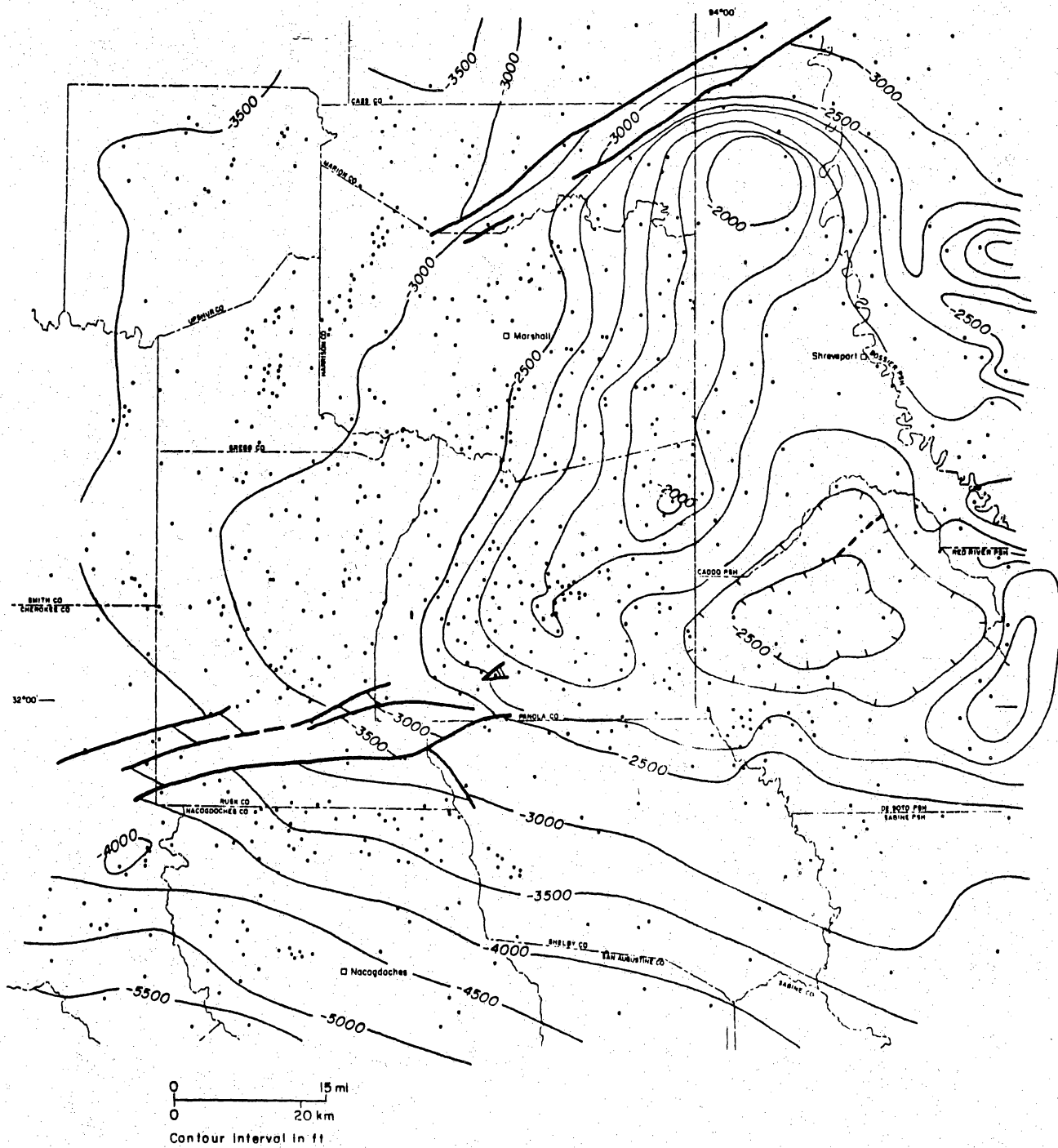


Figure 25. Structure map of the base of the Massive Anhydrite, Sabine Uplift area.



been penetrated in Gregg, Harrison, and Marion Counties. Thicknesses of Eagle Mills greater than 1,000 ft (300 m) are present in north-central Louisiana (Hazzard and others, 1945b).

A depositional hiatus existed during the early Jurassic. The Werner Anhydrite and overlying Louann Salt, which covered a large area of the widening Gulf of Mexico, were deposited in the mid- to late Jurassic. Original salt thickness may have reached 2,500 ft (760 m) or more in the central part of the East Texas Basin (Jackson and Seni, 1983) but was probably no greater than 2,000 ft (600 m) over the Sabine Uplift, based on the absence of large salt structures there. Late Jurassic deposits include about 100 ft (30 m) of Norphlet clastics overlain by relatively thin mud and carbonate deposits, the Smackover and Buckner Formations and the Gilmer Limestone of the Louark Group (Jackson and Seni, 1984b). Final thickness of Louark Group deposits reached about 1,500 ft (460 m) over the Sabine Uplift.

Near the end of Jurassic time a thick clastic wedge, the Cotton Valley Group, was deposited as a delta system in the northern parts of the East Texas and North Louisiana basins; equivalent inner shelf deposits extended into the central parts of the basins and across the Sabine Uplift area (Anderson, 1979). Erosion of Cotton Valley sediments took place in updip areas before and perhaps during progradation of the younger Travis Peak Formation, but evidence of a Cotton Valley/Travis Peak unconformity in the East Texas Basin, over the Sabine Uplift, or in the North Louisiana Basin is unsubstantiated (Saucier, 1985; Johnson, 1958).

Lower Cretaceous Depositional History

Saucier (1985) interpreted the Travis Peak Formation as a fluvial-deltaic depositional system. Major depocenters trend southeast in the eastern East Texas Basin and southwest in northeastern Louisiana. Marine shelf muds were deposited in

the North Louisiana Basin. Saucier's (1985) highly interpretive map of the Travis Peak - Sligo isopach interval (fig. 27) shows gradual thickening from northwest to southeast across East Texas, away from the northwest source direction. A major feature of this map is the Gibsland salt withdrawal basin in north-central Louisiana.

In this study, the lowest isopach interval mapped was the Pine Island, James, and Rodessa interval (fig. 28), which shows gradual thickening to the east and to the southeast. McFarlan's (1977) two regional cross sections, crossing the East Texas Basin and the North Louisiana Basin from north to south (fig. 29), indicate a facies change in the Pine Island, James, and Rodessa interval from outer shelf (skeletal, oolitic, and pelletal limestone) in the East Texas Basin to middle and inner shelf (micritic skeletal, oolitic, and pelletal limestone and shale) in the North Louisiana Basin. Eastward thickening may therefore be caused by more rapid subsidence in the North Louisiana Basin than in Texas. Irregular contours on figure 28 that occur in the southwest corner, in Panola County, and in Bossier Parish can probably be attributed to early growth of salt structures (see section on salt structures).

The Massive Anhydrite and upper Glen Rose isopach map (fig. 30) shows the same gradual thickening to the east as the lower Glen Rose units (fig. 28). Dome-shaped features in Caddo and Bossier Parishes are interpreted to be salt structures, as are the areas of thin sediments over the northeastern corner of Panola County and in southwest De Soto Parish. Thinning along the southern margin of the study area is due to reef formation at the Cretaceous shelf edge, a condition that persisted during deposition of much of the Lower Cretaceous (Siemers, 1978). Detailed facies maps by Pittman (1985) show substantial thinning of the Massive Anhydrite in this area as it merged into the Glen Rose reef. Upper Glen Rose deposits in East Texas and Louisiana are middle and outer shelf carbonates, merging into prodelta facies in north-central Louisiana (McFarlan, 1977) (fig. 29).

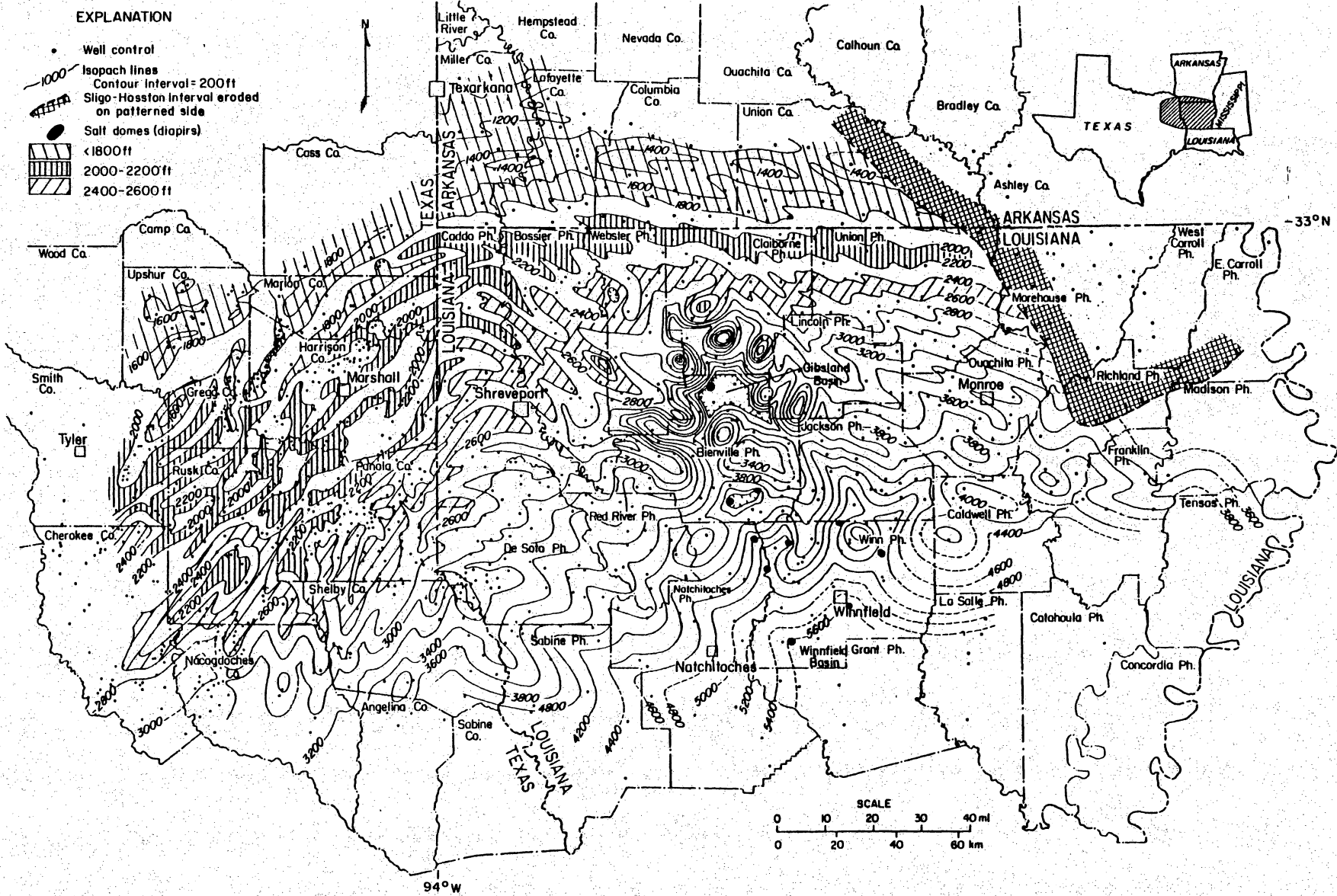


Figure 27. Stratigraphic section for the Sabine Uplift area. Adapted from Braunstien and others (in press).

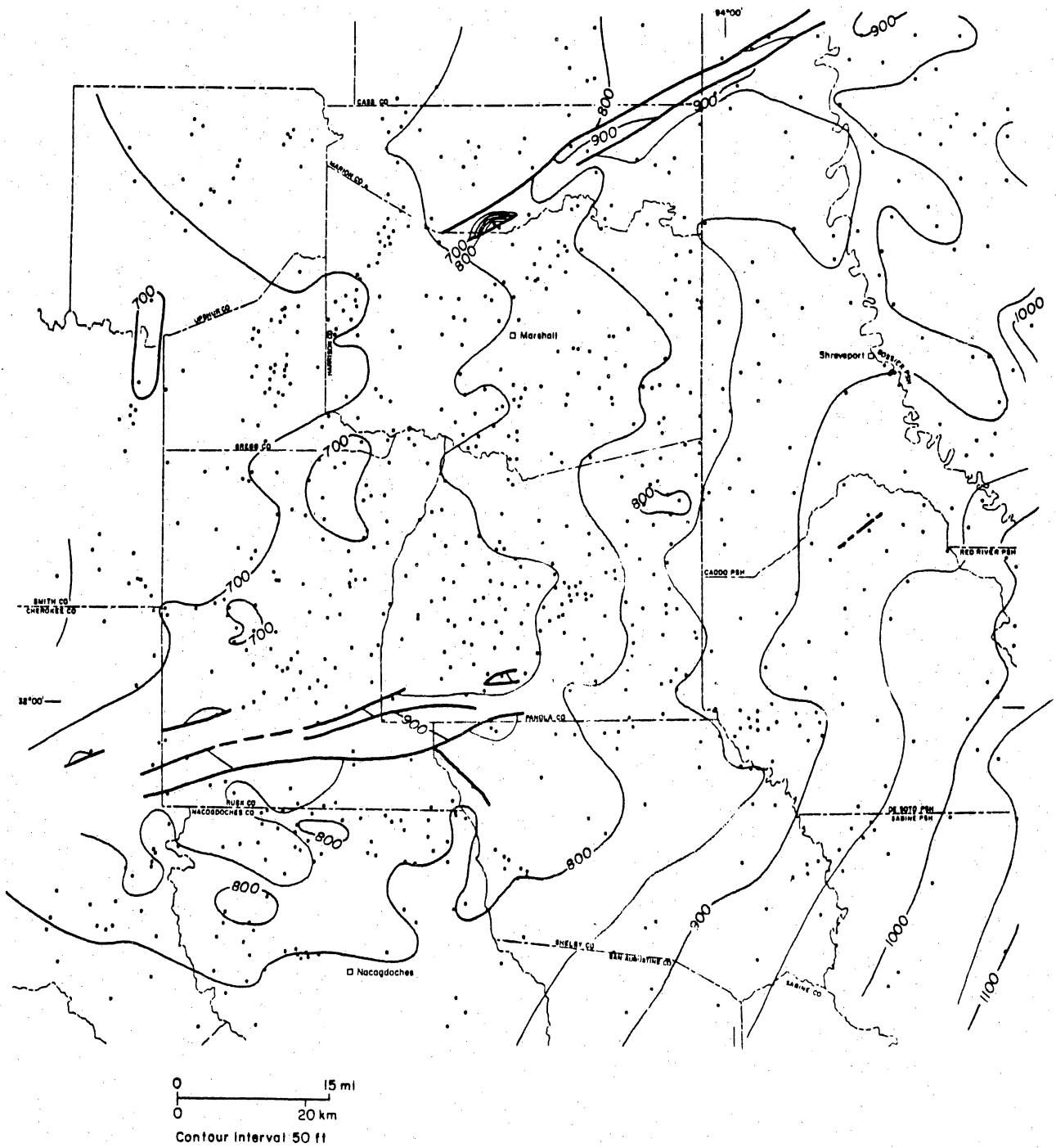


Figure 28. Isopach map of the Pine Island, James, and Rodessa Members of the Trinity Group, Sabine Uplift area.

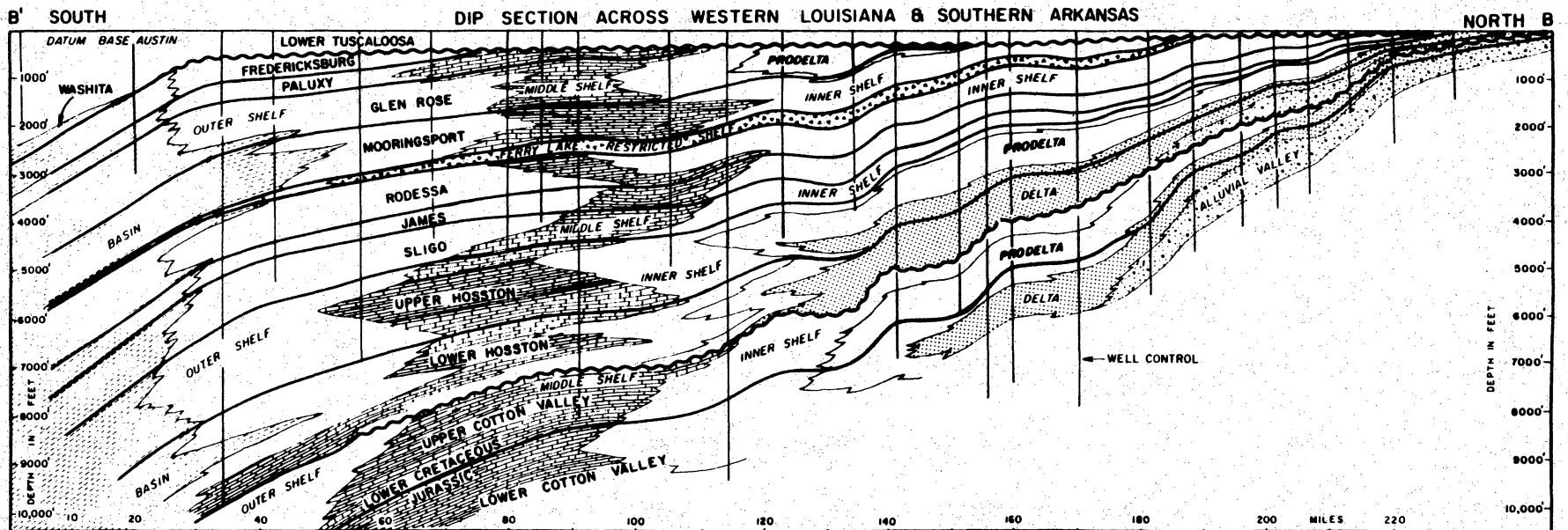
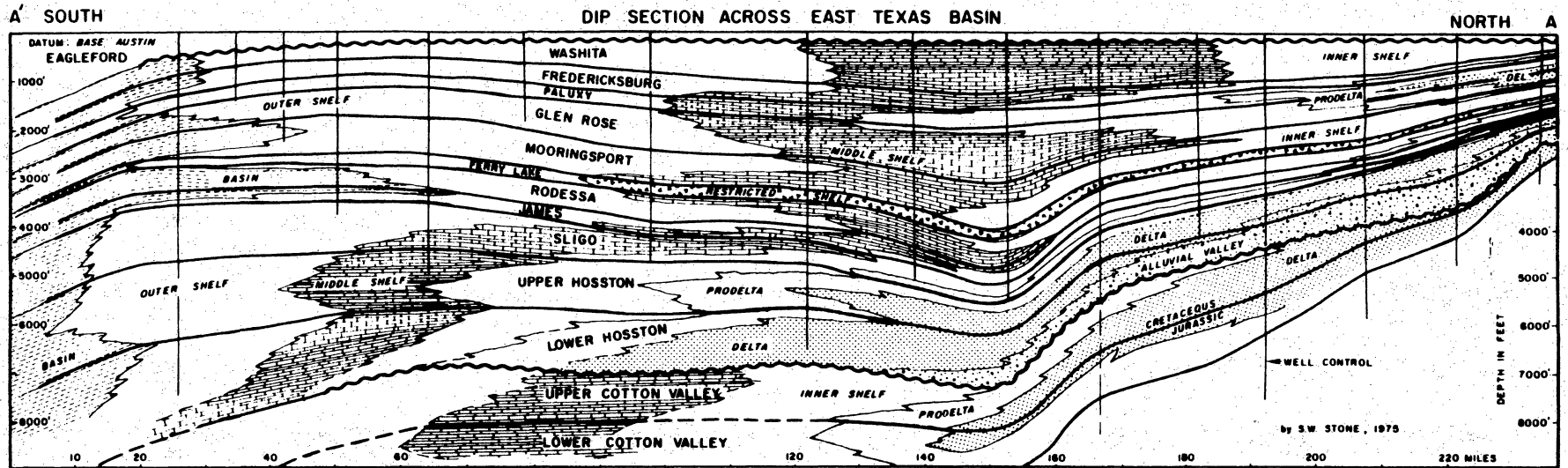


Figure 29. Representative stratigraphic dip sections across East Texas and western Louisiana. Cross-section locations on figure 19. From McFarlan (1977).

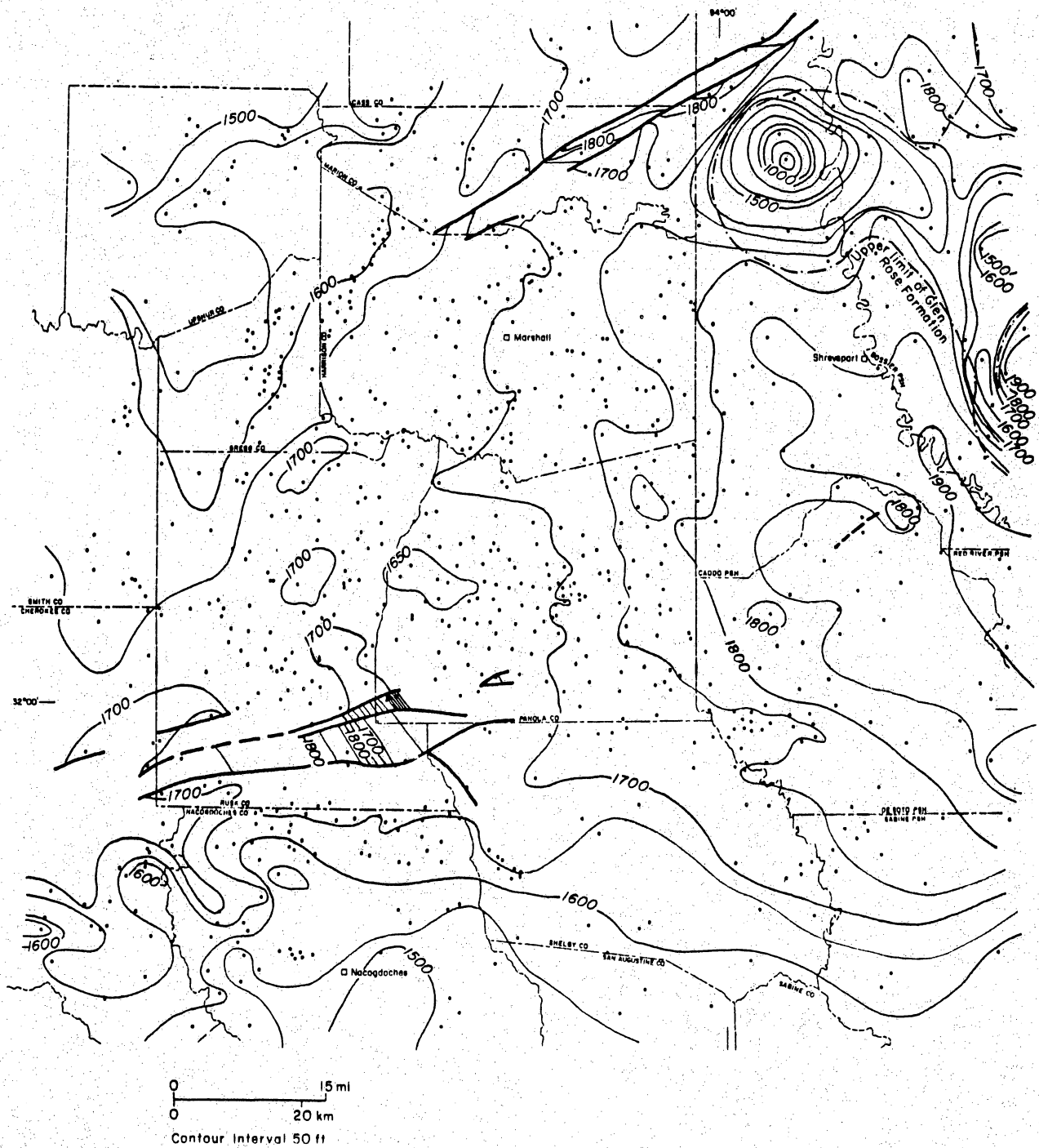


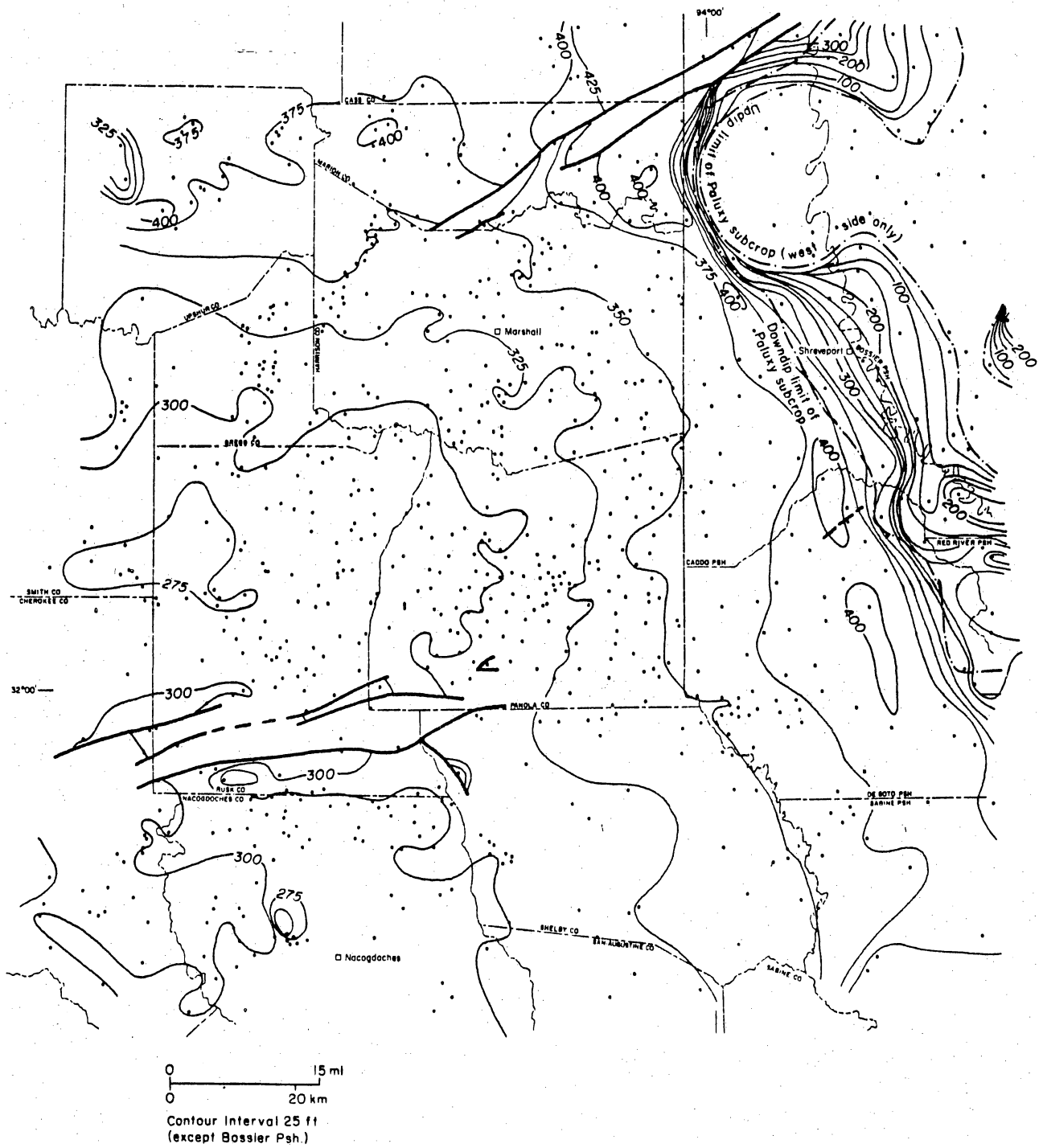
Figure 30. Isopach map of the upper Glen Rose and Massive Anhydrite, Sabine Uplift area.

The isopach map of the Paluxy Formation (fig. 31) shows that the formation thickens to the east until it reaches the downdip limit of the subcrop, east of which erosion of the Paluxy has resulted in thinning and absence of the unit. A slight thickening of the Paluxy Formation may be observed toward the northwest, near the source area (Caughey, 1977). The Paluxy unit is only recognized as a formation in sandstone and shale facies in and north of Smith, Rusk, and Panola Counties, and in Caddo Parish. South of this region facies equivalents are shales, marls, and limestones of the Walnut Formation shelf deposits (Caughey, 1977; McFarlan, 1977). Thinning in Cherokee and Upshur County is caused by salt structures. These counties are in the low- and intermediate-amplitude salt pillow provinces of Seni and Jackson (1984b). Also notice that the contour interval used on this map is half that used on figures 28 and 30; the Paluxy has a nearly uniform thickness across the study area.

In northwestern Louisiana the Tuscaloosa sand overlies both the Paluxy and upper Glen Rose Formations in erosional contact. Sands in both the Paluxy and upper Glen Rose Formations and the complexity of salt structures in Caddo and Bossier Parishes make the Tuscaloosa sand difficult to map using electric logs in these parishes. Therefore, Tuscaloosa-equivalent strata were grouped with the underlying formation, either Paluxy or upper Glen Rose.

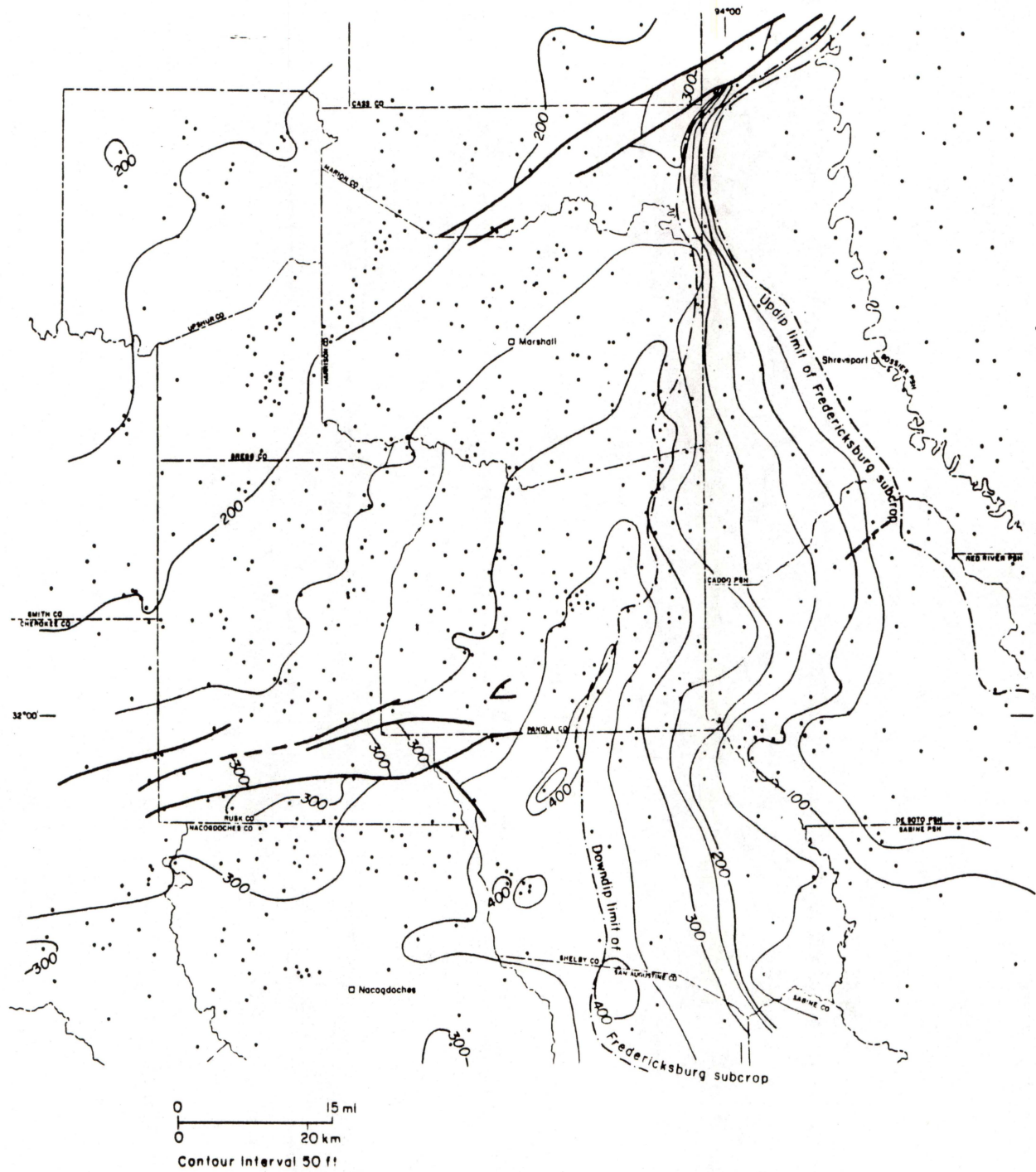
The Fredericksburg interval, composed of outer and middle carbonate shelf deposits (McFarlan, 1977) (fig. 29), thickens gradually to the southeast into Panola County (fig. 32). Similar to trends on the Paluxy map (fig. 31), the Fredericksburg Group thickens to the downdip limit of the subcrop and then thins eastward because of erosion.

The erosional remnants of the Washita Group outer and middle carbonate shelf deposits (McFarlan, 1977) (fig. 29) thicken westward away from the Sabine Uplift (fig. 33). Only on the eastern edge of the East Texas Basin is a complete thickness



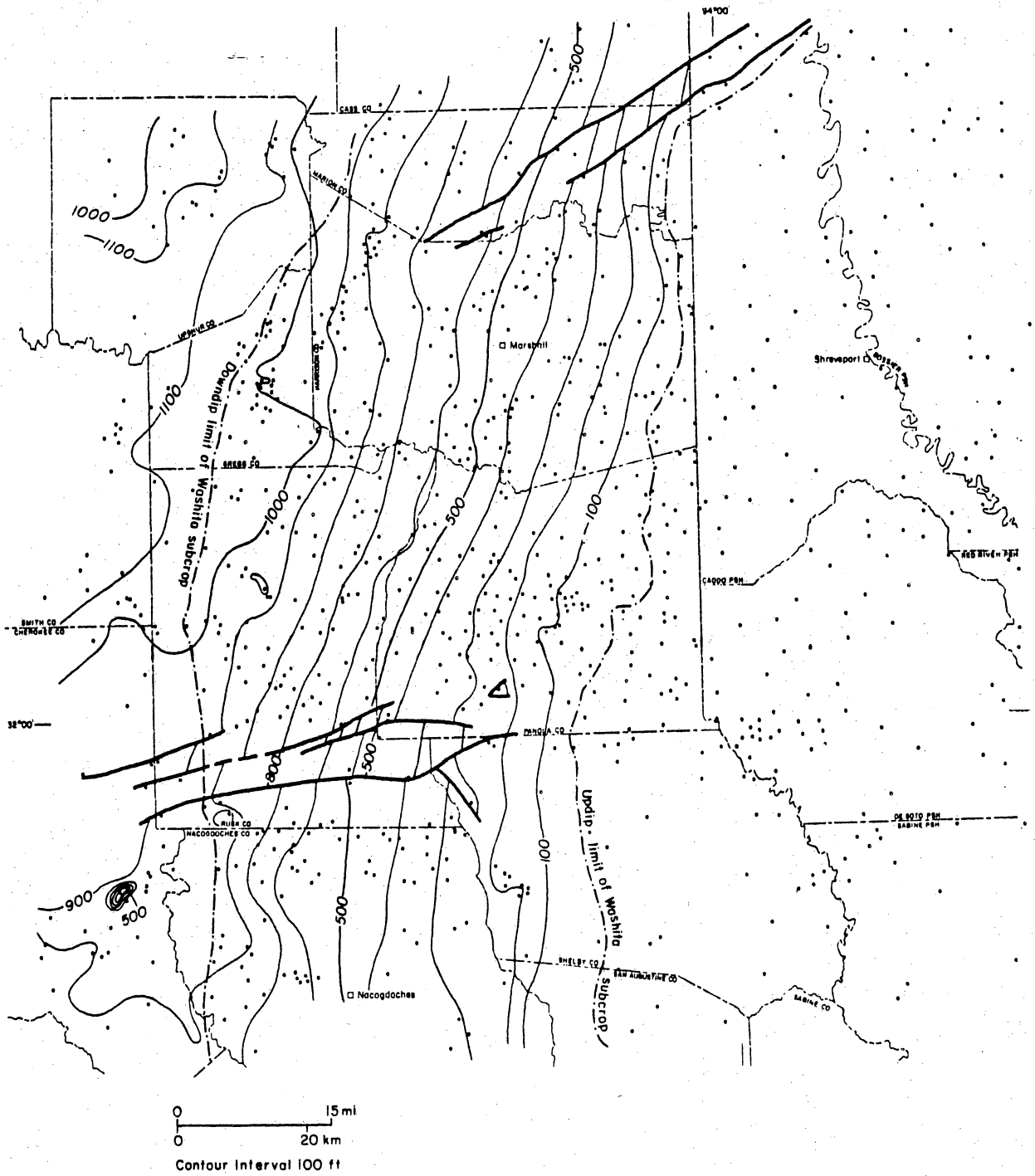
QA 7013

Figure 31. Isopach map of the Paluxy Formation, Sabine Uplift area.



QA 7022

Figure 32. Isopach map of the Fredericksburg Group, Sabine Uplift area.



QA 7015

Figure 33. Isopach map of the Washita Group, Sabine Uplift area. Downdip limit of the Washita Group subcrop is the updip subcrop limit of the Woodbine Group.

of the Washita Group present, and here the unit thickens 200 ft (60 m) from south to north, in the opposite direction from the trends of underlying intervals. Salt-cored uplifts near the Cherokee-Nacogdoches County boundary and in central Rusk County are evident, and thinning to the northwest in Upshur County is also caused by salt mobilization (Seni and Jackson, 1984).

Basal Upper Cretaceous Depositional History

The basal Upper Cretaceous Woodbine Group was mapped in detail by Oliver (1971), and was interpreted as a high-destructive delta system, derived from the northeast, that prograded into the East Texas Basin. The thickest part of the Woodbine reaches 400 feet (120 m) in Smith and adjacent Henderson Counties (Oliver, 1971). Time-equivalent strata on the eastern side of the Sabine Uplift are Tuscaloosa sands (Forgotson, 1958), extending across north-central Louisiana at an average thickness of 200 ft (60 m) (Hazzard and others, 1945a). The Tuscaloosa Group thickens basinward into central Louisiana and Mississippi to more than a thousand feet (Hazzard and others, 1945a). South and east of Cherokee County, in the East Texas Basin, the Woodbine sand facies merges into a prodelta unit designated the Pepper Shale (Oliver, 1971). This unit extends eastward and is the downdip facies equivalent of the Tuscaloosa Group in Louisiana (Anderson, 1979).

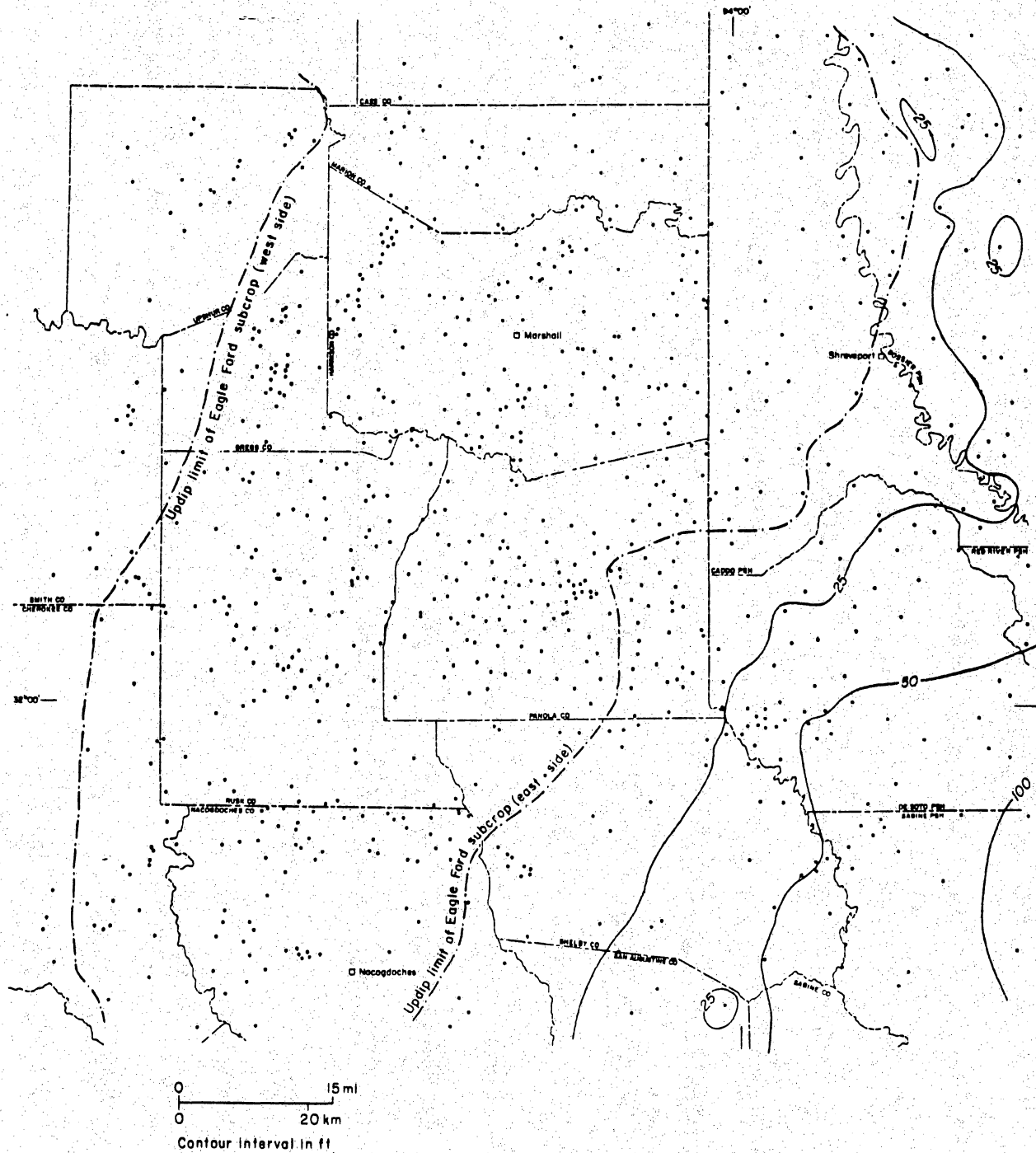
The Woodbine Group subcrops along the eastern edge of the Sabine Uplift, beginning at the downdip limit of the Washita Group subcrop (fig. 33), and extends to the west side of the East Texas Basin where it outcrops. The lower contact of Woodbine and Tuscaloosa sands is unconformable in northern Texas and Louisiana. South of the East Texas Basin, in Tyler County, the Woodbine interval is conformable to the underlying Washita Group and to the overlying Eagle Ford (Siemers, 1978).

The marine Eagle Ford Group lies above the Woodbine (fig. 24). This unit is less than 100 ft (30 m) thick in the study area (fig. 34) and extends across northern Louisiana with thicknesses of 100 to 200 ft (30 to 60 m) (Hazzard and others, 1945a). The Eagle Ford reaches 400 ft (120 m) in thickness in the East Texas Basin (Oliver, 1971). Eagle Ford sediments represent shelf deposits that formed as the East Texas Basin subsided (relative to sea level) following Woodbine deposition.

The Eagle Ford Group is conformable with the Woodbine Group in the central East Texas Basin and pinches out against Woodbine sediments on the east side of the Sabine Uplift (Gussow, 1973). In contrast, the Eagle Ford overlaps both Woodbine and older Buda sediments on the west edge of the East Texas Basin (Stephenson, 1927) and Tuscaloosa sand on the west edge of the North Louisiana Basin (Granata, 1963). In south and central Texas and in Louisiana the Eagle Ford is conformable with the Austin Group (Waters and others, 1955; Anderson, 1979).

A separate mid-Cretaceous deltaic unit, the Harris Sand, was deposited on the western flank of the Sabine Uplift. It has been correlated with both Woodbine and Eagle Ford deposits and may contain eroded Woodbine sediments (Oliver, 1971). Buda, Woodbine, and Eagle Ford ammonites are closely related, making age determinations difficult; all three units were once considered to be Cenomanian in age (Sellards and others, 1932).

Nichols (1964) shows truncation of Eagle Ford sediments in the southwestern part of the East Texas Basin and states that the Eagle Ford was eroded before the Austin was deposited. If Eagle Ford shales covered Woodbine and Harris sands on the west side of the Sabine Uplift, then erosion must have removed the Eagle Ford there before Austin deposition (compare figs. 33 and 34). Nichols' (1964) areas of Eagle Ford truncation may coincide with salt diapirs, however, many of which have no Eagle Ford over their tops (Jackson and Seni, 1984a). Gussow (1973), apparently



QA 7020

Figure 34. Isopach map of the Eagle Ford Group, Sabine Uplift area.

basing his observations on detailed electric-log correlations, states that there was little or no erosion of the Eagle Ford. If this is so, then updip Harris and Woodbine sands were never covered with Eagle Ford clay, and perhaps not submerged, until deposition of the Ector Chalk began.

Upper Cretaceous and Tertiary Depositional History

Granata (1963) made isopach maps of the Upper Cretaceous carbonate shelf deposits, comprising the Austin, Taylor, and Navarro Groups. Granata's map of the Austin Group shows thinning over the area of the Sabine Uplift. The Taylor Group is very uniform in thickness across the uplift region, but biogenic deposits are abundant over the Sabine Uplift (Stehli and others, 1972). The Navarro Group thickens sourceward to the north, where the carbonate facies become sandy.

The Cretaceous-Tertiary boundary lies above the Kemp shale, a few hundred feet above the Nacatoch Sand and below the Midway Group (Wood and Guevara, 1981a) (fig. 24). This period of time was marked by worldwide retreat of the seas (Vail and others, 1977); a break in faunal assemblages exists at the Navarro-Midway outcrop (Sellards and others, 1932) and a period of subaerial erosion may have occurred in updip regions before the Midway was deposited (Young, 1972). Midway shales cannot be distinguished from Navarro Group shales on an electric log, however. Midway strata and upper Navarro shales thicken by only a few hundred feet from Rusk County into the East Texas Basin (Wood and Guevara, 1981b). The shales were deposited in about 300 ft (90 m) of water (Sellards and others, 1932).

Wilcox continental deposits accumulated over broad regions in Texas and Louisiana (Fisher and McGowen, 1967; Galloway, 1968). Accurate Wilcox thickness estimates over the Sabine Uplift cannot be made because the basal Wilcox contact is

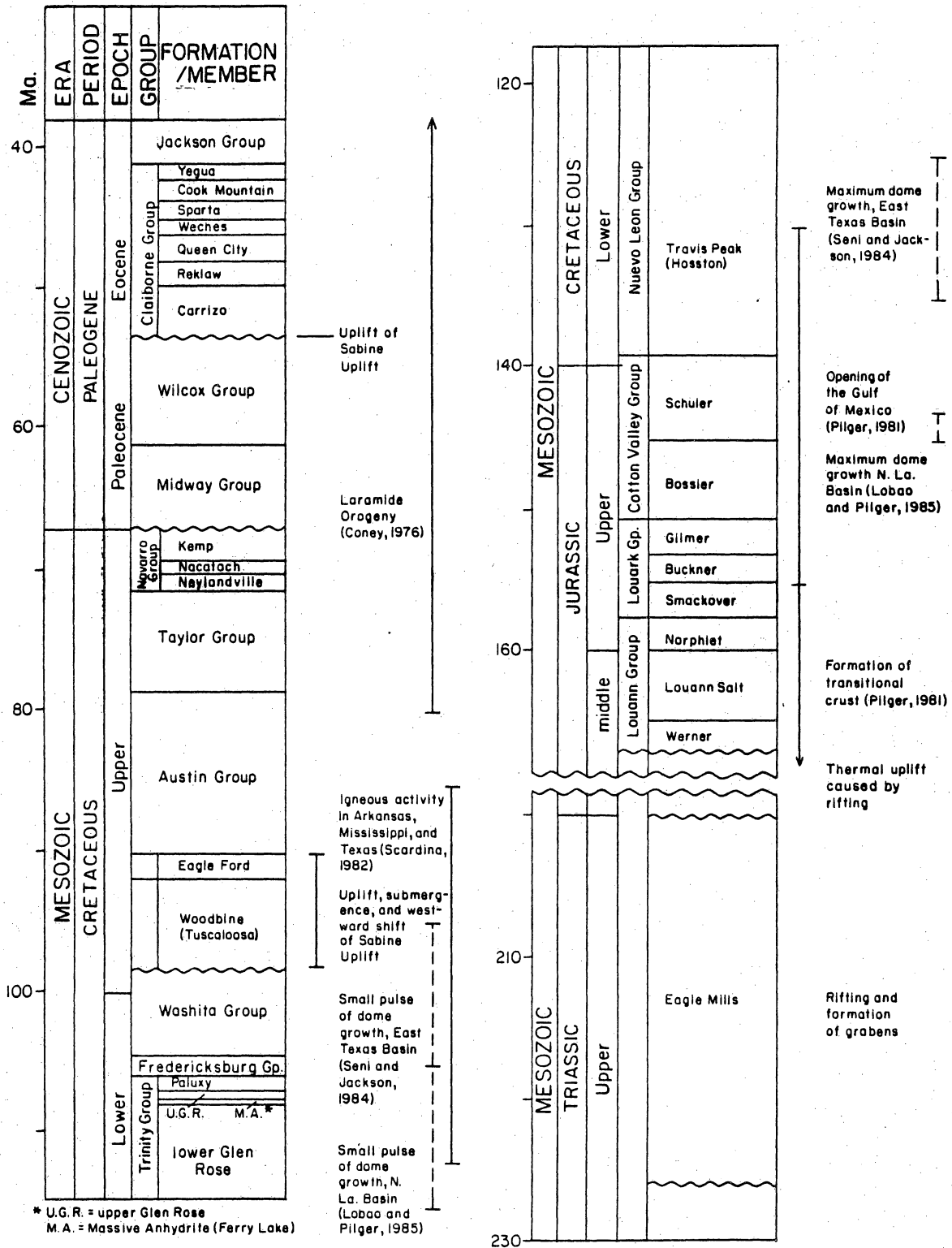
gradational and time-transgressive, and the upper contact, where present, is erosional. However, thick (greater than 6 ft, 2 m) lignite deposits on the south flank of the Sabine Uplift (Kaiser and others, 1986) indicate that major Wilcox fluvial axes bypassed the Sabine Uplift. Therefore, original Wilcox deposits over the Sabine Uplift may have been thinner than the adjacent basin deposits.

After a period of erosion, sedimentation continued in the Claiborne with deposition of the Carrizo Sand in northeast Texas. The Sabine Uplift did not receive sediment during Queen City time (Hobday, 1980), but nearshore sediments were deposited on its flanks during Weches time (Eckel, 1938). Sparse data indicate low sand percentages and strike-trending sand bodies in Late Eocene sediments that lie south of the Sabine Uplift, indicating low levels of sediment input across the uplift region (Kaiser and others, 1980). Depositional rates continued at low levels in the area until denudation began in the Late Tertiary.

MESOZOIC AND CENOZOIC STRUCTURAL HISTORY

Late Jurassic and Early Cretaceous Events

Initial rifting of the Gulf of Mexico formed a shallow evaporite basin (180-155 mya) (fig. 35), which subsided slowly through the early Late Jurassic. The Sabine Uplift area received thinner Louann and Louark deposits than surrounding areas. Late Jurassic Cotton Valley deltas initiated rapid subsidence of the Sabine Uplift area, and this depositional style was continued during the deposition of the Travis Peak. Maximum rates of salt diapirism occurred during this time. Basin configuration revealed by Cotton Valley and Travis Peak lithofacies and isopach maps (Saucier, 1985; Anderson, 1979) shows that the Sabine Uplift was not a structural high during



* U.G.R. = upper Glen Rose
M.A. = Massive Anhydrite (Ferry Lake)

EXPLANATION

┆ Tectonic events ┆ Salt-related events

QA 7033

Figure 35. Tectonic and salt-related events in the Sabine Uplift area. Time scale adapted from Braunstien and others (in press).

this time, but was a site for lower delta plain deposition. Regional slope of the basin floor from the East-Texas Basin across the Sabine Uplift area and still deeper into the North Louisiana Basin persisted during late Early Cretaceous carbonate and minor clastic deposition (Glen Rose Formation, Paluxy Formation, and Fredericksburg Group). This can be seen by comparison of figures 28 (lower Glen Rose) and 30 (upper Glen Rose) with figure 36 (Glen Rose) and comparison of figure 31 (Paluxy) with the stratigraphically equivalent figure 37. The eastward deepening is also shown by the greater thickness of sediment present in the North Louisiana Basin than in the East Texas Basin (fig. 29). Thickening of Glen Rose, Paluxy, and Fredericksburg sediments occurred regionally from the Mexia-Talco fault zone area in the north and west to the North Louisiana Basin in the south and east.

Arching at the End of the Early Cretaceous

A broad arch formed at the end of the Early Cretaceous (fig. 35), uplifting sediments in an elongate region extending from the Sabine Uplift area to northeast Louisiana. The highest part of this structure was at the Monroe Uplift (fig. 27). The complete sequence of Lower Cretaceous sediments was removed in the North Louisiana region, and Cotton Valley Group sediments were exposed at the surface (Johnson, 1958). Erosion of approximately 1,200 ft (370 m) of sediment occurred over the Sabine Uplift area, removing the Lower Cretaceous sequence down to the Glen Rose (fig. 38), and tilting the remaining strata gently toward the west. This arching event was coincident with a postulated worldwide sea-level drop (Vail and others, 1977), which marks the end of Lower Cretaceous deposition in East Texas and Louisiana. At the end of this erosional period, the Sabine Uplift was probably at or slightly below sea level (Halbouty and Halbouty, 1982).

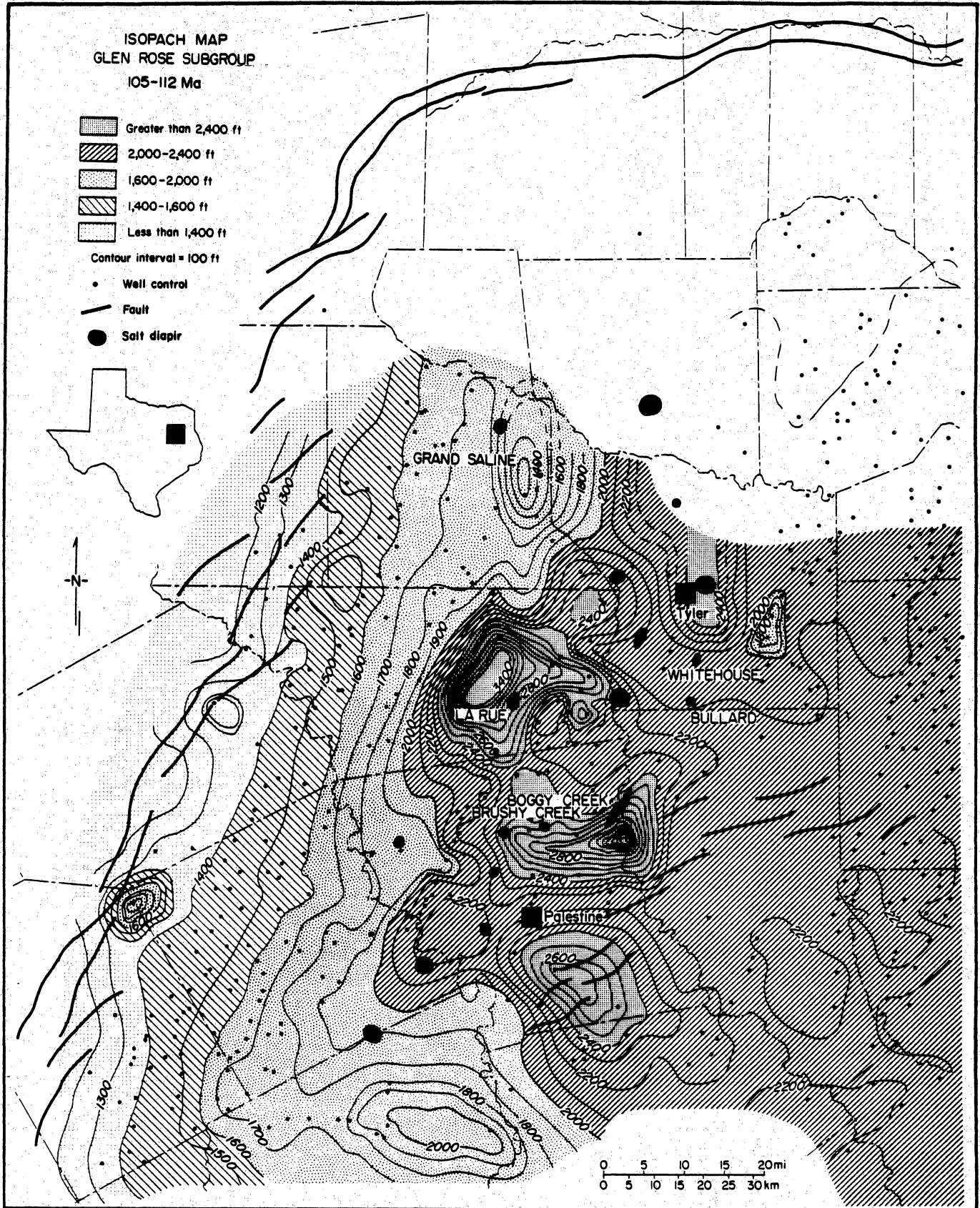


Figure 36. Regional isopach map of the Glen Rose Subgroup, East Texas Basin. From Seni and Jackson (1984).

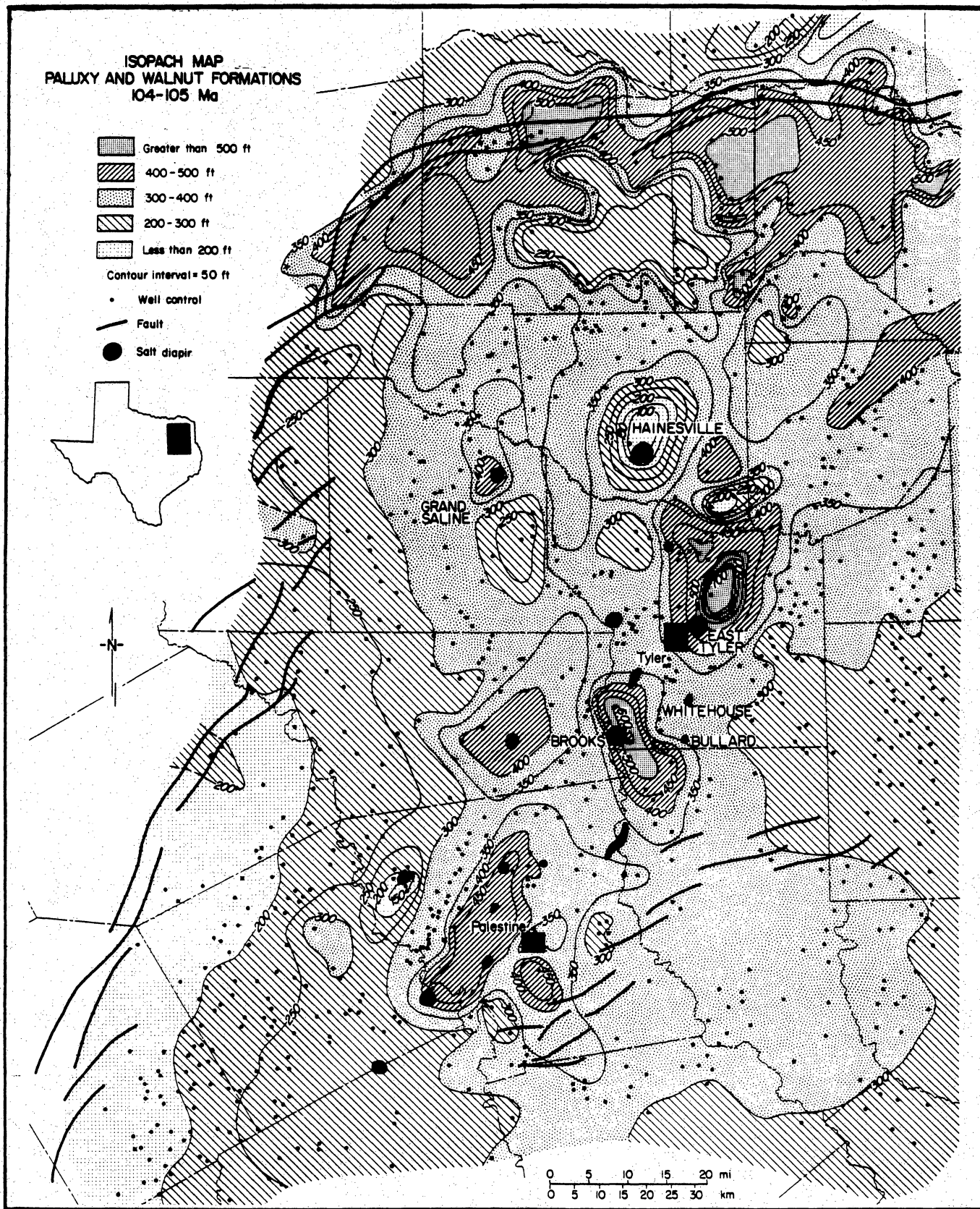


Figure 37. Regional isopach map of the Paluxy Formation, East Texas Basin. From Seni and Jackson (1984).

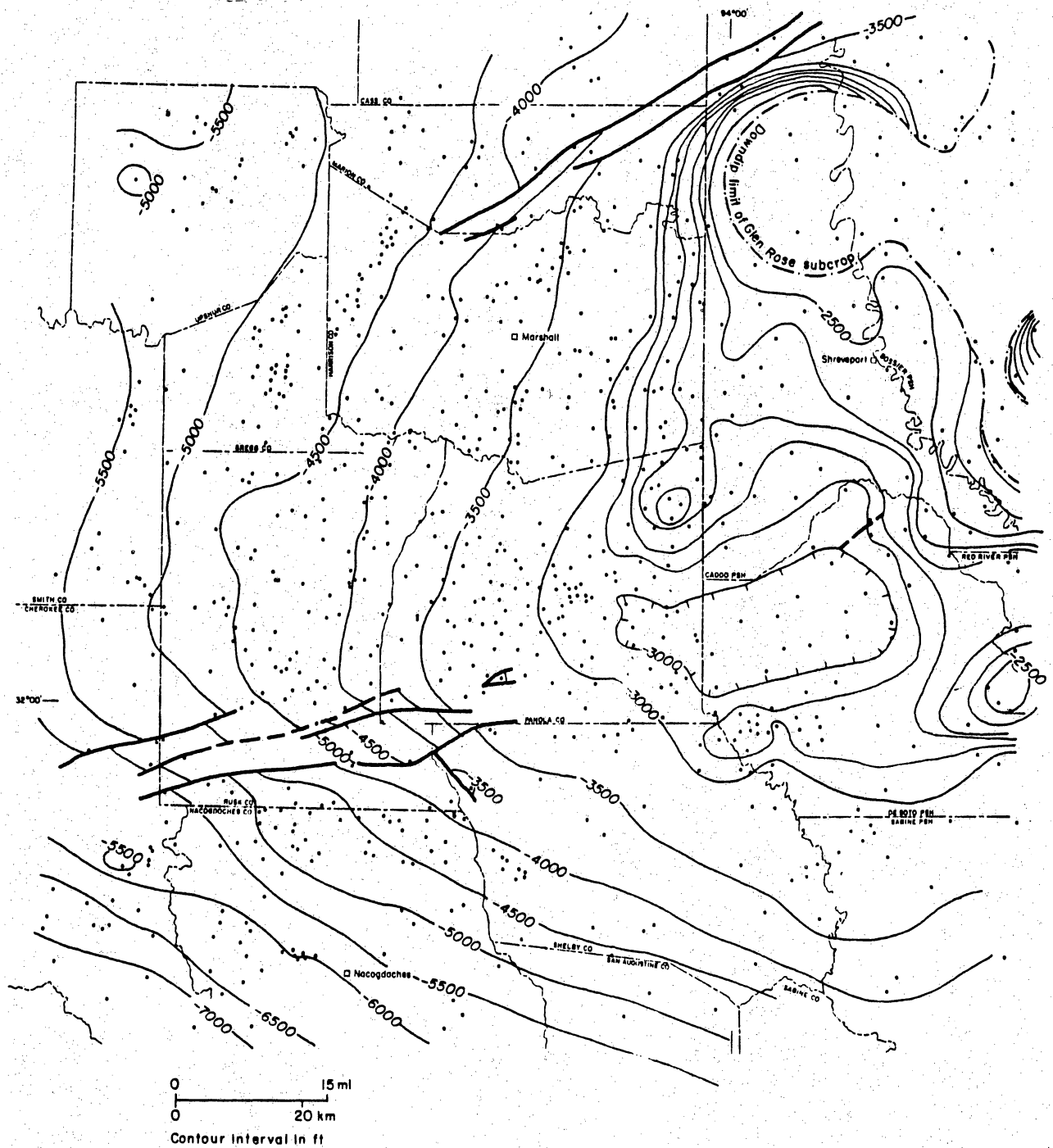


Figure 38. Structure map on the top of the upper Glen Rose Formation, Sabine Uplift area.

A smaller emergent episode (or episodes) occurred following the major pre-Woodbine uplift and submergence. Many versions of this period of Cenomanian-Turonian depositional history have been published (table 7). A possible sequence of events begins with deposition of the Woodbine Formation across a barely submergent Sabine Uplift. Although the Woodbine is not present across the area today, Oliver (1971) reported that the uplift area was not a barrier to longshore currents until near the end of Woodbine deposition. At this time the Sabine Uplift became subaerially exposed, and the Harris deltas formed on the west flank. It is not known if Eagle Ford deposits extended over the Sabine Uplift, but if Harris deltas are early Eagle Ford in age, the Eagle Ford sea probably did not cover the uplift until late Turonian time, if at all.

A second low-amplitude emergence may have occurred at the end of Eagle Ford time, during which Eagle Ford sediments were eroded from the west flank of the Uplift, exposing Woodbine sediments.

The simultaneous onlapping (east) and offlapping (west) position of the Eagle Ford Group on the Sabine Uplift implies that the structural axis of uplift shifted between Woodbine and Eagle Ford time. Development of Harris deltas in the Eagle Ford-Woodbine sea (with possible updip erosion of Woodbine-age sediments) on the west side of the Sabine Uplift and transgression of the Eagle Ford sea (onlapping the Woodbine) on the east side of the uplift suggests that the axis of uplift shifted to the west (Granata, 1963; Oliver, 1971).

The time span from the end of Buda deposition to the beginning of Woodbine Group deposition, encompassing the major mid-Cretaceous arching event, may have lasted only 1 m.y. (fig. 35). The actual amount of uplift and its effect on the underlying sediments was smaller than is apparent from the structure maps. The palinspastic map constructed on the base of the Massive Anhydrite shows the

Table 7. References pertaining to mid-Cretaceous erosional history on the Sabine Uplift.

Author	Unconformities present (in East Texas Basin or on Sabine Uplift)			Timing of erosion of 1,200 ft of Cretaceous sediments	
	Wb/Cret	EF/Wb	Aust/EF ⁺	pre-Woodbine	other
Anderson, 1979	yes	yes	yes	x	
Bailey and others, 1945	yes	--#	--	--	
Bornhauser, 1958	--	--	yes		after Woodbine
Forgotson, 1958	yes	--	--	x	
Granata, 1963	yes	yes	yes	x	
Gussow, 1973	yes	no	no	x	
Halbouty and Halbouty, 1982	yes	no	yes	x	
Hazzard and others, 1945a	yes	yes	yes	x	
Nichols, 1964	yes	yes	yes	x	
Nichols and others, 1968	yes	no	yes		during & after Eagle Ford
Oliver, 1971	yes	yes	--	x	
Siemers, 1978	*	*	*	--	
Stephenson, 1927	yes	*	yes	x	
Waters and others, 1955	yes	no	yes	x	

* in some areas

+ Wb = Woodbine, Cret = Cretaceous, EF = Eagle Ford, Aust = Austin

#--not addressed by authors

structural configuration prior to deposition of the Austin Group (fig. 39). Steep dips at the Angelina-Caldwell Flexure Zone, produced by Cenozoic deltaic sediment loading, did not exist at the end of the lower Cretaceous. Dip on the palinspastic surface is about 5 ft/mi (1 m/km); the arching was a low-amplitude movement.

Late Cretaceous and Tertiary Events

Lithofacies and biofacies maps indicate that the Sabine Uplift area was "generally positive," although submerged, throughout the Upper Cretaceous (Stehli and others, 1972; Stehli and Creath, 1964). The Angelina-Caldwell Flexure Zone was also a relatively high area at this time (Stehli and others, 1972). The uplift subsided slowly through Midway deposition and slightly faster during Wilcox time. Subsidence of the Angelina-Caldwell Flexure Zone probably began with the advancement of Wilcox deltas, which accumulated to thousands of feet in thickness in San Augustine and Sabine Counties.

The Sabine Uplift arched again at the end of Wilcox time (early Eocene), and the strata were tilted in all directions away from the crest of the uplift. Up to 2,000 ft (600 m) of sediment may have been removed from the highest regions of the uplift, according to vitrinite reflectance of a lignite sample from a well in southern Panola County (P. Mukhopadhyay, personal communication, 1986). The arching episode may coincide with a lowstand of sea level that extended east to Georgia (Gibson and Bybell, 1981).

The magnitude of deformation caused by the arching event can be measured by comparing the palinspastic map of the base of the Massive Anhydrite with a structural map of the same horizon (figs. 25 and 39). The magnitude of structural relief produced by the Early Tertiary episode approximately equals the amount produced by the mid-Cretaceous episode; present structural dip is almost double the palinspastic rate.

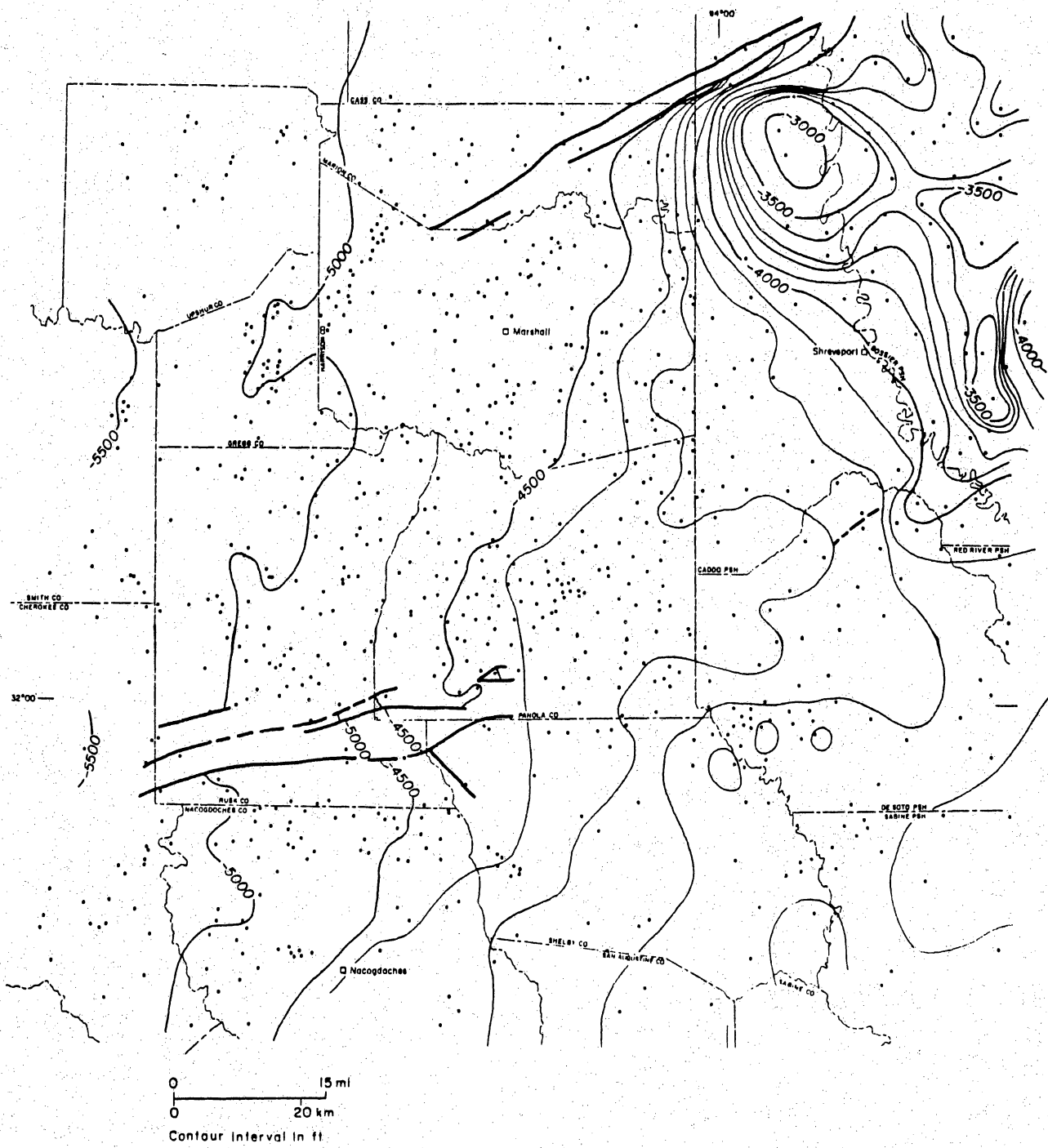


Figure 39. Palinspastic map on the base of the Massive Anhydrite. Sabine Uplift area.

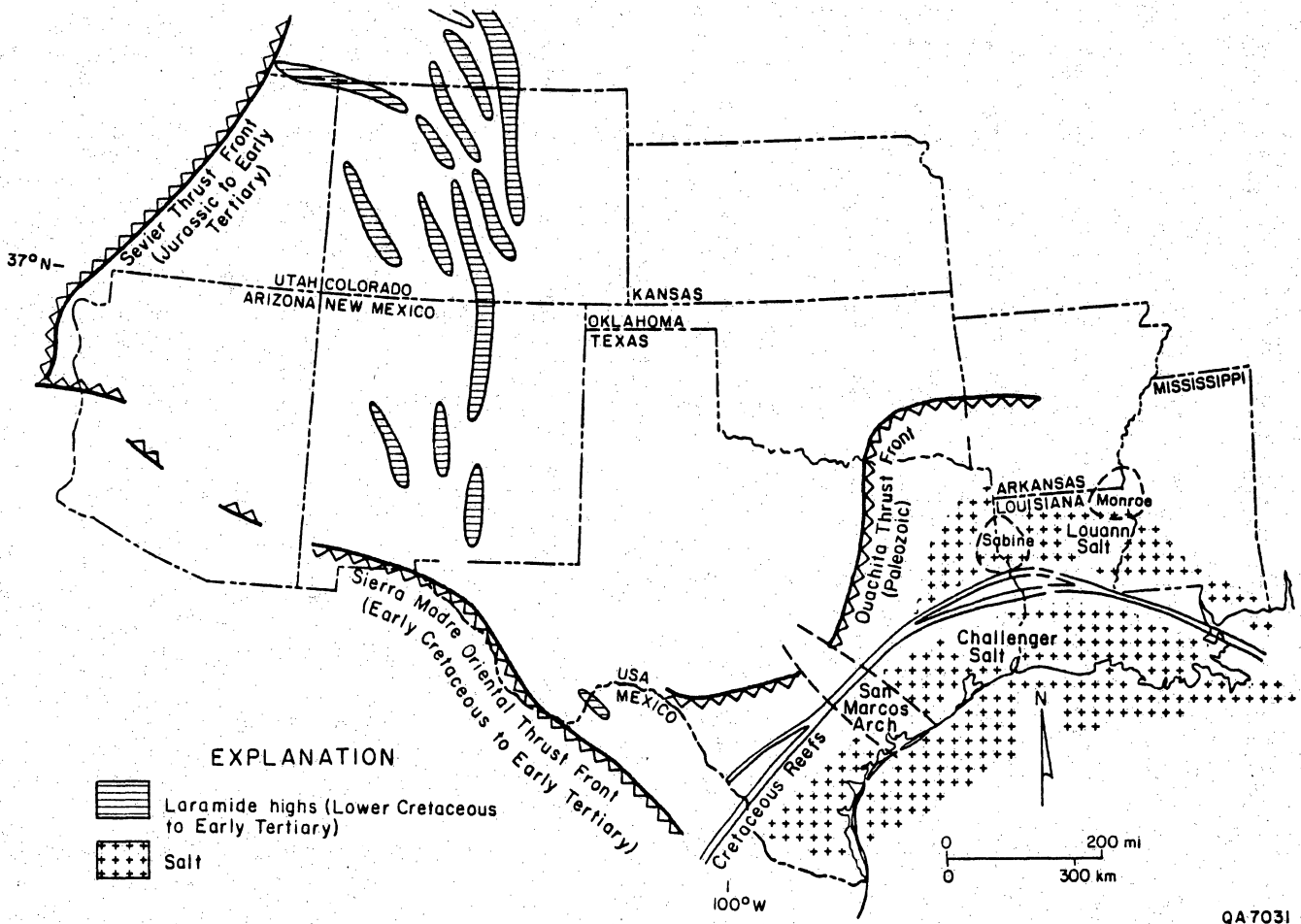
The Sabine Uplift remained a structurally high area through much of the Eocene. The uplift may have been subaerially exposed during deposition of the Queen City Formation and may have acted as a minor sediment source (Hobday, 1980). It was nearly emergent during Weches deposition (Eckel, 1938).

Tertiary sediments thousands of feet thick were deposited in Shelby, San Augustine, and Sabine Counties and along the Texas and Louisiana coasts, resulting in downwarping of the Gulf margin (Murray, 1948). In response to this event, isostatic rebound took place along the landward edge of the Gulf of Mexico. This uplift began in the mid-Tertiary (Seni and Jackson, 1984) and was probably responsible for erosion of any post-Wilcox sediments deposited over the Sabine Uplift.

SALT-RELATED STRUCTURES ON THE SABINE UPLIFT

Jurassic salt was deposited in two major basins, forming the Louann Salt and the Challenger Salt (Seni and Jackson, 1984) (fig. 40). The Louann salt basin can be divided into three inland basins, the East Texas, North Louisiana, and Mississippi. Areas between these basins contain comparatively thin salt. The Louann salt basins are separated from the Challenger Salt to the south by the Lower Cretaceous reef, which lies at the updip edge of the Angelina-Caldwell Flexure Zone.

Halokinesis, or salt movement, has affected sediments over the Sabine Uplift only slightly compared with the effects of the mid-Cretaceous and early Tertiary uplifts. Salt thicker than about 2,000 ft (600 m) will form low-amplitude salt pillows, and thicker salt will form intermediate-amplitude salt pillows and salt diapirs (Jackson and Seni, 1983). The original thickness of salt over the Sabine Uplift was not great enough to produce low-amplitude salt pillows. Based on the absence of large salt structures, therefore, original thickness of salt over the uplift was probably less than 2,000 ft (600 m). Halokinesis in the crestal area of the uplift has, however, produced



QA7031

Figure 40. Structural features in southwestern United States. From Dickinson and Snyder (1978), Seni and Jackson (1984), Reynolds and others (1986), and Ewing (in preparation).

a number of small salt structures (fig. 41). Identification of these features was based on structures visible on structure maps of the intervals studied in this report (figs. 25, 26, 38, 42, and 43). A ring-shaped area of salt structures, beginning at the Pine Island salt pillow on the north, extends southward along a structural ridge to the Waskom anticline, the Bethany anticline, and the Joaquin-Logansport anticline, and then across into Louisiana to the Spider anticline and the Red River - Bull Bayou structure. From there the ring is completed across the Sligo anticline in Bossier Parish. It is very likely that these structural features are salt-cored and were caused by salt movement. The large closed depression in De Soto Parish that is present on structure maps (figs. 25, 26, 38, and 42) is probably a salt-withdrawal basin.

Salt has been penetrated in the Waskom, Bethany, and Joaquin-Logansport areas, but values for total thickness of the salt over the Sabine Uplift is not available in the literature. The Pine Island salt pillow has been drilled through to basement and has a salt thickness of 1,176 ft (358 m) (appendix A). Salt has also been penetrated in two places in the Carthage gas field in Panola County (fig. 41). Although the Carthage structure is extremely low amplitude and larger in areal extent than other salt structures, the circular shape of the structure implies that it was formed by salt movement.

Salt flowage may have affected the Travis Peak Formation either during or after Travis Peak deposition, or both. Sediment thinning over a salt structure may be caused by salt movement during deposition or the presence of a topographic high due to salt movement prior to deposition. The isopach map of the Sligo-Travis Peak interval (fig. 27) shows that the Waskom, Bethany, Carthage, and Joaquin-Logansport salt structures affected Sligo-Travis Peak sedimentation. Growth of these small salt structures probably started before Travis Peak deposition, because salt flowage can begin under relatively low overburden pressure (Hughes, 1968). Hughes (1968) has

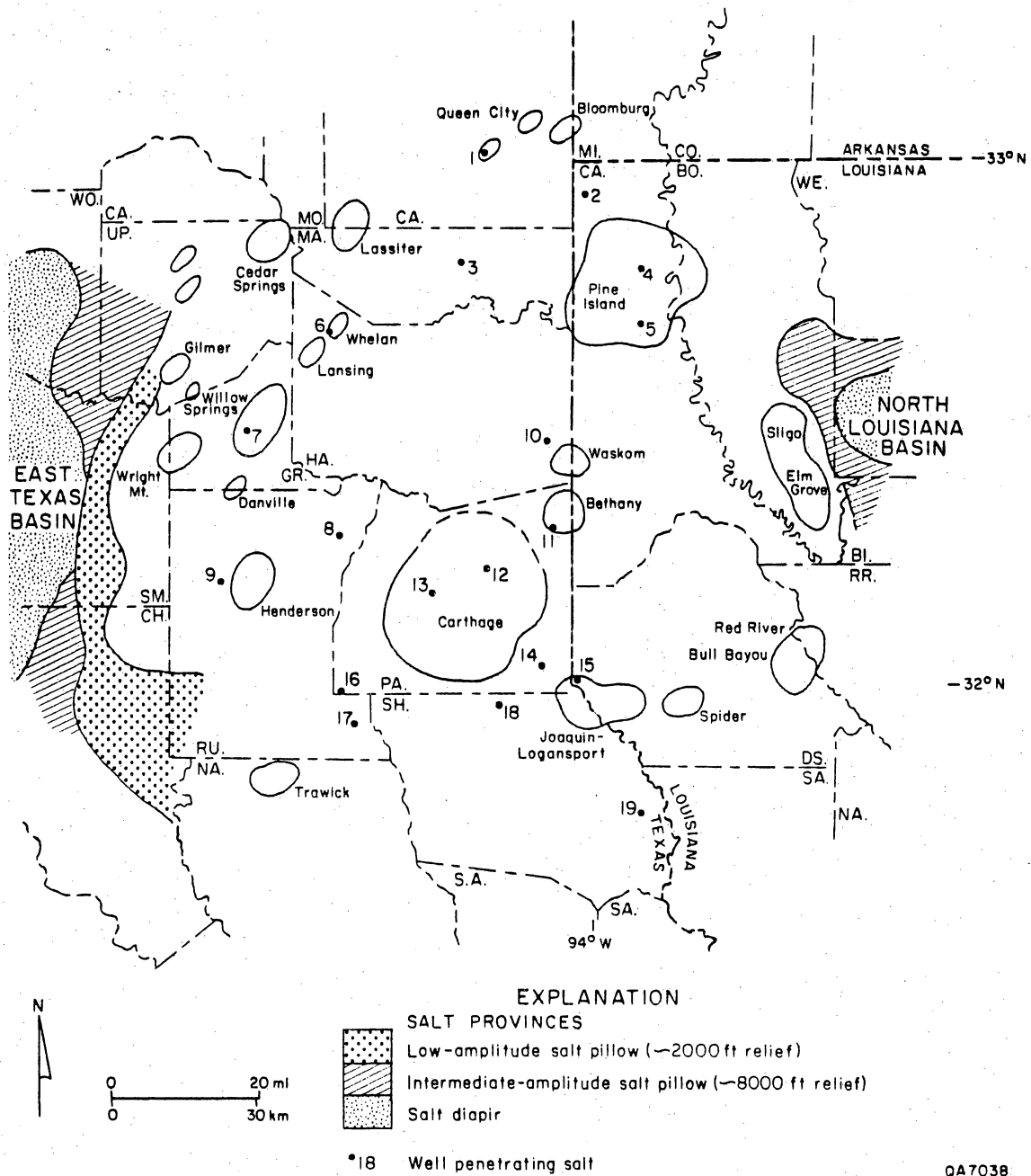


Figure 41. Salt-related structures in the Sabine Uplift area. Names of oil fields associated with some of the structures are shown. Salt structures in Upshur County and vicinity are from Geomap. Salt provinces in Texas from Seni and Jackson (1984); numbered wells are listed in appendix A.

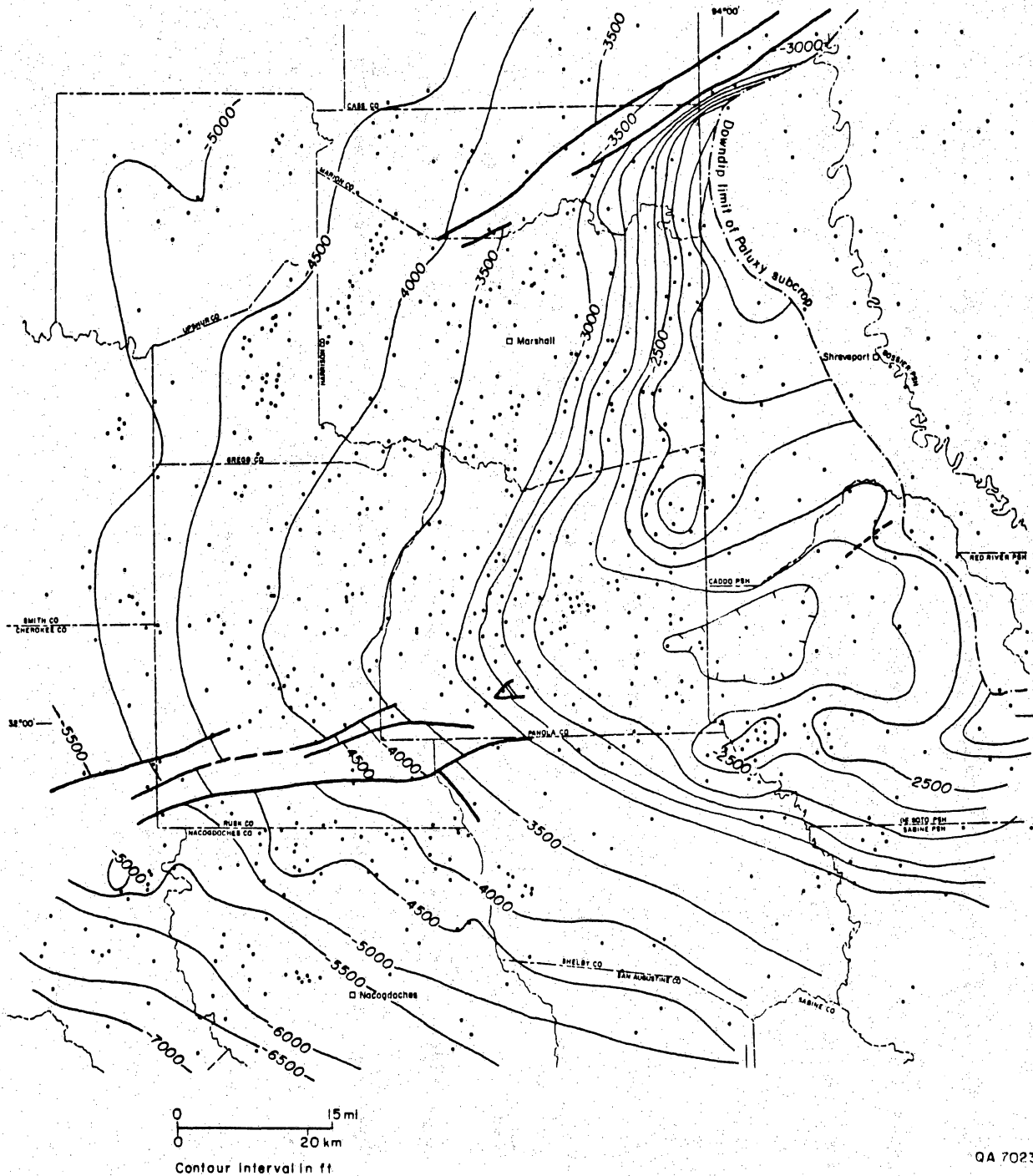


Figure 42. Structure map on the top of the Paluxy Formation, Sabine Uplift area.

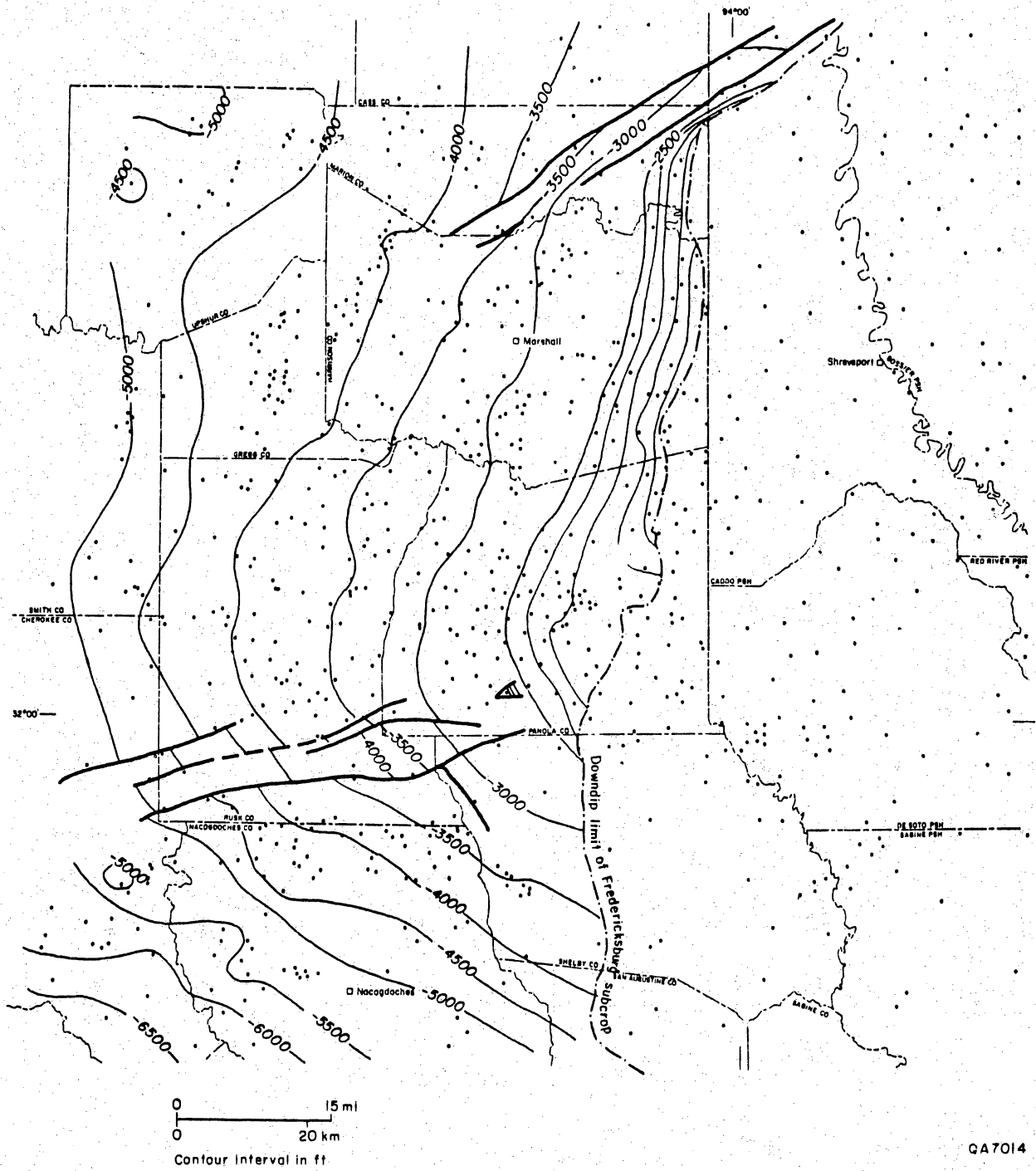


Figure 43. Structure map on the top of the Fredericksburg Group, Sabine Uplift area.

shown that salt structure formation had already begun by the end of Norphlet time in the Mississippi salt basin.

The Pine Island salt pillow did not reach its present size until after the smaller salt structures in the ring had formed. The isopach map of the Sligo-Travis Peak interval (fig. 27) shows that a high in central Caddo Parish is smaller than and lies to the south of the present Pine Island pillow. Only a hint exists of the other small salt structures over the uplift. The isopach map of the next highest interval, the lower Glen Rose (fig. 28), shows that small salt structures had formed, but no pillow is indicated at the present Pine Island structural position. Sediments are thinner over the pillow area than to the south, however. The isopach map of the upper Glen Rose (fig. 30) shows dramatic thinning over the Pine Island area, but because a full thickness of upper Glen Rose is not present over the area, it is impossible to tell how much thinning was caused by pillow growth and how much was caused by erosion. Maximum growth of the Pine Island salt structure may have occurred during upper Glen Rose time; this was also a time of diapir growth in the North Louisiana salt basin (Lobao and Pilger, 1985) (fig. 35). The isopach map of the Paluxy Formation (fig. 31) does not show influence from salt structures in the study area, indicating that salt movement on the uplift had probably ceased at that time. Overlying intervals are eroded in the area of salt structures, so salt movement during Fredericksburg and Washita intervals (late Early Cretaceous) cannot be determined.

PROPOSED ORIGIN FOR THE SABINE UPLIFT

Examination of the early Mesozoic tectonic history of the Gulf of Mexico is important in evaluating theories for the origin of the Sabine Uplift. During the Early

Triassic, South and North America were joined along the Ouachita Front (fig. 40). Continental rifting began in the Late Triassic, forming attenuated crust in the Sabine Uplift area. Eagle Mills red beds were deposited in the resultant grabens (Salvador and Green, 1980). Early stage graben geometry is poorly known but may be reflected in the distribution of diapiric salt basins, where salt deposits were thickest. Thermal uplift and erosion in the Early Jurassic (Jackson, 1981) were followed by deposition of middle Jurassic Werner Anhydrite, Louann Salt, and Norphlet clastics. The Sabine Uplift was a relative high during this time, but the presence of salt across the uplift (fig. 41) indicates that its surface was level with surrounding areas in the latter part of Louann time. Cotton Valley and Travis Peak clastics buried the Sabine Uplift area under four thousand feet of sediment. The isopach maps in this study show that the Sabine Uplift was part of a large basinal area during the Late Jurassic and Early Cretaceous. Thus the Sabine Uplift does not appear to have been a large Jurassic horst that remained in a structurally high position through the Cretaceous and Tertiary, as is commonly depicted in the literature (Pindell, 1985; Buffler and Sawyer, 1985; Scott and Kidson, 1977).

Possible mechanisms for uplift in the Sabine area include differential thermal subsidence during rifting, differential response to sediment loading due to crustal inhomogeneities, thermal uplift caused by crustal anomaly (hot spot activity), incipient rifting, or folding caused by compression. Early authors, before the advent of plate tectonic theory, favored a plutonic origin for the uplift (Bornhauser, 1958; Moody, 1931).

Thermal subsidence models (Nunn and others, 1984; Royden and others, 1980) for passive rift margins like the Gulf Coast predict rapid, short-duration subsidence followed by slow, prolonged subsidence. The models do not account for the mid-Cretaceous and Early Tertiary uplift events. The long axis of the Sabine Uplift is

oriented north-south; this is not easily accounted for in the east-northeast-oriented sea-floor spreading models proposed by Pindell (1985), Buffler and Sawyer (1985), and Salvador and Green (1980) for the opening of the Gulf of Mexico.

Timing, orientation, and magnitude of Sabine arching indicate that the Sabine Uplift may have been produced by northeast-directed tectonic events related to orogenic activity in the southern North American Cordillera and the Sierra Madre Oriental in Mexico (fig. 40). Orogenic activity in the southern North American Cordillera during the mid-Cretaceous is not well understood, but it involved subduction along Middle America and the southern North American Cordillera (Dickinson, 1981). The Late Cretaceous-Early Tertiary Laramide Orogeny (fig. 35) caused uplifts in areas up to 400 mi (700 km) east of the Sevier fold-thrust belt (Dickinson and Snyder, 1978). This distance, if measured from the Sierra Madre Oriental, would reach to within 100 mi (160 km) of the Sabine Uplift. Differences in the type of continental crust, brittle in the inland areas and attenuated on the Gulf margin, could account for differences in structural style of uplifts and allow for low-amplitude uplifts at great distances from an orogenic thrust front.

SUMMARY

This study creates a regional database that supports detailed research on the pattern and timing of fracture propagation in the Travis Peak Formation, from which a stress history can be derived. Documentation of the uplift history demonstrates that some widely held beliefs concerning the structural history of this region may be erroneous. Isopach maps of Lower Cretaceous intervals show conclusively that the Sabine Uplift was not a positive feature in the lower Cretaceous but rose substantially, although with low relief, during the Cenomanian. Erosion of more than

1,200 ft (370 m) of dominantly carbonate sediments accompanied the uplift. Following a shift in the axis of uplift, Upper Cretaceous sediments were deposited during a structurally quiescent period. Tertiary clastic deposition was interrupted in the early Eocene by a second broad upwarp that resulted in erosion of another 1,200 ft (370 m) of sediment. Tertiary deposition resumed, but the uplift continued to be a positive feature, influencing clastic deposition. Erosion caused by isostatic rebound began about 40 mya and continues in the area today.

A possible driving force for arching of the Sabine Uplift is orogenic activity that occurred along the southern North American Cordillera and Sierra Madre Oriental during the early Tertiary and possibly also during the mid-Cretaceous. Plate collision causing thrusting and subduction in a northeasterly direction could be responsible for rejuvenation of the Sabine Uplift.

ACKNOWLEDGMENTS

This work was prepared for, and funded by, the Gas Research Institute under contract no. 5082-211-0708, Robert J. Finley, Principal Investigator. The author is greatly indebted to Steve Laubach for stimulating discussions and encouragement concerning theories on the origin of the Sabine Uplift. The author gratefully acknowledges the assistance of Steve Seni, Shirley Dutton, Walt Ayers, Malcolm Light, Mary McBride, and Tim Jackson in the formulation of ideas and review of the literature.

Word processing of this manuscript was done by Dorothy C. Johnson under the direction of Lucille C. Harrell. Illustrations were prepared by Nan Minchow-Newman under the direction of Richard L. Dillon. The manuscript was reviewed by Robert J. Finley and Edward C. Bingler. Technical editorial review was by Jules Dubar, and Diane Callis Hall edited the manuscript.

REFERENCES

- Andersen, H. V., 1960, Geology of Sabine Parish: Louisiana Department of Conservation, Geological Bulletin No. 34, 164 p.
- Anderson, E. G., 1979, Basic Mesozoic study in Louisiana, the northern coastal region and the Gulf Basin Province: Louisiana Geological Survey Folio Series No. 3, 58 p.
- Andrews, D. I., 1960, The Louann salt and its relationship to Gulf Coast salt domes: Gulf Coast Association of Geological Societies Transactions, v. 10, p. 215-240.
- Bailey, G. B., Dwyer, J. L., Francica, J. R., and Feng, M. S., 1984, Update on the use of remote sensing in oil and gas exploration, in Davidson, M. J., and Gottlieb, B. M., eds., Unconventional methods in exploration for petroleum and natural gas III, Symposium: Southern Methodist University, Dallas, Texas, p. 231-253.
- Bailey, T. L., Evans, F. G., and Adkins, W. S., 1945, Revision of stratigraphy of part of Cretaceous in Tyler Basin, Northeast Texas: American Association of Petroleum Geologists, v. 29, no. 2, p. 170-186.
- Bannister, E., 1980, Joint and drainage orientation of southwest Pennsylvania: Zeitschrift fur Geomorphologie N. F., v. 24, no. 3, p. 273-286.
- Barnes, V. E., 1967a, Palestine sheet: The University of Texas at Austin, Bureau of Economic Geology, Geologic Atlas of Texas, scale 1:250,000.
- _____ 1967b, Sherman sheet: The University of Texas at Austin, Bureau of Economic Geology, Geologic Atlas of Texas, scale 1:250,000.
- _____ 1972, Dallas sheet: The University of Texas at Austin, Bureau of Economic Geology, Geologic Atlas of Texas, scale 1:250,000.
- _____ 1975, Tyler sheet: The University of Texas at Austin, Bureau of Economic Geology, Geologic Atlas of Texas, scale 1:250,000.
- _____ 1979a, Texarkana sheet: The University of Texas at Austin, Bureau of Economic Geology, Geologic Atlas of Texas, scale 1:250,000.
- _____ 1979b, Waco sheet: The University of Texas at Austin, Bureau of Economic Geology, Geologic Atlas of Texas, scale 1:250,000.
- Berger, Z., 1982, The use of Landsat data for detection of buried and obscured geologic structures in the East Texas Basin, U.S.A.: Proceedings, International Symposium on Remote Sensing of Environment, Second Thematic Conference, Remote Sensing for Exploration Geology, Ft. Worth, Texas, p. 579-589.
- Bornhauser, Max, 1958, Gulf Coast tectonics: American Association of Petroleum Geologists Bulletin, v. 42, no. 2, p. 339-370.

- Braunstien, Jules, Huddleston, Paul, McLemore, William, and Biel, Ralph, coordinators, in press. Correlation of stratigraphic units in North America, Gulf Coast Province region: American Association of Petroleum Geologists, correlation chart series.
- Brown, R. O., Forgotson, J. M., and Forgotson, J. M., Jr., 1980, Predicting the orientation of hydraulically created fractures in the Cotton Valley Formation of east Texas: Society of Petroleum Engineers of AIME, 55th Annual Fall Conference, Dallas, Texas, Paper SPE 9269, 12 p.
- Buffler, R. T., and Sawyer, D. S., 1985, Distribution of crust and early history, Gulf of Mexico Basin: Gulf Coast Association of Geological Societies Transactions, v. 35, p. 333-344.
- Bushaw, D. J., 1968, Environmental synthesis of the East Texas Lower Cretaceous: Gulf Coast Association of Geological Societies Transactions, v. 18, p. 416-438.
- Caran, S. C., Woodruff, C. M., Jr., and Thompson, E. J., 1981, Lineament analysis and inference of geologic structure--examples from the Balcones/Ouachita trend of Texas: Gulf Coast Association of Geological Societies Transactions, v. 31, p. 59-69.
- Carlson, S. M., 1984, Investigations of recent and historical seismicity in East Texas: The University of Texas at Austin, Master's thesis, 197 p.
- Caughey, C. A., 1977, Depositional systems in the Paluxy Formation: The University of Texas at Austin, Bureau of Economic Geology Geological Circular 77-8, 59 p.
- Cheeny, R. F., 1983, Statistical methods in geology: Boston, George Allen and Unwin, 169 p.
- Dickinson, K. A., 1968, Upper Jurassic stratigraphy of some adjacent parts of Texas, Louisiana, and Arkansas: U.S. Geological Survey Professional Paper No. 594-E, 25 p.
- Dickinson, W. R., 1981, Plate tectonics and the continental margin of California, in Ernst, W. G., ed., The geotectonic development of California: Rubey v. 1, Englewood Cliffs, New Jersey, Prentice-Hall, p. 2-28 (chapter 1).
- Dickinson, W. R., and Snyder, W. S., 1978, Plate tectonics of the Laramide orogeny, in Matthews, V., III, ed., Laramide folding associated with basement block faulting in the western U. S.: Geological Society of America Memoir 151, p. 355-366.
- Dix, O. R., and Jackson, M. P. A., 1981, Statistical analysis of lineaments and their relation to fracturing, faulting, and halokinesis in the East Texas Basin: The University of Texas at Austin, Bureau of Economic Geology Report of Investigations No. 110, 30 p.
- Drury, S. A., 1986, Remote sensing of geological structure in temperate agricultural terrains: Geological Magazine, v. 123, no. 2, p. 113-121.

- Dutton, S. P., 1985. Petrography and diagenesis of the Travis Peak (Hosston) Formation, East Texas: The University of Texas at Austin, Bureau of Economic Geology, topical report prepared for the Gas Research Institute under contract no. 5082-211-0708, 71 p.
- Echols, D. J., and Malkin, D. S., 1948; Wilcox (Eocene) stratigraphy, a key to production: American Association of Petroleum Geologists Bulletin, v. 32, no. 1, p. 11-33.
- Eckel, E. B., 1938. The brown iron ores of eastern Texas: U. S. Geological Survey Bulletin 902, 155+ p.
- El-Etr, H. A., 1976. Proposed terminology for natural linear features, in Hodgson, R. A., Gay, S. P., Jr., and Benjamins, J. Y., eds.: Proceedings, First International Conference on the New Basement Tectonics, Salt Lake City, Utah Geological Association Publication No. 5, p. 480-489.
- Etheridge, M. A., Branson, J. C., and Stuart-Smith, P. G., 1985. Extensional basin-forming structures in Bass Strait and their importance for hydrocarbon exploration, in 25 years, a national achievement: APEA Journal, APEA Conference, Perth, Australia, v. 25, pt 1, p. 344-361.
- Ewing, T. E., compiler, in preparation, Tectonic map of Texas: The University of Texas at Austin, Bureau of Economic Geology, scale 1:750,000.
- Fenneman, N. M., 1938, Physiography of eastern United States: New York, McGraw-Hill Book Company, Inc., 714 p.
- Finley, R. J., 1984. Geology and engineering characteristics of selected low-permeability gas sandstones: The University of Texas at Austin, Bureau of Economic Geology Report of Investigations No. 138, 220 p.
- Finley, R. J., and Gustavson, T. C., 1981. Lineament analysis based on Landsat imagery, Texas Panhandle: The University of Texas at Austin, Bureau of Economic Geology Geological Circular 81-5, 37 p.
- Fisher, W. L., and McGowen, J. H., 1967. Depositional systems in the Wilcox Group of Texas and their relationship to occurrence of oil and gas: The University of Texas at Austin, Bureau of Economic Geology Geological Circular 67-4, p. 105-125.
- Fisk, H. N., 1944. Geological investigation of the alluvial valley of the lower Mississippi River: U. S. Army Corps of Engineers, Mississippi River Commission, 78 p.
- Forgotson, J. M., 1956. A correlation and regional stratigraphic analysis of the formations of the Trinity Group of the Comanchean Cretaceous of the Gulf Coastal Plain; and the genesis and petrography of the Ferry Lake Anhydrite: Gulf Coast Association of Geological Societies Transactions, v. 6, p. 91-108.
- _____, 1958. The basal sediments of the Austin Group and the stratigraphic position of the Tuscaloosa Formation of Central Louisiana: Gulf Coast Association of Geological Societies Transactions, v. 8, p. 117-125.

- Fracasso, M. A., Finley, R. J., and Dutton, S. P., 1986, Subregional stratigraphic relations, diagenesis, and reservoir quality of Travis Peak tight gas sandstones, Sabine Uplift area, Texas: Proceedings, 1986 East Texas Regional Meeting, sponsored by the East Texas section of Society of Petroleum Engineers in cooperation with East Texas Geological Society and the Gas Research Institute, SPE No. 14666, p. 133-142.
- Frost, R.T.C., 1977, Tectonic patterns in the Danish region (as deduced from a comparative analysis of magnetic, Landsat, bathymetric and gravity lineaments): *Geologie en Mijnbouw*, v. 56, no. 4, p. 351-362.
- Galloway, W. E., 1968, Depositional systems of the lower Wilcox Group, north-central Gulf Coast basin: *Gulf Coast Association of Geological Societies Transactions*, v. 18, p. 275-289.
- Geomap Company, 1981, Executive's geologic atlas for East Texas: scale 1:48,000.
- Gibson, T. G., and Bybell, L. M., 1981, Facies changes in the Hatcherigbee Formation in Alabama-Georgia and the Wilcox-Claiborne Group unconformity: *Gulf Coast Association of Geological Societies Transactions*, v. 31, p. 301-306.
- Gough, D. I., and Bell, J. S., 1982, Stress orientations from borehole wall fractures with examples from Colorado, east Texas, and northern Canada: *Canadian Journal of Earth Sciences*, v. 19, no. 7, p. 1358-1370.
- Granata, W. H., Jr., 1963, Cretaceous stratigraphy and structural development of the Sabine Uplift area, Texas and Louisiana, in Hermann, L. A., ed., Report on selected North Louisiana and South Arkansas oil and gas fields and regional geology: *Shreveport Geological Society Reference Volume 5*, p. 50-95.
- Gussow, W. C., 1973, East Texas field, the classic trap, has new interpretation: *Oil and Gas Journal*, v. 71, no. 7, p. 134-136.
- Haimson, B. C., 1978, Near surface and deeper hydrofracturing stress measurements in the Waterloo Quartzite (abs.): *EOS Transactions, American Geophysical Union*, v. 59, p. 327-328.
- _____ 1979, New hydrofracturing measurements in the Sierra Nevada Mountains and the relationship between shallow stresses and surface topography: 20th U.S. Symposium on Rock Mechanics, Austin, Texas, p. 675-682.
- Halbouty, M. T., 1980, Geologic significance of Landsat data for 15 giant oil and gas fields: *American Association of Petroleum Geologists Bulletin*, v. 64, no. 1, p. 8-36.
- Halbouty, M. T., and Halbouty, J. J., 1982, Relationships between East Texas field region and Sabine Uplift in Texas: *American Association of Petroleum Geologists Bulletin*, v. 66, no. 8, p. 1042-1054.
- Haley, B. R., 1976, Geologic map of Arkansas: *Arkansas Geological Commission*, scale 1:500,000.

- Hazzard, R. T., Blanpied, B. W., and Spooner, W. C., 1945a, Notes on correlations of the Cretaceous of East Texas, South Arkansas, North Louisiana, Mississippi, and Alabama, in Reference report on certain oil and gas fields of north Louisiana, South Arkansas, Mississippi, and Alabama: Shreveport Geological Society, v. 2, p. 472-481.
- Hazzard, R. T., Spooner, W. C., and Blanpied, B. W., 1945b, Notes on the stratigraphy of the formations which underlie the Smackover limestone in South Arkansas, northeast Texas, and north Louisiana, in Reference report on certain oil and gas fields of north Louisiana, South Arkansas, Mississippi, and Alabama: Shreveport Geological Society, v. 2, p. 483-503.
- Hobbs, W. H., 1904, Lineaments of the Atlantic border region: Geological Society of America Bulletin, v. 15, p. 483-506.
- Hobday, D. K., 1980, Geology of the Queen City Formation and associated units, in Perkins, B. F., and Hobday, D. K., eds., Middle Eocene coastal plain and nearshore deposits of East Texas, a field guide to the Queen City Formation and related papers: Gulf Coast Section, Society of Economic Paleontologists and Mineralogists, field trip guidebook, p. 1-45.
- Hughes, D. J., 1968, Salt tectonics as related to several Smackover fields along the northeast rim of the Gulf of Mexico Basin, Gulf Coast Association of Geological Societies Transactions, v. 18, p. 320-330.
- Huntley, L. G., 1923, The Sabine Uplift: American Association of Petroleum Geologists Bulletin, v. 7, no. 2, p. 179-180.
- Imlay, R. W., 1943, Jurassic formations of Gulf region: American Association of Petroleum Geologists Bulletin, v. 27, no. 11, p. 1407-1533.
- Jackson, M.P.A., 1981, Tectonic environment during early infilling of the East Texas Basin, in Kreitler, C. W., and others, Geology and geohydrology of the East Texas Basin, a report on the progress of nuclear waste isolation feasibility studies: The University of Texas at Austin, Bureau of Economic Geology Geological Circular 81-7, p. 7-11.
- _____ 1982, Fault tectonics of the East Texas Basin: The University of Texas at Austin, Bureau of Economic Geology Geologic Circular 82-4, 31 p.
- Jackson, M.P.A., and Seni, S. J., 1983, Geometry and evolution of salt structures in a marginal rift basin of the Gulf of Mexico, East Texas: Geology, v. 11, p. 131-135.
- _____ 1984a, Atlas of salt domes in the East Texas Basin: The University of Texas at Austin, Bureau of Economic Geology Report of Investigations No. 140, 102 p.
- _____ 1984b, Suitability of salt domes in the East Texas Basin for nuclear waste isolation: The University of Texas at Austin, Bureau of Economic Geology Geologic Circular 84-1, 128 p.
- Johnson, O. H., Jr., 1958, The Monroe Uplift: Gulf Coast Association of Geological Societies Transactions, v. 8, p. 24-37.

- Kaiser, W. R., Ayers, W. B., Jr., and La Brie, L. W., 1980. Lignite resources in Texas: The University of Texas at Austin, Bureau of Economic Geology Report of Investigations No. 104, 52 p.
- Kaiser, W. R., Jackson, M. L. W., and Collins, G. F., 1986. Geology of deep-basin lignite in the Wilcox Group, Sabine Uplift area, in Kaiser, W. R., and others, Geology and ground-water hydrology of deep-basin lignite in the Wilcox Group of East Texas: The University of Texas at Austin, Bureau of Economic Geology Special Publication, p. 11-20.
- Kupfer, D. H., Crowe, C. T., and Hessenbruch, J. M., 1976. North Louisiana basin and salt movements (halokinetics): Gulf Coast Association of Geological Societies Transactions, v. 26, p. 94-110.
- Lin, Z. S., 1985. Reservoir engineering properties and production characteristics of selected fields in the Travis Peak Formation, East Texas Basin, in Finley, R. J., and others, The Travis Peak (Hosston) Formation: geologic framework, core studies, and engineering field analysis: The University of Texas at Austin, Bureau of Economic Geology, topical report prepared for the Gas Research Institute under contract no. 5082-211-0708, p. 127-188.
- Lindenlaub, J. C., 1976. The physical basis of remote sensing: Fundamentals of remote sensing, Purdue University Minicourse Series, 13 p.
- Lobao, L. L., and Pilger, R. H., Jr., 1985. Early evolution of salt structures in the north Louisiana salt basin: Gulf Coast Association of Geological Societies Transactions, v. 35, p. 189-198.
- Louisiana Geological Survey, 1984. Geologic map of Louisiana: scale 1:500,000.
- McFarlan, E., Jr., 1977. Lower Cretaceous sedimentary facies and sea level changes, U. S. Gulf Coast, in Bebout, D. G., and Loucks, R. G., eds., Cretaceous carbonates of Texas and Mexico: The University of Texas at Austin, Bureau of Economic Geology Report of Investigations No. 89, p. 5-11.
- McKenzie, D., 1978. Some remarks on the development of sedimentary basins: Earth and Planetary Science Letters, v. 40, no. 1, p. 25-32.
- McMahan, C. A., Frye, R. G., and Brown, K. L., 1984. The vegetation types of Texas, including cropland: Texas Parks and Wildlife Department, PWD Bulletin 7000-120, 40 p.
- Moody, C. L., 1931. Tertiary history of region of Sabine Uplift, Louisiana: American Association of Petroleum Geologists Bulletin, v. 15, no. 5, p. 531-551.
- Murray, G. E., 1948. Geology of DeSoto and Red River Parishes: Department of Conservation, Louisiana Geological Survey Geological Bulletin No. 25, 312 p.
- _____ 1961. Geology of the Atlantic and Gulf Coastal Province of North America: New York, Harper, 692 p.

- Murray, G. E., Jr., and Thomas, E. P., 1945. Midway-Wilcox surface stratigraphy of Sabine Uplift, Louisiana and Texas: American Association of Petroleum Geologists Bulletin, v. 29, no. 1, p. 45-70.
- Nichols, P. H., 1964. The remaining frontiers for exploration in northeast Texas: Gulf Coast Association of Geological Societies Transactions, v. 14, p. 7-22.
- Nichols, P. H., Peterson, G. E., and Wuestner, C. E., 1968. Summary of subsurface geology of northeast Texas, *in* Beebe, B. W., ed., Natural gases of North America: American Association of Petroleum Geologists, Memoir 9, v. 1, p. 982-1004.
- Norman, J. W., 1976. Photogeological fracture analysis as a subsurface exploration technique: Transactions, American Institute of Mining and Metallurgy, Section B, v. B, p. B52-B61.
- Nunn, J. A., Scardina, A. D., and Pilger, R. H., Jr., 1984. Thermal evolution of the north-central Gulf Coast: Tectonics, v. 3, no. 7, p. 723-740.
- Oliver, W. B., 1971. Depositional systems in the Woodbine Formation (upper Cretaceous), northeast Texas: The University of Texas at Austin, Bureau of Economic Geology Report of Investigations No. 73, 28 p.
- Orton, R. B., 1964. The climate of Texas and the adjacent Gulf waters: U.S. Department of Commerce, Weather Bureau, 195 p.
- Pilger, R. H., Jr., 1981. The opening of the Gulf of Mexico: implications for the tectonic evolution of the northern Gulf Coast: Gulf Coast Association of Geological Societies Transactions, v. 31, p. 377-381.
- Pindell, J. L., 1985. Alleghenian reconstruction and subsequent evolution of the Gulf of Mexico, Bahamas, and Proto-Caribbean: Tectonics, v. 4, no. 1, p. 1-39.
- Pittman, J. G., 1985. Correlation of beds within the Ferry Lake Anhydrite of the Gulf Coastal Plain: Gulf Coast Association of Geological Societies Transactions, v. 35, p. 251-260.
- Powers, S., 1920. The Sabine Uplift, Louisiana: American Association of Petroleum Geologists Bulletin, v. 4, no. 2, p. 117-136.
- Rainwater, E. H., 1971. Possible future petroleum potential of lower Cretaceous, western Gulf basin, *in* Cram, I. H., ed., Future petroleum provinces of the United States--their geology and potential: American Association of Petroleum Geologists Memoir 15, p. 901-926.
- Reynolds, S. J., Spencer, J. E., Richard, S. M., and Laubach, S. E., 1986. Mesozoic structures in west-central Arizona, *in* Beatty, B., and Wilkinson, P. A. K., eds., Frontiers in geology and ore deposits of Arizona and the southwest: Arizona Geological Society Digest, v. 16, p. 35-51.

- Royden, Leigh, Sclater, J. G., and von Herzen, R. P., 1980, Continental margin subsidence and heat flow: important parameters in formation of petroleum hydrocarbons: American Association of Petroleum Geologists Bulletin, v. 64, no. 2, p. 173-187.
- Salvador, Amos, and Green, A. R., 1980, Opening of the Caribbean Tethys (origin and development of the Caribbean and the Gulf of Mexico), in Colloque C5: Geologie des chaines alpines issues de la Tethys: Bureau de Recherches Geologiques et Minieres, Memoire 115, p. 224-229.
- Saucier, A. E., 1984, The Gibsland salt stock family in northwestern Louisiana: Gulf Coast Association of Geological Societies Transactions, v. 34, p. 401-410.
- _____ 1985, Geologic framework of the Travis Peak (Hosston) Formation of East Texas and north Louisiana, in Finley, R. J., and others, The Travis Peak (Hosston) Formation: geologic framework, core studies, and engineering field analysis: The University of Texas at Austin, Bureau of Economic Geology, topical report prepared for the Gas Research Institute under contract no. 5082-211-0708, 77 p.
- Scott, R. W., and Kidson, E. J., 1977, Lower Cretaceous depositional systems, West Texas, in Bebout, D. G., and Loucks, R. G., eds., Cretaceous carbonates of Texas and Mexico: The University of Texas at Austin, Bureau of Economic Geology Report of Investigations No. 89, p. 5-11.
- Sellards, E. H., Adkins, W. S., and Plummer, F. B., 1932, The geology of Texas: The University of Texas, Austin, Bureau of Economic Geology Bulletin No. 3232, v. 1, 1007 p.
- Seni, S. J., and Jackson, M. P. A., 1984, Sedimentary record of Cretaceous and Tertiary salt movement, East Texas Basin: times, rates, and volumes of salt flow and their implications for nuclear waste isolation and petroleum exploration: The University of Texas at Austin, Bureau of Economic Geology Report of Investigations No. 139, 89 p.
- Siegel, S., 1956, Nonparametric statistics for the behavioral sciences: New York, McGraw-Hill, 312 p.
- Siemers, C. T., 1978, Submarine fan deposition of the Woodbine-Eagle Ford interval (upper Cretaceous), Tyler County, Texas: Gulf Coast Association of Geological Societies Transactions, v. 28, p. 493-533.
- Spoooner, W. C., 1926, Interior salt domes of Louisiana: American Association of Petroleum Geologists Bulletin, v. 10, p. 217-292.
- Stehli, F. G., and Creath, W. B., 1964, Foraminiferal rations and regional environments: American Association of Petroleum Geologists Bulletin, v. 48, no. 11, p. 1810-1827.
- Stehli, F. G., Creath, W. B., Upshaw, C. F., and Forgotson, J. M., Jr., 1972, Depositional history of Gulfian Cretaceous of East Texas embayment: American Association of Petroleum Geologists Bulletin, v. 56, no. 1, p. 38-67.

- Stenzel, H. B., 1938. The geology of Leon County, Texas: University of Texas, Austin, Publication No. 3818, 295 p.
- Stephenson, L. W., 1927, Notes on the stratigraphy of the upper Cretaceous Formations of Texas and Arkansas: American Association of Petroleum Geologists Bulletin, v. 11, no. 1, p. 1-17.
- Strubhar, M. K., Fitch, J. L., and Glenn, E. E., Jr., 1975, Multiple, vertical fractures from an inclined wellbore--a field experiment: Journal of Petroleum Technology, v. 27, p. 641-647.
- Thomas, G. E., 1974, Lineament-block tectonics: Williston-Blood Creek Basin: American Association of Petroleum Geologists Bulletin, v. 58, no. 7, p. 1305-1322.
- Tullis, T. E., 1981, Stress measurements via shallow overcoring near the San Andreas Fault, in Carter, N.L., Friedman, M., Logan, J. M., and Stearns, D. W., eds., Mechanical behavior of crustal rocks: American Geophysical Union, Geophysical Monograph 24, The Handin Volume, p. 199-213.
- Uttamo, W., 1979, Application of Landsat imagery for regional geologic and geomorphic mapping, northern Mississippi: The University of Mississippi, The Mississippi Mineral Resources Institute, Report of Student Investigations No. 791, 64 p.
- Vail, P. R., Mitchum, R. M., Jr., and Thompson, S., III, 1977, Seismic stratigraphy and global changes of sea level, part 4: global cycles of relative changes of sea level, in Payton, C. E., ed., American Association of Petroleum Geologists Memoir 26, p. 83-97.
- Vernon, R. C., 1971, Possible future petroleum potential of pre-Jurassic, western Gulf Basin, in Cram, I. H., ed., Future petroleum provinces of the United States--their geology and potential: American Association of Petroleum Geologists Memoir 15, p. 954-979.
- Vistelius, A. B., 1966, Structural diagrams: New York, Pergamon Press, 178 p.
- Waters, J. A., McFarland, P. W., and Lea, J. W., 1955, Geologic framework of Gulf coastal plain of Texas: American Association of Petroleum Geologists Bulletin, v. 39, no. 9, p. 1821-1850.
- Williams, R. S., Jr., 1983, Geological applications, in Colwell, R. N., ed., Manual of remote sensing: American Society of Photogrammetry, 2d ed., v. 2, Estes, J. E., ed., Interpretation and applications, p. 1667-1953.
- Wise, D. U., 1969, Pseudo-radar topographic shadowing for detection of sub-continental sized fracture systems: Proceedings, Sixth International Symposium on Remote Sensing of Environment, v. 1, p. 603-615.
- Withjack, M. O., and Scheiner, C., 1982, Fault patterns associated with domes--an experimental and analytical study: American Association of Petroleum Geologists Bulletin, v. 66, no. 3, p. 302-316.

Wood, D. H., and Guevara, E. H., 1981a, Regional structural cross sections and general stratigraphy, East Texas Basin: The University of Texas at Austin, Bureau of Economic Geology Cross Sections.

_____ 1981b, Regional structural cross sections and general stratigraphy, East Texas Basin: The University of Texas at Austin, Bureau of Economic Geology Open-File Cross Sections, East Texas Waste Isolation project.

Woodruff, C. M., Jr., and Caran, S. C., 1984, Lineaments of Texas--possible surface expressions of deep-seated phenomena: The University of Texas at Austin, Bureau of Economic Geology, final report prepared for U. S. Department of Energy, Division of Geothermal Energy, under contract no. DE-AS07-79ID12057, Geothermal resource assessment for the State of Texas, 68 p.

Yamaguchi, Y., 1985, Image-scale and look-direction effects on the detectability of lineaments in radar images: Remote sensing of environment, v. 17, no. 2, p. 117-127.

Young, Keith, 1972, Mesozoic history, Llano region, in Barnes, V. E., and others, Geology of the Llano region and Austin area: The University of Texas at Austin, Bureau of Economic Geology Guidebook 13, p. 41-46.

Zoback, M. D., Tsukahara, H., and Hickman, S., 1980, Stress measurements at depth in the vicinity of the San Andreas Fault: implications for the magnitude of shear stress at depth: Journal of Geophysical Research, v. 85, no. B11, p. 6157-6173.

Zoback, M. L., and Zoback, M., 1980, State of stress in the conterminous United States: Journal of Geophysical Research, v. 85, no. B11, p. 6113-6156.

APPENDIX A. Wells that penetrate salt over the Sabine Uplift.
 --- Base salt noted where penetrated. Depths in feet.

Map No.	Operator	No.	Lease	T.D.	Remarks	Reference*
1	Ridley et al. (So. Union)	1	Hardin	12,080	top salt 11,701	---
2	Norton	1	Payne	11,486	top salt 11,470	AS, H
3	Chevron USA	1	Livingston	12,514	top salt 11,076 base salt 11,390	---
4	Stanolind	131	Dillon	11,419	top salt 10,160 base salt 11,335	H, AN
5	Texaco	1	Gish	10,556	top salt 10,556	---
6	Placid	2	Dunn Unit 1	14,283	top salt 12,470 base salt 13,440	AN, V
7	Western	1	Stevens	14,316	top salt 11,681 base salt 13,045	---
8	Fair	1	Waters	12,255	top salt 11,850	---
9	Beacon	1	Lloyd	12,620	top salt 12,114	---
10	Ark-La Gas	1	Waskom Smack-over Unit	11,341	top salt 10,999	---
11	Tenneco (Tx.Co.)	1	Adams	11,105	top salt 11,067	H
12	Glassell	27	Carthage Gas Unit	12,202	top salt 11,232	AS
13	Carthage (Chicago)	2 (1)	Unit 3 (Allison)	11,441	top salt 11,117 base salt 11,315	AS, AN
14	Skelly	K-2	Werner	11,320	top salt 11,299	AS
15	Skelly	1	Thelma Nash	11,664	top salt 11,652	AN
16	Humble	1	Johnson	16,884	top salt 11,920 base salt <13,820	V
17	Gulf	1	Langston	12,281	top salt 12,163	---
18	Amerada	1	Strickland	12,533	anhydrite with salt	AN, V
19	Humble	1	Pickering	12,230	top salt 12,230	AS, AN

* AN = Anderson, 1979; AS = Andrews, 1960; H = Hazzard and others, 1945b;
 V = Vernon, 1971